AD-A083 699 ROYAL AIRCRAFT ESTABLISHMENT FARNBOROUGH (ENGLAND) F/G 9/5
A THICK FILM MICROSTRIP BUTLER MATRIX FOR THE FREQUENCY RANGE 1--ETC(U)
SEP 79 A G TABB
UNCLASSIFIED RAE-TR-79118 DRIC-BR-72772 NL

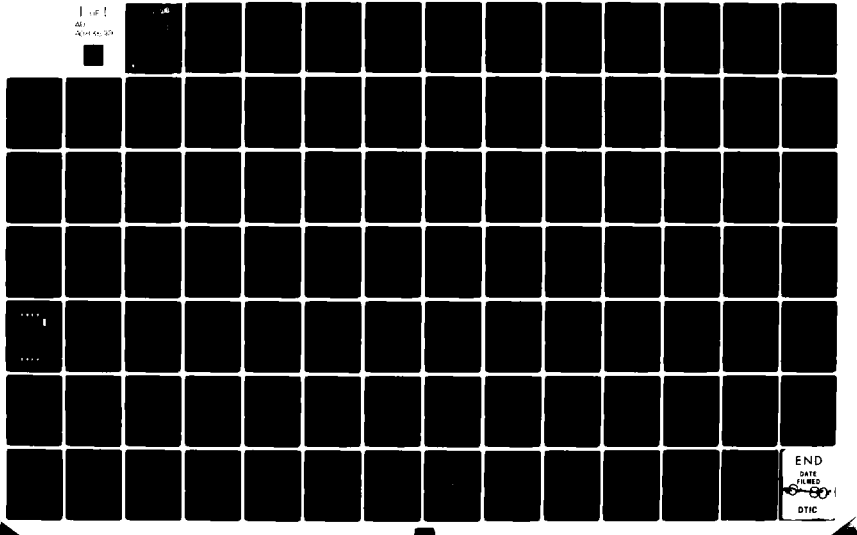

END
DATE FILMED
DTIC

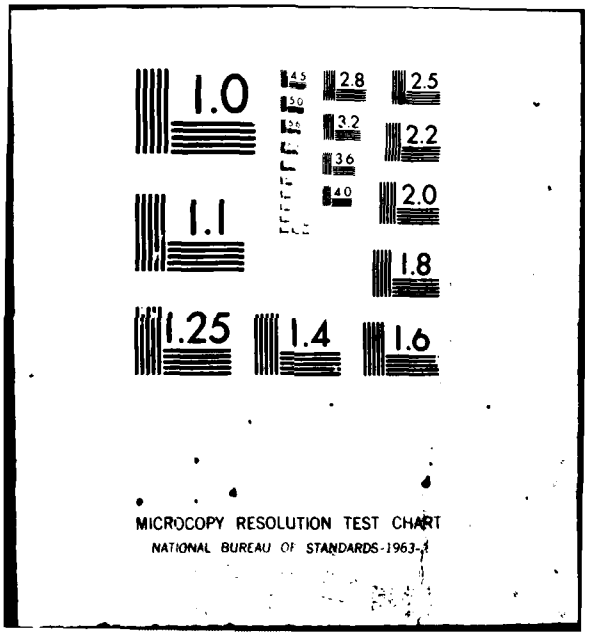
1.0
1.1
1.25
1.4
1.6
1.8
2.0
2.2
2.5
2.8
3.2
3.6
4.0
4.5
5.0
MICROCOPY RESOLUTION TEST CHART
NATIONAL BUREAU OF STANDARDS-1963-A

ROYAL AIRCRAFT ESTABLISHMENT

*

(9) Technical Report 79118
(11) September 1979

(6) A THICK FILM MICROSTRIP BUTLER MATRIX FOR THE FREQUENCY RANGE 1.5-1.7 GHz

by

(10) A.G. Tabb

(12) 96

*

Procurement Executive, Ministry of Defence
Farnborough, Hants

UDC 621.396.67 : 621.396.679.4 : 621.3.038.615 : 621.3.029.64 : 621.396.4:
621.3.049.77-418

ROYAL AIRCRAFT ESTABLISHMENT

Technical Report 79118

Received for printing 10 September 1979

A THICKFILM MICROSTRIP BUTLER MATRIX FOR THE FREQUENCY RANGE 1.5-1.7 GHz

by

A. G. Tabb

SUMMARY

This Report describes the design, construction and electrical measurement of a 4 × 4 Butler Matrix for the 1.5-1.7 GHz frequency range. The Matrix was constructed in thickfilm technology on an alumina substrate. A computer aided design package was used for the circuit synthesis.

Departmental Reference: Space 568

LIST OF CONTENTS

LIST OF CONTENTS (concluded)

1 INTRODUCTION

A Butler Matrix is a passive multiport component which when loaded with radiating elements enables production of a beam of microwave energy in a specified direction in space, dependent upon which input port is activated.

This Report describes the general design procedure and analysis of Butler Matrices up to order 5 (*ie* 32 input and output ports). In particular it describes the design and measurement of a 1.5-1.7 GHz, 4 × 4 Butler Matrix constructed in microstrip on alumina by thick film technology.

2 THE BUTLER MATRIX

The Butler Matrix consists of an equal number of input and output ports connected through an array of phase shifters and couplers such that when a signal is applied to any input port it produces equal amplitude signals at all output ports.

There are two main types:

2.1 The broadside beam Matrix[2]

Here, the signal impressed on one input gives rise to equi-amplitude equi-phase outputs (broadside beam condition), whereas on any other input the applied signal gives rise to equi-amplitude signals at all outputs but the phase difference between any two adjacent output ports is a function of the input port number. It requires the provision of a -3dB coupler giving a π-phase difference between the outputs when one input is energised and equi-phase outputs for the other input energisation. Such a coupler is shown in Fig 1a.

For the Matrix with 2^k inputs and outputs (where k is a positive integer) the phase length between any input and output can be given by

$$\psi_{mn} = \psi_0 + (n - 1)m \frac{2\pi}{2^k}$$

where ψ_{mn} is the phase shift between input m, output n,

ψ_0 is the phase shift from broadside $m = 0$ to any output,

m is the input port number $-2^{k-1} \leqslant m \leqslant 2^{k-1} - 1$

and

n is the output port number $1 \leqslant n \leqslant 2^k$.

A Matrix of this size would require a total of $k2^{k-1}$ couplers and $(k - 1)2^k$ phase shifters allowing a total of 2^k different beams to be radiated simultaneously.

2.2 The non-broadside beam Matrix

Here, a signal applied to any input port produces equi-amplitude signals at all output ports but with a constant phase difference between them resulting in formation of beams at a certain angle in space. It requires a coupler giving a $\pi/2$ phase difference between output ports for either input port energisation (Fig 1b).

The phase difference $\Delta\phi$ between radiating elements for this Matrix with 2^k input and output ports and for a scan angle θ is given by[3] (Fig 2a):

$$\Delta\phi = \frac{2\pi d}{\lambda} \sin\theta$$

where d is the element spacing,
θ is the scan angle,
λ is the wavelength.

This type, as the broadside type, requires $k2^{k-1}$ couplers and $(k-1)2^k$ phase shifters.

3 GENERAL MATRIX DESIGN

A general design procedure is available in the literature[4] but in this section a somewhat simpler systematic approach is outlined for the non-broadside beam Matrix, showing how the input and output port numbering is achieved and giving the phase shifter values for each rank.

A systematic design approach for the broadside beam Matrix is available in the literature[2].

Section 2.2 explains what happens for a signal applied to a given input. For a basic 4 × 4 Matrix array four beams are possible as shown in Fig 2b.

The beams to the left of the array axis are named first left, second left (working away from the axis) and those to the right, first right and second right. To link the beam formed to the input forming it, the inputs are labelled 1L, 2L, 1R and 2R but due to the various phasing sections of the Matrix (although symmetric) the numbering sequence of the input ports does not run concurrently.

3.1 Input port numbering

The derivation of an input port numbering sequence for a Matrix of order $N = 2^k$ (*ie* N beams) is an iterative process. It builds upon the numbering sequence derived for the Matrix one order lower ($\frac{N}{2}$ beams, where $\frac{N}{2} = 2^{k-1}$) and so

on back to $\frac{N}{2^{k-2}} = 2^2$, *ie* four beams as starting point. The sequence for two beams is an exception to the method but is simple enough to annotate at sight. The examples which follow will illustrate the method described below.

To derive the input numbering sequence for a Matrix of order $N = 2^k$, add 2^{k-2} to each term of the first half of the input port numbering sequence derived for the Matrix of order 2^{k-1}. Reverse this new sequence in pairs and interleave in pairs with the original sequence (order 2^{k-1}) after the first term. Append the mirror image to this sequence and the resultant is that required for the input port numbering of order $N = 2^k$. The terms are then lettered alternately R and L to relate them to the beams they produce at output.

(i) $k_1 = 1$, $N_1 = 2$	1R 1L	exception to the rule
(ii) $k_2 = 2$, $N_2 = 4$	1	half of input port numbering sequence derived in (i) for k_1 = 1, *ie* $k_2 - 1$
	2	$+2^{k_2-2}$
	1 2	interleave
	1 2 2 1	mirror image
	1R 2L 2R 1L	
(iii) $k_3 = 3$, $N_3 = 8$	1 2	half of input port numbering sequence derived in (ii) for $k_2 = 2$, *ie* $k_3 - 1$
	3 4	$+2^{k_3-2}$
	4 3	reverse as pairs
	1 4 3 2	interleave
	1R 4L 3R 2L 2R 3L 4R 1L	mirror image and add R, L
(iv) $k_4 = 4$, $N_4 = 16$	1 4 3 2	half of input port numbering sequence derived in (iii) for $k_3 = 3$
	5 8 7 6	$+2^{k_4-2}$
	8 5 6 7	reverse as pairs
	1 8 5 4 3 6 7 2	interleave as pairs after first term
	1R 8L 5R 4L 3R 6L 7R 2L 2R 7L 6R 3L 4R 5L 8R 1L	mirror and add R, L

3.2 Output port numbering

For a Matrix of order $N = 2^k$ write down the first N numbers of the normal number sequence provided the layout is as in Fig 3.

3.3 Phase shifter values

From a design such as Fig 4, it will be seen that the number of rows of phase shifters for an order $N = 2^k$ Matrix is $k - 1$ and each unit must insert a multiple of $-\pi/2^k$ radians, derived by an iterative process starting from the values for the $k_4 = 4$ case.

In general for the first row of phase shifters take half the sequence for the $k_n - 1$ case and repeat it. Alternately add and subtract 1, ignoring zeros for this treatment, to the half-way point in the sequence and mirror. Add to the original sequence and mirror.

For the second row take half the sequence for the $k_n - 1$ case (as for first row) and repeat each number 2^1 times multiplying each by 2^1, then mirror. This gives the sequence for the second row of phase shifters.

For the nth row take half the sequence for the $k_n - n + 1$ case and repeat each number 2^{n-1} times, multiplying each by 2^{n-1}, then mirror resulting in the sequence for the nth row of phase shifters.

(i) In the case of $k_1 = 1$ no phase shifters are required.

(ii) For $k_2 = 2$ it can be seen from Fig 3 that this case requires one row of phase shifters, multiples of $-\pi/4$, arranged sequentially as:

1 0 0 1 .

(iii) For $k_3 = 3$ two rows of phase shifters, multiples of $-\pi/8$, are required.

For the first row take the sequence for $k_3 - 1$

1 0 0 1 .

Add and subtract 1.

2 0 0 0 .

Add this to the original sequence ($k_3 - 1$) and mirror to give the required phase shifter values for the first row.

3 0 0 1 1 0 0 3 .

From $k_4 = 4$ onwards the method follows the iteration process described above.

(iv) $k_4 = 4$ three rows of phase shifters, multiples of $-\pi/16$, are required.

The first row uses half the sequence for $k_4 - 1$, repeated.

3 0 0 1 3 0 0 1 .

Alternately add and subtract 1, ignoring zeros to the half-way point and then mirror.

4 0 0 0 0 0 0 4 .

Add this to the original sequence and mirror, giving the first row sequence:

7 0 0 1 3 0 0 5 5 0 0 3 1 0 0 7 .

For the second row of phase shifters take half the sequence for the $k_4 - 1$ case and repeat each number twice multiplying each by 2, then mirror.

3 0 0 1
6 6 0 0 0 0 2 2
6 6 0 0 0 0 2 2 2 2 0 0 0 0 6 6 .

For the third row take half the sequence for the $k_4 - 2$ case and repeat each number four times, multiplying each by 4 and mirror.

1 0
4 4 4 4 0 0 0 0
4 4 4 4 0 0 0 0 0 0 0 0 4 4 4 4 .

Appendix A gives a complete example of the input and output port numbering and phase shifter values for an order N = 32 Matrix.

Fig 4 shows a complete basic block diagram for one half of this 32 × 32 Matrix, the other half being a mirror image apart from the output port numbering.

Note that each line of phase shifters adds up to $-N\pi/8$ and that the $-\pi/4$ phase shifters are always at the row of couplers next to the antenna array.

Equal phase shift magnitudes are found in places symmetric to the Matrix axis, the smallest phase shift value being $-\pi/N$.

3.4 Design specification

Below is detailed a typical design specification for a 4 × 4 Butler Matrix.

Frequency band	:	1.535-1.66 GHz
Transmit band	:	1.535-1.5585 GHz
Receive band	:	1.6365-1.66 GHz
Centre frequency:		1.5975 GHz
Total losses	:	-1.5 dB target
		-2.0 dB maximum
Phase error	:	$\pm 5.0^{\circ}$ target
VSWR	:	1.2 : 1 any input, output
Isolation	:	-20 dB minimum
Dimensions	:	no specific requirements - as small as possible
Weight	:	no specific requirements - as light as possible
Connectors	:	SMA type
Technology	:	suitable for space qualification.

Plus the following:

Transmission medium	microstrip
Technology	thickfilm
Substrate type	alumina (MRC superstrate) $\varepsilon_r = 9.8$
Maximum substrate size	50.8 × 101.6 × 0.635 mm
Conductor ink	Plessey EMD C5700 fritless gold
Ground plane ink	Englehard T894 silver
Screen mesh size for thickfilm printing	325 meshes/square inch .

4 CHOICE OF MATRIX COMPONENTS

For the Butler Matrix there are two basic components that have to be selected: the hybrid coupler and the phase shifter. It will be seen below that while one is free to select the particular type of hybrid considered to be optimum for the task in hand, in the case of the phase shifter there are fundamental considerations of dispersion which restrict the choice to some extent.

Since the chosen transmission medium is microstrip, several types of coupler and phase shifter exist that can be used in the design, each having various advantages and disadvantages.

4.1 Couplers

The couplers considered were:

4.1.1 The Lange interdigitated coupler

The Lange interdigitated quadrature hybrid coupler[5] (Fig 5) has the advantages of being broadband and coupling in the forward direction thus simplifying layout procedure, requiring shorter tracks hence lower insertion loss. The problem of decreasing directivity with increasing frequency is avoided by using cross-strapping between alternate lines but this makes the device less robust and more difficult to manufacture. Unfortunately no general design data have been published.

4.1.2 The Schiffman coupler

The Schiffman coupler[6] (Fig 6) is very broadband but presents design difficulties due to the even and odd mode velocity differences in the coupled lines.

4.1.3 The 90° hybrid coupler

This coupler (Fig 7) is relatively narrow band, couples in the forward direction hence simplifying layout and constitutes no great design difficulties. It has a $\pi/2$-phase shift between coupled and through arms and presents a low VSWR to the connecting circuit even when the output lines are equal but not exactly 50 ohm.

4.1.4 The 180° hybrid coupler

The conventional microstrip rat-race has three branches of $\lambda/4$ and one of $3\lambda/4$. To reduce frequency sensitivity one of the arms can be replaced by a coupled pair of grounded $\lambda/4$ lines[7] (Fig 8) producing a π-phase shift. This coupler has the disadvantages of diagonally opposite coupled ports and, in the wideband version, a very narrow coupling gap and shorting holes in the substrate. The narrow coupling gap can be overcome if the complication of a sandwich construction can be tolerated to obtain the required mutual coupling.

4.1.5 The broadside coupler

This relatively wideband coupler providing good isolation and a straightforward layout is shown in Fig 9a. The coupling mechanism is special in that a wave travelling in one direction on one of the lines couples only to a wave going in the opposite direction on the other line. Hence the disadvantage of diagonally opposite direct and coupled ports and a greater disadvantage of low level coupling (-5 dB possible with laser trimming).

4.1.6 The Podell coupler

The Podell coupler[8] of Fig 9b overcomes even and odd mode velocity dispersion by using a sawtooth design on the inner edge. This sawtooth effectively slowing the odd mode as it propagates along the inside edge while the even mode remains unaffected along the outside edge. Its advantage is that its layout, (similar to the broadside coupler), only involves thickfilm printing. Its disadvantages are the necessity to use tandem coupling for a 3 dB split (thus greater insertion losses) and the coupled and through arms are diagonally opposite, leading to complicated overall layouts. Also no design information is available in the literature.

4.2 Phase shifters

In the explanation given in section 2 of the working of the Butler Matrix, a spot frequency only was considered in the interests of simplicity. If however, the Butler Matrix is to be of any practical use it must operate correctly over the information bandwidth, *ie* dispersion over this bandwidth must be prevented. To achieve this, identical phase frequency slopes must be designed into sets of phase shifters having different electrical lengths.

The following passive phase shifters were considered:

4.2.1 The dielectrically loaded line phase shifter

This phase shifter is achieved by placing lumped constant, high permittivity material on a uniform microstrip line. This has the unfortunate disadvantage of setting up moding in the line and introducing mismatches (hence greater VSWRs).

4.2.2 The meanderline phase shifter

Meanderlines are easy to design but the line lengths necessary for a full set of shifters (for larger matrices) causes greater insertion losses.

4.2.3 The loaded line phase shifter

Loaded line sections with short or open circuit stubs can be used to distort the phase-frequency slope of a uniform transmission line over a narrow bandwidth. The simplest type cannot produce greater than π-phase shift unless open or shorted stubs are used in combination.

5 COMPONENT DESIGN

5.1 Couplers

For ease of layout and design using the proposed technology the 90° hybrid coupler of section 4.1.3 was ideally suited. For the relatively narrow bandwidth

required (8%) a single section coupler was adequate and previous experience[2] has shown that in a square geometry this coupler performed more closely to theoretical predictions than in a circular geometry.

The basic configuration shown in Fig 7 required some length modifications to compensate for the somewhat unpredictable junction discontinuities involved when two different impedance lines meet[9].

5.2 Discontinuities and fringing effects

In addition to the main point made in section 4.2 there is the possibility of slight dispersion of the information frequencies by the microstrip line itself. At the frequencies of interest and the bandwidth requirements in the specification of section 3, errors due to this problem have been rendered insignificant by the best compromise design. It should therefore be mentioned that the dispersive effects of microstrip lines, although not too important at these frequencies, are a problem in circuit design and dispersion is dependent on the permittivity of the substrate and the physical dimensions of the lines. Its effects are noticeable when more of the field becomes contained in the substrate thus increasing the effective permittivity (phase velocity) and lowering the characteristic impedance of the microstrip lines.

Effective permittivity varies across the substrate and, more so, from substrate to substrate, so average effective permittivity values must be used in calculating line lengths, these values having been measured for lines of differing impedance.

Junction and open end effects have also to be accounted for, though again it is not absolutely necessary at these lower frequencies.

In the Butler Matrix component design, the microstrip dispersive effects compromised were line lengths (by using effective permittivities), junction effects and open circuit effects.

5.3 Phase shifters

From line length considerations, ease of design layout and relatively narrow bandwidth requirements, meanderline phase shifters were chosen in conjunction with loaded line sections. The choice of meanderlines was made primarily for ease of layout, but it will be appreciated that this choice automatically sets the phase frequency slope which has to be designed into the loaded lines.

In the loaded line there is a choice of open or shorted stubs but the latter would necessitate numerous holes being drilled at various points in the substrate

and so, from the point of view of cost and ease of manufacture, phase shifter design was limited to loaded sections with open circuit stubs.

To obtain the required value of insertion phase while ensuring an identical phase-frequency slope, each set (being the complete set of phase shifters between any two ranks of couplers) was designed together.

Fig 10 shows a typical loaded line section and its equivalent circuit.

For any line or filter section the characteristic impedance is given by

$$Z_0 = \sqrt{Z_{sc} Z_{oc}} = \frac{1}{\sqrt{Y_{sc} Y_{oc}}}$$

and the propagation constant γ is given by

$$\tanh(\gamma) = \sqrt{\frac{Z_{sc}}{Z_{oc}}} = \sqrt{\frac{Y_{oc}}{Y_{sc}}}$$

and

$$\gamma = \alpha + j\beta$$

where α is the *attenuation constant* ($\alpha = 0$ *for a lossless network*),

β is the phase constant or delay of the section *viz* the angle in radians by which the current leaving the section lags the current entering it,

Z_{sc} is the short circuit impedance $\left(= \frac{1}{Y_{sc}}\right)$

and

Z_{oc} is the open circuit impedance $\left(= \frac{1}{Y_{oc}}\right)$.

Hence, for a lossless network

$$\tanh(\gamma) = \tanh(j\beta) = j \tan(\beta)$$

$$\therefore \beta = \tan^{-1}\left[-j\sqrt{\frac{Y_{oc}}{Y_{sc}}}\right].$$

Appendix B gives a detailed solution of the phase-frequency slope problem of section 4.2 in terms of the normalised admittances of the lines and stubs, the phase shift of a section at midband and the change of this phase shift with frequency (the phase slope). An equivalence is made between this phase slope and that produced by a length of transmission line of normalised admittance 1.

The equation of this length of transmission line and the equivalent loaded line section are used in an iterative program[10] to compute the desired phase shifter design values. Hence a set of phase shifters is designed with the same phase slope as that of a known length of meanderline. This constant phase slope is necessary to ensure a constant phase difference between each phase shifter over the frequency band of interest.

Typical examples of the program output are shown in Table 1.

Since, in this project, a 4 × 4 Matrix was being designed the single rank of phase shifters required consisted of $\pi/4$ and 0 degree phase shifters. As the phase differences, output to output, were constant for each input stimulus, and all output phases were relative to the 1R, 1 plane of the Matrix, the phase shift values need not necessarily have been identically $\pi/4$ and 0 degrees. Provided there was a $\pi/4$ phase difference between them, any pair of the set shown in Table 1 could be used.

For ease of layout on a 101.5 × 50.8 mm substrate (the largest processable) the 135° meanderline and 90° loaded line sections were chosen.

The basic configuration of these phase shifters had to have some length modifications to the values given in Table 1 to compensate them for the open circuit and junction effects of microstrip lines.

6 PRACTICAL DESIGN OF A COMPLETE MATRIX

As can be seen by comparing the Matrix schematics of Figs 1 and 11 there was a physical layout problem for Matrices of greater than order N = 2 due to their non-flat nature especially since the chosen transmission medium was microstrip. The configuration as it stood, required crossover lines which in any adverse environment would have introduced reliability problems besides increased complexity in the thickfilm processing.

Fig 12 shows a compromise situation, suitable only for the Matrix of order N = 4, where the circuit was orientated in such a way that no crossovers were required and the circuit was purely of flat geometry. Although the circuit now had no crossovers and was straightforward to produce, it had the disadvantage of having inputs diagonally opposite each other and also outputs opposite each other on the other diagonal.

Because of the limited size of substrate available for processing some thought was given to the actual positioning of the components on the substrate.

In order to keep the surface area taken up by the meanderline to a minimum it had to be folded while maintaining a minimum separation between lines, to prevent cross-coupling, and a minimum bending radius, to allow the centre line to be taken as the correct electrical length. It was also necessary to maintain a minimum separation between the transmission lines and adjacent loaded line sections to prevent any possible interaction.

Additional lengths of 50 ohm line used for joining sections together had to be the same length in each part of the Matrix either input or output section, but not necessarily both, although it did simplify the design. For the practical layout, see Fig 13.

Connection to the external circuit was by SMA connectors (type OSM 14107A) between which a minimum distance had to be maintained to facilitate connection and disconnection of external apparatus. These connectors used pressure contact with the microstrip line in the breadboard models.

The printed, dried and fired substrate was mounted on an aluminium block to facilitate connection of the SMA connectors. To ensure adequate grounding between the substrate ground plane and the mounting block the circuit was stuck to the block using DAG, a silver loaded ink. This grounding method produced more consistent results than using other grounding materials. It also had the added advantage of inhibiting movement of the circuit under the pressure contact connectors when it was being handled.

Fig 14 shows the finished breadboard model.

7 THEORETICAL ANALYSIS OF THE DESIGN

Using an in-house microwave analysis program, REDAP38, available on the RAE computer the basic circuits were analysed.

Table 2 shows an example program for the phase shifters on the test circuit the outputs being insertion gain, insertion phase and VSWR which are shown plotted in Fig 15. It must be noted that this program was for ideal lossless transmission lines although some allowance was made for effective permittivity of the substrate for different impedance lines.

Loss in the line could be allowed for, each impedance requiring its own attenuation factor in dB per metre, though this would not affect the insertion phase and would not add a significant amount (only 0.1 dB) to the insertion loss.

The line lengths used were exactly the same as those on the test circuit but no allowance was made for the SMA-microstrip transitions because of their virtually unknown effects.

The coupler test circuit was synthesised similarly and results plotted in Figs 16 and 17.

The final design of the Matrix was tackled in much the same way, the complete program being shown in Table 3. The computed phase shift, insertion loss, isolation and VSWR are shown plotted in Figs 18 to 22 for the actual design.

8 MEASUREMENTS

Using a Hewlett Packard network analyser a full set of RF measurements were made on two test substrates containing the 90° hybrid coupler and the two phase shifters, and also on two samples of the breadboard Butler Matrix. Measurements were made at selected spot frequencies over the range 1.5-1.7 GHz.

8.1 Measurement of test pieces

8.1.1 Phase shift

The apparatus setup was as shown in Fig 23. It was calibrated for zero phase shift through the 1R, 1 ports of the coupler at the centre frequency of 1.5975 GHz and then the phase shift for the other output port was measured relative to this. Next the phase shifts for input 1L to both outputs were measured. All outputs not connected to the test gear were terminated in 50 ohm loads. Fig 24 shows the phase shifts versus frequency for the coupler.

For the phase shifters, the 90° loaded line section was taken as the zero reference for setting up and hence the 135° meander line phase-frequency response is shown relative to this in Fig 25.

8.1.2 Insertion loss

This was measured using the same setup as for phase with the exception that the apparatus was calibrated for zero dB before inserting the circuit under test. In this way all effects monitored during test were due to the actual circuit itself (and connectors), thus the insertion loss of the 90° hybrid coupler was not taken relative to the -3 dB split inherent in the device.

The phase shifters were also measured for insertion loss versus frequency. Figs 24 and 25 show the insertion loss versus frequency for the coupler and phase shifters respectively.

8.1.3 Return loss

Return loss was measured with all output ports correctly terminated in 50 ohm loads and is shown in Figs 26 and 27 for the coupler and phase shifters respectively. Return loss is related to VSWR through the expressions

$$\text{VSWR} = \frac{1 + |\rho|}{1 - |\rho|}$$

where $$|\rho| = \frac{1}{\log^{-1}(0.05 \times \text{return loss})} ,$$

the correspondence of VSWR being shown on the curves.

8.1.4 Isolation

This parameter was measured versus frequency for the 90° hybrid coupler between each input, both outputs terminated in 50 ohm loads. Results are shown in Fig 24.

All these measurements were made prior to the design of the complete Matrix to ensure that the required results were being obtained. Table 4a&b summarises these results for the transmit band centre 1.54675 GHz, centre frequency 1.5975 GHz and receive band centre 1.64825 GHz.

8.2 Butler Matrix measurement and measurement accuracy

8.2.1 *Phase measurement*

The same apparatus setup was used as for the test pieces. The phase shift for each input to all output ports was measured relative to the 1R, 1 ports which were used for calibration of zero phase at the design centre frequency. Shown in Figs 28 to 31 are the phase shifts through the Butler Matrix for each input to all outputs.

Table 5 shows the ideal design values of phase compared with the actual measured values for the complete Matrix; the 45° difference is relative and can be ignored.

Accuracy of phase measurement was difficult to assess since non-repeatability of the transitions microstrip-SMA connector and SMA-coaxial line had significant effect on phase rather than on amplitude.

It was noted that the least discernible bending of the flexible cable produced ±0.8° change in phase and during measurement calibration was checked regularly and was correct within ±2°. Assuming ±3° for non-repeatability of connections the total expected accuracy of the phase measurement was ±5.8°.

8.2.2 Insertion loss

Again the setup was as before but was calibrated with the test circuit omitted from the apparatus. Thus insertion loss was not measured relative to the -6 dB split due to the Matrix couplers.

Figs 32 to 35 show the typical results obtained.

Bearing in mind that connections had to be made and broken a number of times for each set of readings, errors of ±0.5 dB could have occurred. Checking zero at intervals during measurement gave errors of ±0.3 dB and flexing of the cable ±0.1 dB so total accuracy on insertion loss measurements was probably within ±1.0 dB.

8.2.3 Return loss

Fig 36 shows the measured return loss with all output ports of the Matrix 50 ohm loaded. Also shown is some measure of the VSWR.

Here accuracy of measurement was not great for reasons mentioned before which affected the matching, especially the SMA-microstrip transitions which represented unknown and unmeasurable errors. No test through the connectors and leads alone wac made to assess residual VSWR and hence return loss errors, because this would only have taken account of inserting one particular length of line in place of the Butler Matrix.

Results are thought to be accurate to within ±1.5 dB for the lower levels of return loss but may be ±4 dB at the higher levels, (30 dB return loss say).

8.2.4 Isolation

This parameter versus frequency is shown in Figs 37 to 40 for the bread-board Matrix. Apparatus setup was as before and the Matrix was correctly terminated at all non-used ports. Accuracy of measurement was probably within those of section 8.2.3.

9 A PRACTICAL APPLICATION

An application for this Butler Matrix is as a submatrix for a 16 × 16 Matrix which could be part of the feed system of a satellite borne steerable beam phased array of radiators allowing complete earth coverage.

As a first step this 4 × 4 submatrix was packaged and its performance measured with a small planar array of four circular microstrip radiators. The basic layout of the array in block form is shown in Fig 41. The array was designed to operate at 1575 MHz with both left hand and right hand circular

polarisation. The complete array was backed by a square of RAM (radio absorbent material). Measurements of the radiation patterns were made at the Antenna Test Range, Lasham, using a RHC polarised helix antenna as the receiving element with the array excited with RHC polarisation.

First, however, to qualify the array the radiation pattern of a single element disc antenna similar to those used in the array was measured (Fig 42). From this polar diagram it can be seen that no attempt has been made, at this stage, to minimise the ripple around the pattern apart from verifying it is usable. Other polar cuts show the pattern to be roughly a solid of revolution.

Fig 43 shows the basic setup of the Matrix fed array and Fig 44, the range setup for polar radiation pattern measurements.

The radiation patterns are taken with each Matrix input being excited individually, all others being terminated in their characteristic impedances. The rotating pole upon which the array is mounted is then turned through 360°, while the radiation pattern is plotted.

Figs 45 to 48 show these resultant polar diagrams. The dependence of beam steering on which Butler Matrix input was excited can be seen clearly and from Appendix C all beam nulls will be seen to occur at certain common angles with the main beam peaks occurring near to one or other of these same common angles.

In Appendix C the polar diagram for an array fed by a Butler Matrix is calculated and a comparison is made between some ideal basic parameters to be obtained from such a beam forming technique and the corresponding measured values.

Reasonable precautions were taken over the array dimensioning and angular measurements on the Lasham Range, and the beam aiming discrepancies of the results have been largely accounted for in theory.

10 DISCUSSION AND CONCLUSIONS

The most noticeable differences between the computed and measured responses of the test pieces and Matrix breadboard models were the different phase slopes of the plots. One reason not already mentioned was that the REDAP Analysis Program only synthesised the actual circuit on the substrate; no allowance was made for either the extra length of coaxial line used on the input to facilitate measurement or the microstrip-SMA transition or indeed the SMA connectors themselves which would alter the phase frequency slope of the circuit and in some respects the other measurable parameters.

The network analyser could itself be set up with an initial phase frequency slope, this not invalidating any of the phase results obtained since they were all of a relative nature.

Omission of the attenuation factor in the REDAP program would not affect the phase responses and would only slightly increase values of insertion loss and isolation (only -0.1 dB).

The phase shifters had a measured insertion loss of <0.25 dB and a VSWR <1.3 : 1 (compared to a computed value of <1.2:1) over the 1.535-1.66 GHz band of interest.

Computer analysis of a component would ideally only produce an accurate prediction of a device's performance if access was available to a complete data set relating to that component and its precise mode of operation. Since the REDAP macro itself was not equipped for dealing with them in any way, the junction effects entered in the program were dealt with as an increase in line length, hence the computed isolation and return loss for the coupler (Figs 16 and 17) peaked at a frequency lower than the design centre frequency.

The -3 dB power split of the coupler was not quite achieved but was within the tolerance level of -3 ± 0.25 dB over the band of interest. Computed VSWRs were <1.25:1 over the band and were measured at <1.22:1. A good VSWR was to be expected in this coupler because the power reflected goes to the isolated port and is absorbed.

For the breadboard Matrix, discrepancies occurred between the responses of some input and output port combinations that should ideally have been identical, however these were within expected tolerance levels. Most significant was the insertion loss for the 2L, 3 and 2R, 2 ports at the low frequency end (Figs 33 and 34). These results were re-checked a month later and found to be within 0.2 dB of the original measurement.

Table 6 summarises errors in phase shift (measured and computed) relative to the ideal values (shown in Fig 11b) for the various input and output port combinations. Small transmission-line discontinuities which could give rise to significant reflections and transmission losses usually presented a very small phase shift to the circuit.

Isolation was more critically dependent on across-the-substrate permittivity tolerances, through the coupler changes and bad transitions. Measured isolation on all inputs was better than -16 dB, this being the worst case at the lower band-edge. The computed value being -20 dB.

Insertion loss was <1.2 dB for all the input-output port combinations measured, in most cases being <0.8 dB. The computed value was <0.25 for the ideal circuit.

The shape and magnitude of the return loss curves could have been affected by the input and output connectors and the connections themselves. VSWRs for all inputs were <1.5:1 over the band of interest (this being the worst case value) compared with a computed value of <1.25:1 for the ideal Matrix.

The VSWR given in the design specification (section 3.4) may have been a little optimistic for thickfilm microstrip, the transitions and the cables used in the measurements.

As an exercise in basic design principles the Butler Matrix described largely met its specification (albeit a general rather than a specific requirement).

Improvements could possibly be achieved by accurate prediction of the junction effects between differing impedance lines but there is a shortage of accurate data available on general microstrip discontinuities and connector-microstrip transitions.

A more realistic computer prediction would have been obtained if attenuation factors for the various lines had been used in the program (typically 2.5-3.5 dB per metre for 33 ohm and 50 ohm microstrip lines respectively, using Plessey C5700 gold conductor paste).

Section 3 gave an example of how complicated Butler Matrix design could become for greater than order 4, especially from the layout point of view. Larger Matrices must, of necessity, be made up of an assembly of 2 × 2 or 4 × 4 submatrices with transmission line crossovers made externally.

A second difficulty in larger Matrix design is the large numbers of measurements to be made during final electrical testing. As an example[10], for a 16 × 16 Matrix the following measurements are necessary per frequency: 16 measurements of VSWR, 240 of input to input isolation and 256 each of input to output insertion loss and phase shift, making a grand total of 768 measurements per frequency, each taking approximately one minute.

With the Matrix used as a feed to a breadboard four element planar array the parameters obtained from the polar radiation patterns measured at Lasham on the Antenna Test Range appear to be in good agreement with the ideal parameters of Appendix C.

The array had not been optimised in any way but the ripples around the polar diagram of the single disc element were considered acceptable, however this hampered the fitting of a theoretical curve to the measured patterns when trying to predict beam aiming.

The nulls and crossovers and to a lesser extent the peaks of the beams occur at the anticipated positions and the dead ahead crossover levels are in good agreement with the ideal.

Appendix C shows that an asymmetric lobe is to be expected whose maximum will differ slightly in angle from the in-phase angle (which would give a maximum for isotropic sources). Hence, the angles between -3 dB or -10 dB points cannot be bisected to determine the angle of the lobe maximum.

However it must be noted that the null angle due to phasing is independent of the element patterns and should therefore provide a check on the accuracy of the element spacing and the phasing of the Butler Matrix. Alternatively a check can be made by curve fitting to the measured element pattern and substituting this expression for cos θ in the array pattern of Appendix C.

Acknowledgments

The author would like to thank the Space Department Drawing Office for preparing the artwork, Mr A.G. Millet and Miss D. Carver for fabrication of the circuits, Mr M. Sidford (R & N) for permission to use the radiation patterns of the planar array fed by the breadboard Matrix and Mr R.W. Hogg for many stimulating discussions.

Appendix A

BLOCK DIAGRAM OF A 32 × 32 BUTLER MATRIX

The following procedure is an example of input and output port numbering and calculation of phase shifter values for a 32 × 32 Matrix. The Matrix consists of 5 rows each of 16 couplers and 4 rows each of 32 phase shifters.

A.1 Input port numbering

$k_5 = 5$, $N_5 = 32$.

Half series for $k_5 - 1$ from section 3.1 (iv):

1 8 5 4 3 6 7 2

$+ 2^{k_5-2}$ viz 8:

9 16 13 12 11 14 15 10

reverse as pairs:

16 9 12 13 14 11 10 15

interleave with original half series in pairs after first term:

1 16 9 8 5 12 13 4 3 14 11 6 7 10 15 2

mirror and affix R, L for complete set:

1R 16L 9R 8L 5R 12L 13R 4L 3R 14L 11R 6L 7R 10L 15R

2L 2R 15L 10R 7L 6R 11L 14R 3L 4R 13L 12R 5L 8R 9L

16R 1L.

A.1.1 Output port numbering

Because of the chosen layout the first 32 numbers of the normal number sequence are used.

A.1.2 Phase shifter values

There are four rows of shifters whose values are multiples of $-\pi/32$.

A1.2.1 First row: take half the sequence for $k_5 - 1$ (*ie* as derived for the first row of $k_4 = 4$ in section 3.3 (iv)) and repeat

7 0 0 1 3 0 0 5 7 0 0 1 3 0 0 5 .

Alternately add and subtract 1, ignoring zeros to the half way point, then mirror.

8 0 0 0 4 0 0 4 4 0 0 4 0 0 0 8 .

Add to the original sequence and mirror.

15 0 0 1 7 0 0 9 11 0 0 5 3 0 0 13 13 0 0 3 5 0

0 11 9 0 0 7 1 0 0 15 .

A.1.2.2 For the second row take, as in A1.2.1, half the sequence for $k_5 - 1$

7 0 0 1 3 0 0 5 .

Repeat each number twice, multiplying by 2 then mirror

14 14 0 0 0 0 2 2 6 6 0 0 0 0 10 10 10 10 0 0 0

0 6 6 2 2 0 0 0 0 14 14 .

A.1.2.3 For the third row take half the sequence for the $k_5 - 2$ case (*ie* as derived from section 3.3 (iii))

3 0 0 1 .

Repeat each number four times multiplying by 4 and mirror

12 12 12 12 0 0 0 0 0 0 0 0 4 4 4 4 4 4 4 4 0 0

0 0 0 0 0 0 12 12 12 12 .

A.1.2.4 For the fourth row take half the sequence for the $k_5 - 3$ case (*ie* as derived in section 3.3 (ii))

1 0 .

Repeat each number eight times, multiplying by 8 and mirror

8 8 8 8 8 8 8 8 0 0 0 0 0 0 0 0 0 0 0 0 0 0

0 0 8 8 8 8 8 8 8 8 .

Appendix B

THEORY OF LOADED LINE PHASE SHIFTERS

The A matrices* of the lossless network of Fig 10 are

$$\begin{vmatrix} E_1 \\ I_1 \end{vmatrix} = \begin{vmatrix} 1 & 0 \\ jBY_1 & 1 \end{vmatrix} \begin{vmatrix} 1 & \frac{j \tan \theta_2}{Y_2} \\ jY_2 \tan \theta_2 & 1 \end{vmatrix} \begin{vmatrix} 1 & 0 \\ jBY_1 & 1 \end{vmatrix} \begin{vmatrix} E_2 \\ I_2 \end{vmatrix}$$

$$= \begin{vmatrix} 1 - \tan \theta_2 B \frac{Y_1}{Y_2} & \frac{j \tan \theta_2}{Y_2} \\ 2jBY_1 + jY_2 \tan \theta_2 - jB^2 \frac{Y_1^2}{Y_2} \tan \theta_2 & 1 - B \frac{Y_1}{Y_2} \tan \theta_2 \end{vmatrix} \begin{vmatrix} E_2 \\ I_2 \end{vmatrix} .$$

Now the short-circuit and open-circuit admittances of the network are given by

$$Y_{sc} = A_{22}/A_{12} \tag{B-1}$$

$$Y_{oc} = A_{21}/A_{11} . \tag{B-2}$$

Hence

$$Y_{sc} = \frac{Y_2 - BY_1 \tan \theta_2}{j \tan \theta_2} \tag{B-3}$$

$$Y_{oc} = \frac{2jBY_1Y_2 + jY_2^2 \tan \theta_2 - jB^2Y_1^2 \tan \theta_2}{Y_2 - BY_1 \tan \theta_2} . \tag{B-4}$$

The characteristic admittance is then

$$Y_0 = \sqrt{Y_{oc}Y_{sc}}$$

$$= \frac{(2BY_1Y_2 + Y_2^2 \tan \theta_2 - B^2Y_1^2 \tan \theta_2)(Y_2 - BY_1 \tan \theta_2)}{(Y_2 - BY_1 \tan \theta_2)(\tan \theta_2)} . \tag{B-5}$$

---

* different from Butler Matrix

Normalising to Y_0, and letting Y_1, Y_2 be the characteristic admittances of Y_1, Y_2 normalised to Y_0 and $B_{norm} = \tan\theta_1 = 1$ for $\lambda/8$ stubs, (B-5) becomes

$$1 = \frac{2Y_1Y_2 + Y_2^2 \tan\theta_2 - Y_1^2 \tan\theta_2}{\tan\theta_2} .$$

But $\tan\theta_2 = \infty$ for $\lambda/4$ line

$$\therefore 1 = Y_2^2 - Y_1^2 . \qquad \text{(B-6)}$$

Also

$$j \tan\beta = \sqrt{\frac{Y_{oc}}{Y_{sc}}} \qquad \text{(from section 5.3)}$$

$$= j \frac{\sqrt{\left(2BY_1Y_2 + Y_2^2 \tan\theta_2 - B^2Y_1^2 \tan\theta_2\right)\tan\theta_2}}{\sqrt{(Y_2 - BY_1 \tan\theta_2)^2}} .$$

Normalising to Y_0 and letting $\tan\theta_2 = \infty$

$$j \tan\beta = j\sqrt{\frac{Y_2^2 - Y_1^2}{Y_1^2}}$$

$$\therefore \tan\beta = \pm\frac{1}{Y_1}$$

$$\therefore \beta = \tan^{-1}\left[\pm\frac{1}{Y_1}\right] \qquad \text{(B-8)}$$

Now from (B-7) and putting $B = \tan\theta_1$ for open circuited stubs where $2\theta_1 = \theta_2$

$$\tan\beta = \frac{\sqrt{2Y_1Y_2\tan\theta_1\tan\theta_2 + Y_2^2\tan^2\theta_2 - \tan^2\theta_1 Y_1^2\tan^2\theta_2}}{(Y_2 - Y_1\tan\theta_1\tan\theta_2)}$$

and putting $t = \tan\theta_1$, $\frac{2t}{1-t^2} = \tan 2\theta_1 = \tan\theta_2$

$$\tan\beta = \frac{\sqrt{\frac{2Y_1Y_2 2t^2}{1-t^2} + \frac{Y_2^2 4t^2}{(1-t^2)^2} - \frac{t^2Y_1^2 4t^2}{(1-t^2)^2}}}{Y_2 - \frac{Y_1 2t^2}{1-t^2}}$$

$$\therefore \beta = \tan^{-1}\left[2\frac{\sqrt{t^2(1-t^2)Y_1Y_2 + t^2Y_2^2 - t^4Y_1^2}}{Y_2(1-t^2) - 2Y_1t^2}\right]$$

$$= \tan^{-1}(x) . \qquad \text{(B-9)}$$

Now

$$\frac{d\beta}{df} = \frac{d\beta}{dx}\cdot\frac{dx}{dt}\cdot\frac{dt}{d\theta_1}\cdot\frac{d\theta_1}{df} . \qquad \text{(B-10)}$$

For midband $t = 1$ and normalising

$$\left.\frac{d\beta}{dx}\right|_{t=1} = \frac{1}{1+x^2} = \frac{1}{1 + \frac{Y_2^2 - Y_1^2}{Y_1^2}}$$

$$\therefore \frac{d\beta}{dx} = \frac{Y_1^2}{Y_2^2} \qquad \text{(B-11)}$$

$$\frac{dx}{dt} = \left[\frac{\left(Y_2(1 - t^2) - 2Y_1t^2\right)\left(Y_1Y_2(2t - 4t^3) + 2tY_2^2 - 4t^3Y_1^2\right)}{\sqrt{t^2(1 - t^2)Y_1Y_2 + t^2Y_2^2 - t^4Y_1^2}\left(Y_2(1 - t^2) - 2Y_1t^2\right)^2} \right.$$

$$\left. - \frac{2\sqrt{t^2(1 - t^2)Y_1Y_2 + t^2Y_2^2 - t^4Y_1^2}(-2tY_2 - 4tY_1)}{\left(Y_2(1 - t^2) - 2Y_1t^2\right)^2} \right] .$$

At midband and normalising

$$\left.\frac{dx}{dt}\right|_{t=1} = \left[\frac{-2Y_1(-2Y_1Y_2 + 2Y_2^2 - 4Y_1^2)}{\sqrt{Y_2^2 - Y_1^2}\,(-2Y_1)^2} + \frac{2\sqrt{Y_2^2 - Y_1^2}(2Y_2 + 4Y_1)}{4Y_1^2} \right]$$

$$= \frac{-4Y_1Y_2^2 + 4Y_2^3 + 8Y_1Y_2^2}{4Y_1^2\sqrt{Y_2^2 - Y_1^2}}$$

$$= \frac{Y_1Y_2^2 + Y_2^3}{Y_1^2\sqrt{Y_2^2 - Y_1^2}}$$

$$\therefore \left.\frac{dx}{dt}\right|_{t=1} = \frac{Y_2^2}{Y_1^2}\,\frac{Y_1 + Y_2}{\sqrt{Y_2^2 - Y_1^2}} . \qquad \text{(B-12)}$$

$$\frac{dt}{d\theta_1} = 1 + \tan^2\theta_1$$

$$\therefore \left.\frac{dt}{d\theta_1}\right|_{t=1} = 2 \qquad \text{at midband and normalising .} \qquad \text{(B-13)}$$

Assuming air is the dielectric for simplicity, for the stub

$$\theta_1 = \frac{2\pi\ell_1}{\lambda} = \frac{2\pi\ell_1 f}{c}$$

$$\therefore \frac{d\theta_1}{df} = \frac{2\pi\ell_1}{c} \qquad \text{(B-14)}$$

where c is velocity of light *in vacuo*.

Hence, from equations (B-10), (B-11), (B-12), (B-13) and (B-14)

$$\frac{d\beta}{df} = \frac{Y_1^2}{Y_2^2} \cdot \frac{Y_2^2}{Y_1^2} \cdot \frac{Y_1 + Y_2}{\sqrt{Y_2^2 - Y_1^2}} \cdot 2 \cdot \frac{2\pi\ell_1}{c}$$

$$= \frac{4\pi\ell_1}{c} (Y_1 + Y_2) \quad . \qquad \text{(B-15)}$$

Now ℓ_1 for the stub = $\lambda_c/8$ where λ_c is the centre frequency wavelength

$$\therefore \frac{d\beta}{df} = \frac{\pi\lambda_c}{2c} (Y_1 + Y_2) = \frac{\pi}{2f_c} (Y_1 + Y_2) \text{ radians/Hz} . \qquad \text{(B-16)}$$

The corresponding rate of change of phase for a piece of uniform transmission line is

$$\frac{d\theta}{df} = \frac{2\pi\ell}{c} \quad . \qquad \text{(B-17)}$$

For equal rates

$$\frac{2\pi\ell}{c} = \frac{\pi\lambda c}{2c} (Y_1 + Y_2)$$

$$\therefore \ell = \frac{\lambda c}{4} (Y_1 + Y_2) \qquad \text{(B-18)}$$

ie the electrical length of uniform line is

$$\phi_s = \frac{\pi}{2} (Y_1 + Y_2). \qquad \text{(B-19)}$$

Hence for the design of a set of phase shifters we choose Y_1 to give us the required phase shift in accordance with

$$\beta = \tan^{-1}\left(\frac{1}{Y_1}\right)$$

while

$$Y_2^2 - Y_1^2 = 1$$

and $Y_2 + Y_1$ is also fixed at the required phase-frequency slope $\frac{d\beta}{df}$.

Appendix C

POLAR DIAGRAMS OF AN ARRAY FED BY A BUTLER MATRIX

C.1 Suppose an array of 2n omni-radiators spaced 'd' apart is fed by a Butler Matrix with equal amplitude E and progressive phase shifts with respect to some datum at the array centre as shown in Fig 49.

The RF signal reaching a distant receiver in the direction θ will be proportional to:

$$E\left[\sin\left(\omega t + \frac{\phi_1}{2} - \frac{\pi d}{\lambda}\sin\theta\right) + \sin\left(\omega t - \frac{\phi_1}{2} + \frac{\pi d}{\lambda}\sin\theta\right) + \ldots \right.$$

$$\left. + \sin\left(\omega t + \phi_n - \frac{(2n-1)}{\lambda}\pi d \sin\theta\right) \right.$$

$$\left. + \sin\left(\omega t - \phi_n + \frac{(2n-1)}{\lambda}\pi d \sin\theta\right)\right]$$

$$= 2E \sin\omega t\left[\cos\left(\frac{\phi_1}{2} - \frac{\pi d}{\lambda}\sin\theta\right) + \cos\left(\phi_2 - \frac{3\pi d}{\lambda}\sin\theta\right) + \ldots \right.$$

$$\left. + \cos\left(\phi_n - \frac{(2n-1)}{\lambda}\pi d \sin\theta\right)\right]$$

If the Butler Matrix makes $\phi_1, \phi_2, \ldots, \phi_n$ such that the radiation adds in phase at $\theta = \theta_p$ then

$$\frac{\phi_1}{2} = \frac{\pi d}{\lambda}\sin\theta_p\,, \quad \phi_2 = \frac{3\pi d}{\lambda}\sin\theta_p\,, \quad \ldots\,, \quad \phi_n = \frac{(2n-1)}{\lambda}\pi d \sin\theta_p\,,$$

making each cos term unity and giving

$$\phi_2 = \frac{3\phi_1}{2}\,, \quad \ldots\,, \quad \phi_n = \frac{(2n-1)}{2}\phi_1\,.$$

Hence dropping the RF term $\sin(\omega t)$, the distant field is given by:

$$2E\left[\cos\left(\frac{\phi_1}{2} - \frac{\pi d}{\lambda}\sin\theta\right) + \cos 3\left(\frac{\phi_1}{2} - \frac{\pi d}{\lambda}\sin\theta\right) + \ldots + \cos(2n-1)\left(\frac{\phi_1}{2} - \frac{\pi d}{\lambda}\sin\theta\right)\right].$$

This summation is easily made and becomes

$$\frac{2E\left[\sin 2n\left(\frac{\phi_1}{2} - \frac{\pi d}{\lambda}\sin\theta\right)\right]}{2\sin\left(\frac{\phi_1}{2} - \frac{\pi d}{\lambda}\sin\theta\right)}$$

therefore for a uniform array of 2n radiators the polar diagram is given by

$$\frac{E\sin 2n\left(\frac{\phi_1}{2} - \frac{\pi d}{\lambda}\sin\theta\right)}{\sin\left(\frac{\phi_1}{2} - \frac{\pi d}{\lambda}\sin\theta\right)} \quad . \qquad \text{(C-1)}$$

If $\left(\frac{\phi_1}{2} - \frac{\pi d}{\lambda}\sin\theta\right)$ is small (*ie* if d is small and ϕ_1 correspondingly small, which culminates in a distributed source array) then

$$\sin\left(\frac{\phi_1}{2} - \frac{\pi d}{\lambda}\sin\theta\right) \simeq \left(\frac{\phi_1}{2} - \frac{\pi d}{\lambda}\sin\theta\right)$$

and (C-1) becomes

$$\frac{E\sin 2n\left(\frac{\phi_1}{2} - \frac{\pi d}{\lambda}\sin\theta\right)}{\left(\frac{\phi_1}{2} - \frac{\pi d}{\lambda}\sin\theta\right)} \quad .$$

If we now put $E = \frac{E_0}{N}$ where N is the total number of sources, $N = 2n$, the polar diagram is given by:

$$\frac{E_0\sin N\left(\frac{\phi_1}{2} - \frac{\pi d}{\lambda}\sin\theta\right)}{N\left(\frac{\phi_1}{2} - \frac{\pi d}{\lambda}\sin\theta\right)} \qquad \text{(C-2)}$$

which is of the form $\frac{\sin x}{x}$.

In this case however it is more accurate to apply (C-1) as there are $2n = 4$ elements and $d = \lambda/2$. The elements are not isotropic radiators and this must also be allowed for, *eg* if each element were a dipole having a cosine pattern maximising at θ_M , Fig 50, we must replace E by $E_d \cos(\theta_M + \theta)$ in (C-1) and the array pattern shape is then

$$E_d \cos(\theta_M + \theta) \frac{\sin 4\left(\frac{\theta_1}{2} - \frac{\pi}{2}\sin\theta\right)}{\sin\left(\frac{\theta_1}{2} - \frac{\pi}{2}\sin\theta\right)} \qquad \text{(C-3)}$$

element pattern | array pattern

C.2 Results

C.2.1 Beam peak positions assuming isotropic radiating elements occur at values where

$$\sin\theta = \frac{\lambda}{\pi d}\frac{\phi_1}{2}$$

but for the Kth beam

$$\phi_K = \frac{2K-1}{2}\phi_1$$

and

$$\phi_1 = \pm\frac{\pi}{2n} = \pm\frac{\pi}{4}$$

hence

$$\sin\theta = \frac{\lambda}{\pi}\frac{2}{\lambda}\frac{\pi}{4}\frac{1}{2}(2K-1) .$$

For $K = 1$ $\quad \theta = \pm 14.5^\circ$

$K = 2$ $\quad \theta = \pm 48.6^\circ$.

Now, consider the case where $\theta_M = 0$ and $\theta = \theta_P = 48.6^\circ$ corresponding to 135° phase difference between Butler Matrix outputs (where all radiating elements add in phase) giving $\phi_1 = 2.356$ radians.

A plot of $\frac{\sin 4\left(1.178 - \frac{\pi}{2}\sin\theta\right)}{\sin\left(1.178 - \frac{\pi}{2}\sin\theta\right)}\cos\theta$ in dB versus θ° is shown in Fig 51

and an expanded version in Fig 52. This shows the asymmetrical main lobe and three side lobes. The main lobe peak is 7.4° off the in-phase angle (which would give a maximum for isotropic sources).

Similarly if $\theta = \theta_p = 14.5°$, corresponding to 45° phase difference between Butler Matrix outputs, is substituted in the above expression the main lobe in this case peaks at 13.3° which is 1.2° off the in-phase angle (Fig 51).

Comparing with the measured polar plots of Figs 45 to 48 the positions of the main beam peaks are:

Beam number	Measured peak angle	In-phase angle	cos θ element pattern
2R	45°	48.6°	41.2°
1R	15.5°	14.5°	13.3°
1L	-13°	-14.5°	-13.3°
2L	-42°	-48.6°	-41.2°

The differences are due to the element pattern. The array peak angle depends upon the shape of the element pattern, in particular, the slope in the vicinity of the peak of the element pattern. When asymmetry of this element pattern is present the problem is more difficult. In the present case, for simplification, the element pattern was taken as being cosine shape by matching slopes around the known location of the experimental maximum. It was difficult to locate the maximum due to ripples present in the pattern.

The beam nulls resulting from the array pattern (as opposed to the element pattern) occur at angles which are unaffected by the element pattern shape (Fig 51).

C.2.2 The position and levels of beam cross-overs for isotropic radiators.

If θ_c is the angular position of the cross-over of the Kth and K + 1th beams then, equating the amplitudes of these beams

$$\sin \theta_c = \frac{\lambda}{\pi d} (K\phi_1)$$

$$= \frac{\lambda}{\pi} \frac{2}{\lambda} \frac{\pi}{4} \frac{K}{2} .$$

Hence $\theta_c = \pm 30°$, the cross-over of the first and second beams. The 1L, 1R beam cross-over occurs at 0°.

The cross-over level is given by

$$|E|_c = \frac{1}{4} \frac{1}{\sin\left(\frac{\pi}{8}\right)} = 0.65$$

which is approximately -3.7 dB below the peak value, all beams being normalised. In the dead ahead position the measured element pattern was approximately constant over the angle of interest and may therefore be assumed isotropic. In the other cases (given below) the comparison with the above theory is less valid due to the assumption that the element pattern is $\cos\theta$.

Lobes	Measured	In-phase cross-over angle	$\cos\theta$ element pattern
2R + 1R	$+29^o$	$+30^o$	27.5^o
1R + 1L	$+2^o$	0^o	0^o
1L + 2L	-26^o	-30^o	-27.5^o

Lobes	Measured	In-phase cross-over level (below peak)	$\cos\theta$ element pattern
2R + 1R	-3.25 dB	-3.7 dB	-3.25 dB
1R + 1L	-4.4 dB	-3.7 dB	-3.25 dB
1L + 2L	-3.3 dB	-3.7 dB	-3.25 dB

Table 1

OUTPUT FROM PHASE SHIFTER

DESIGN PROGRAM

DESIGN OF SET OF 2 LOADED LINE PHASE SHIFTERS

PHASE SHIFT DEGREES	LOADED LINE STUBS	ADMITTANCES LINE	LINE LENGTH LAMBDAS
0.000	1.0609	1.4579	0.0000
90.000	0.0000	1.0000	0.6297

DESIGN OF SET OF 4 LOADED LINE PHASE SHIFTERS

PHASE SHIFT DEGREES	LOADED LINE STUBS	ADMITTANCES LINE	LINE LENGTH LAMBDAS
0.000	1.3904	1.7127	0.0000
45.000	1.0609	1.4579	0.1461
90.000	0.6719	1.2048	0.3066
135.000	0.0000	1.0000	0.7758

DESIGN OF SET OF 8 LOADED LINE PHASE SHIFTERS

PHASE SHIFT DEGREES	LOADED LINE STUBS	ADMITTANCES LINE	LINE LENGTH LAMBDAS
0.000	1.5443	1.8398	0.0000
22.500	1.3904	1.7127	0.0703
45.000	1.2301	1.5853	0.1422
67.500	1.0609	1.4579	0.2163
90.000	0.8780	1.3307	0.2938
112.500	0.6719	1.2048	0.3769
135.000	0.4182	1.0839	0.4705
157.500	0.0000	1.0000	0.8460

Table 2

COMPUTER REALISATION OF TEST CIRCUITS

```
BMTEST01

LABEL<COUPLER TEST>;
LABEL<MRC SUBSTRATES>;
LABEL<WITH END EFFECTS.>;
LABEL<FOR DESIGN 4X4 BUTLER/02.>;
LABEL<DESIGNED 6/4/77.>;
LINE1 16.457E-3 Z50.0 VR.389 ATT0. I/P1 O/P2 COMMON0;
LINE2 16.457E-3 AS LINE1 I/P7 O/P8 COMMON0;
LINE3 16.458E-3 AS LINE1 I/P3 O/P4 COMMON0;
LINE4 16.458E-3 AS LINE1 I/P5 O/P6 COMMON0;
LINE5 18.723E-3 AS LINE1 I/P2 O/P7 COMMON0;
LINE6 18.723E-3 AS LINE1 I/P6 O/P3 COMMON0;
LINE7 17.885E-3 Z35.355 VR.379 ATT0. I/P2 O/P3 COMMON0;
LINE8 17.885E-3 AS LINE7 I/P7 O/P6 COMMON0;
SOURCE 50 0;
LOAD 50 0;
OUTPUT(PR4,IP,VSWRI);
STEP LIN 1.5E9 1.7E9 0.005E9;

↑**********************************************************************

BMTEST02

LABEL<90 DEGREE PHASER.>;
LABEL<MRC SUBRATES.>;
LABEL<WITH END EFFECTS.>;
LABEL<TEST CIRCUIT,DESIGNED 6/4/77.>;
LINE1 10.734E-3 Z50.0 VR.389 ATT0. I/P1 O/P2 COMMON0;
LINE2 22.0E-3 AS LINE1 I/P4 O/P6 COMMON0;
LINE3 18.066E-3 Z41.501 VR.384 ATT0. I/P2 O/P4 COMMON0;
LINE4 9.423E-3 Z74.416 VR.403 ATT0. I/P2 O/P3 COMMON0;
LINE5 9.423E-3 AS LINE4 I/P4 O/P5 COMMON0;
SOURCE 50 0;
LOAD 50 0;
OUTPUT(PR4,IP,VSWRI);
STEP LIN 1.5E9 1.7E9 0.005E9;

↑**********************************************************************

BMTEST03

LABEL<135 DEGREE PHASER.>;
LABEL<MRC SUBRATES.>;
LABEL<WITH END EFFECTS.>;
LABEL<TEST CIRCUIT,DESIGNED 6/4/77.>;
LINE1 67.043E-3 Z50.0 VR.389 ATT0. I/P1 O/P2 COMMON0;
SOURCE 50 0;
LOAD 50 0;
OUTPUT(PR4,IP,VSWRI);
STEP LIN 1.5E9 1.7E9 0.005E9;

↑**********************************************************************
```

Table 3

COMPUTER REALISATION OF COMPLETE BUTLER MATRIX

```
MBUTW(7)

LABEL<BUTLER MATRIX.>;
LABEL<WITH END EFFECTS.>;
LABEL<LINE3 AND LINE7 CHANGED TO SEE EFFECT,BOTH CHANGED TO THE SAME
LABEL<DESN.5/4/77,FOR MRC SUBSTRATES.>;                          LENGTH.>;
LABEL<EQUIVALENCE OF PORTS.>;
LABEL<INPUTS 1,32,17,16=1L,2R,1R,2L.>;
LABEL<OUTPUTS 10,11,27,26=A,C,B,D.>;
LINE1 13.087E-3 Z50.000 VR.389 ATT0. I/P1 O/P2 COMMON0;
LINE2 17.885E-3 Z35.355 VR.379 ATT0. I/P2 O/P3 COMMON0;
LINE3 11.228E-3 AS LINE1 I/P30 O/P4 COMMON0;
LINE4 18.066E-3 Z41.501 VR.384 ATT0. I/P4 O/P6 COMMON0;
LINE5 9.423E-3 Z74.416 VR.403 ATT0. I/P4 O/P5 COMMON0;
LINE6 9.423E-3 AS LINE5 I/P6 O/P7 COMMON0;
LINE7 11.228E-3 AS LINE1 I/P6 O/P29 COMMON0;
LINE8 17.885E-3 AS LINE2 I/P8 O/P9 COMMON0;
LINE9 13.087E-3 AS LINE1 I/P9 O/P10 COMMON0;
LINE10 18.723E-3 AS LINE1 I/P9 O/P12 COMMON0;
LINE11 18.723E-3 AS LINE1 I/P8 O/P13 COMMON0;
LINE12 13.087E-3 AS LINE1 I/P11 O/P12 COMMON0;
LINE13 17.885E-3 AS LINE2 I/P12 O/P13 COMMON0;
LINE14 56.765E-3 AS LINE1 I/P24 O/P19 COMMON0;
LINE15 17.885E-3 AS LINE2 I/P14 O/P15 COMMON0;
LINE16 13.087E-3 AS LINE1 I/P15 O/P16 COMMON0;
LINE17 13.087E-3 AS LINE1 I/P17 O/P18 COMMON0;
LINE18 18.723E-3 AS LINE1 I/P18 O/P15 COMMON0;
LINE19 18.723E-3 AS LINE1 I/P19 O/P14 COMMON0;
LINE20 17.885E-3 AS LINE2 I/P18 O/P19 COMMON0;
LINE21 11.456E-3 AS LINE1 I/P14 O/P20 COMMON0;
LINE22 9.423E-3 AS LINE5 I/P20 O/P21 COMMON0;
LINE23 18.066E-3 AS LINE4 I/P20 O/P22 COMMON0;
LINE24 9.423E-3 AS LINE5 I/P22 O/P23 COMMON0;
LINE25 11.000E-3 AS LINE1 I/P22 O/P13 COMMON0;
LINE26 18.723E-3 AS LINE1 I/P24 O/P29 COMMON0;
LINE27 17.885E-3 AS LINE2 I/P24 O/P25 COMMON0;
LINE28 13.087E-3 AS LINE1 I/P25 O/P26 COMMON0;
LINE29 18.723E-3 AS LINE1 I/P25 O/P28 COMMON0;
LINE30 13.087E-3 AS LINE1 I/P28 O/P27 COMMON0;
LINE31 17.885E-3 AS LINE2 I/P28 O/P29 COMMON0;
LINE32 56.765E-3 AS LINE1 I/P3 O/P8 COMMON0;
LINE33 17.885E-3 AS LINE2 I/P30 O/P31 COMMON0;
LINE34 18.723E-3 AS LINE1 I/P30 O/P3 COMMON0;
LINE35 18.723E-3 AS LINE1 I/P31 O/P2 COMMON0;
LINE36 13.087E-3 AS LINE1 I/P31 O/P32 COMMON0;
SOURCE 50 0;
LOAD 50 0;
OUTPUT(PR4,IP,VSWR1);
STEP LIN 1.5E9 1.7E9 0.005E9;

↑*************************************************************************
```

Table 4a

COMPUTED COUPLER AND PHASE SHIFTER RESULTS AT TRANSMIT, RECEIVE AND DESIGN FREQUENCIES

	T_x	F_c	R_x	
1R, 1	-11.0	+0.5	+12.5	Coupler phase shift (degrees)
1R, 2	-101.5	-89.5	-77.5	
$\Delta\phi$ Phase difference	-90.5	-90.0	-90.0	
1R, 1	-3.17	-3.03	-3.01	Coupler insertion loss (dB)
1R, 2	-2.975	-3.00	-3.01	
1R, 1L	20.75	30.75	30.25	Coupler isolation (dB)
Meanderline	-10.25	+0.25	-34.0	Phase shifter phase (degrees)
90° loaded line	-55.0	-44.75	+11.0	
$\Delta\phi$ Phase difference	-44.75	-45.0	-45.0	
Meanderline	0	0	0	Phase shifter insertion loss (dB)
90° loaded line	0.0012	0	0.0085	

Table 4b

MEASURED COUPLER AND PHASE SHIFTER RESULTS AT TRANSMIT, RECEIVE AND DESIGN FREQUENCIES

	T_x	F_c	R_x	
1R, 1	-39.0	-0.5	+39.5	Coupler phase shift (degrees)
1R, 2	-130.75	-91.0	-52.0	
$\Delta\phi$ Phase difference	-91.75	-90.5	-91.5	
1R, 1	-3.2	-3.15	-3.25	Coupler insertion loss (dB)
1R, 2	-3.25	-3.31	-3.45	
1R, 1L	-24.0	-37.75	-25.5	Coupler isolation (dB)
Meanderline	-3.0	-45.0	-87.0	Phase shifter phase (degrees)
90^o loaded line	+42.5	0	-42.25	
$\Delta\phi$ Phase difference	-45.5	-45.0	-44.75	
90^o loaded line	0.15	0.10	0.175	Phase shifter insertion loss (dB)

Table 5

IDEAL PHASE VALUES FOR BUTLER MATRIX (FROM FIG 11b)
COMPARED WITH MEASURED VALUES AT CENTRE FREQUENCY

input port number	output port number 1	2	3	4
1R	-45	-90	-135	-180
2L	-135	-0	-225	-90
2R	-90	-225	0	-135
1L	-180	-135	-90	-45

IDEAL

input port number	output port number 1	2	3	4
1R	0	-49	-90	-139
2L	-91	-320	-180	-51
2R	-47	-178	-316	-87
1L	-138	-88	-45	-3.5

MEASURED

Table 6

ERRORS IN PHASE SHIFT (IN DEGREES), MEASURED AND THEORY TO IDEAL AT TRANSMIT, RECEIVE AND DESIGN FREQUENCIES

	1	2	3	4
1R	0	-6.0	-1.0	-5.5
2L	-0.5	-5.5	0	-6.5
2R	-2.5	+2.0	-1.5	+2.5
1L	-5.5	+1.5	-1.0	-3.5

MEASURED

	1	2	3	4
1R	0	-0.1	-0.43	-0.12
2L	-0.43	-0.1	+0.5	-0.1
2R	-0.1	+0.5	-0.1	-0.43
1L	-0.12	-0.43	-0.1	0

THEORY

T_x 1.54675 GHz

	1	2	3	4
1R	0	-4.0	0	-4.0
2L	-1.0	-5.0	0	-6.0
2R	-2.0	+2.0	-1.0	+3.0
1L	-3.0	+2.0	0	-3.5

MEASURED

	1	2	3	4
1R	0	+0.19	-0.11	+0.2
2L	-0.11	+0.1	-0.1	+0.19
2R	+0.19	-0.1	+0.1	-0.11
1L	+0.2	-0.11	+0.19	0

THEORY

F_c 1.5975 GHz

	1	2	3	4
1R	0	-5.0	-1.5	-6.0
2L	-3.0	-7.0	-2.0	-6.0
2R	-3.0	+3.5	-3.0	+2.0
1L	-4.0	0	-1.0	-2.5

MEASURED

	1	2	3	4
1R	0	+0.18	-1.54	+0.1
2L	-1.545	-1.1	+2.4	+0.28
2R	+0.28	+2.4	-1.1	-1.545
1L	+0.1	-1.54	+0.18	0

THEORY

R_x 1.64825 GHz

REFERENCES

No.	Author	Title, etc
1	J. Butler R. Lowe	Beam-forming Matrix simplifies design of electronically scanned antennas. *Electronic Design* 12, 170-173, April 1961
2	J.R. Wallington	Analysis design and performance of a microstrip Butler Matrix. *European Microwave Conference*, Brussels, Vol. 1, pp A14.3 (1973)
3	P.J. Muenzer	Properties of linear phased arrays using Butler Matrices. NTZ Heft 9, 419-422 (1972)
4	H.J. Moody	The systematic design of the Butler Matrix. IEEE Trans AP12, 786-788, November 1964
5	J. Lange	Interdigitated stripline quadrature hybrid. IEEE Trans MTT 17 (12), 1150-1151, December 1969
6	B.M. Schiffman	A new class of broad-band microwave 90° phase shifters. IRE Trans MTT 6, 232-237, April 1958
7	S. March	A wideband stripline hybrid ring. IEEE Trans MTT 16 (6), p 361, June 1968
8	A. Podell	A high directivity microstrip coupler technique. IEEE G-MTT International Microwave Symposium, 33-36 (1970)
9	B. Easter	The equivalent circuit of some microstrip discontinuities. IEEE MTT 23 (8), 655-660, August 1975
10	J.R. Wallington	Private communication. Marconi Research Lab. Gt. Baddow

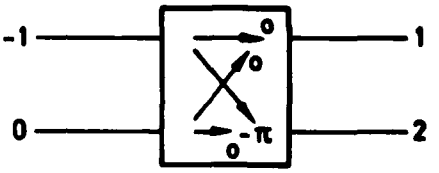

I/P \ O/P	1	2
-1	0	-π
0	0	0

Fig 1a Basic 2 x 2 matrix for broadside Butler matrix

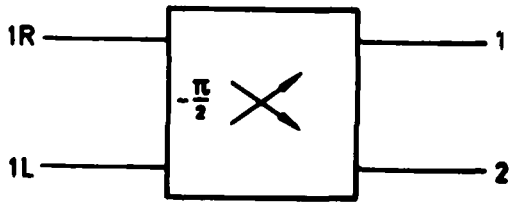

	1	2
1R	0	-π/2
1L	-π/2	0

Fig 1b Basic 2 x 2 matrix for non-broadside Butler matrix

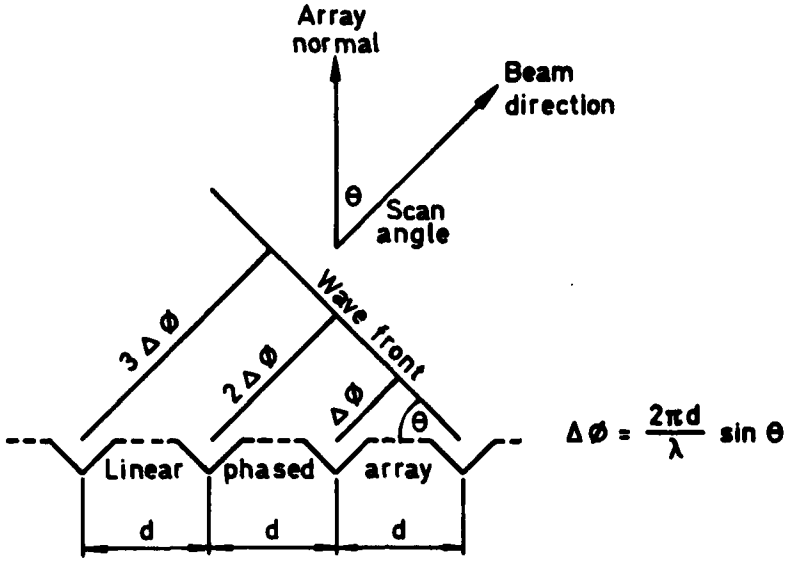

Fig 2a Phase shift between radiating elements fed by a non-broadside matrix

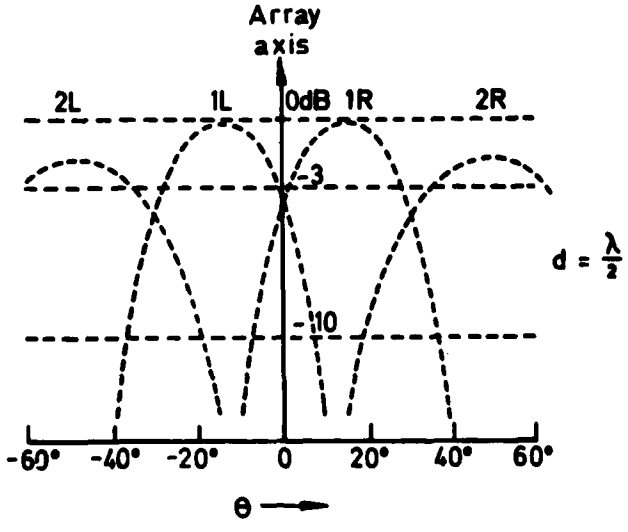

Fig 2b Beam widths and positions of 4 element Butler matrix

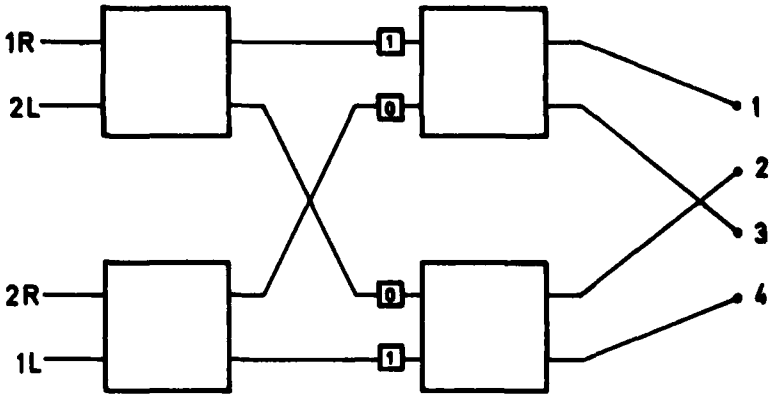

Fig 3 Output port configuration

Fig 4

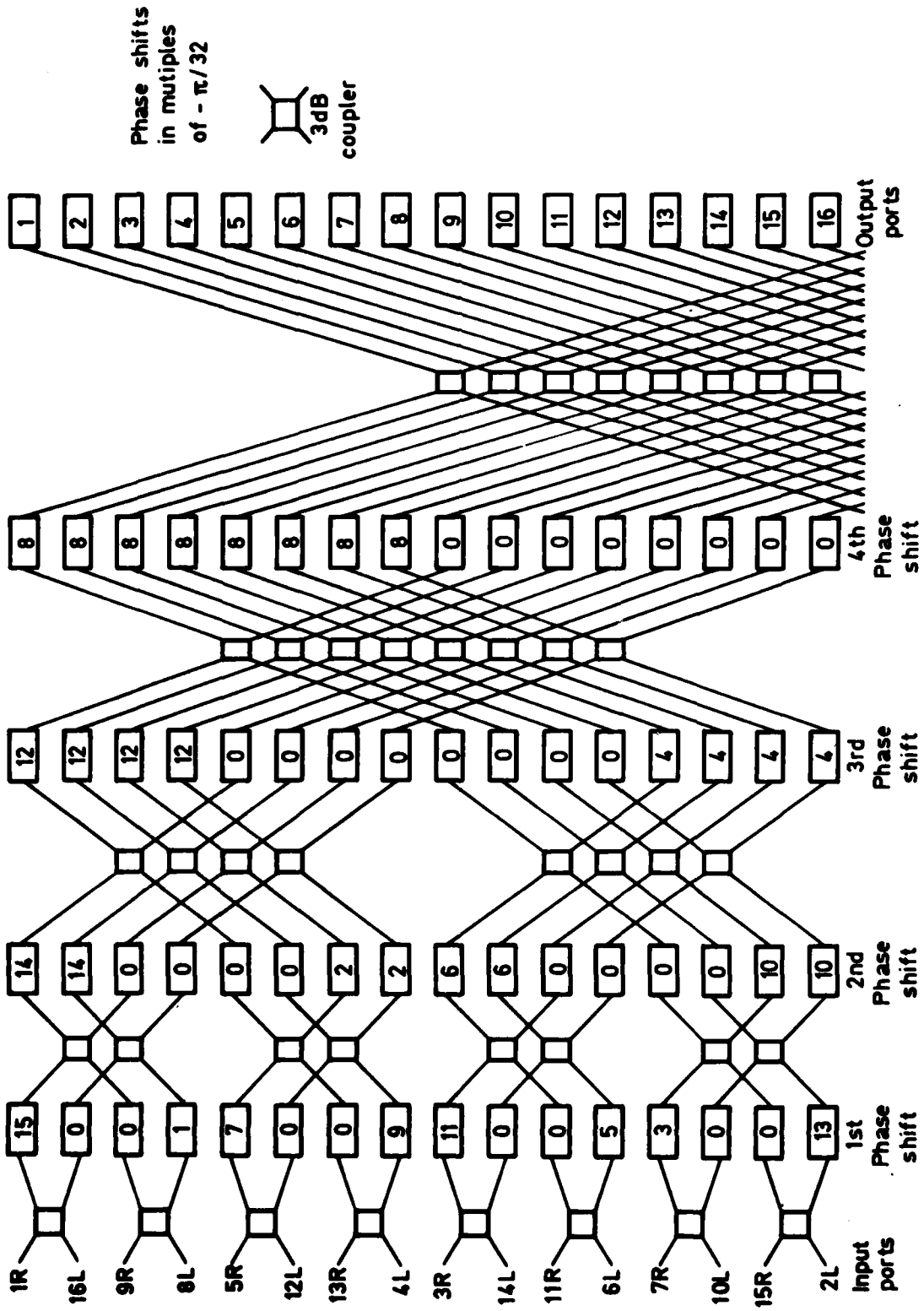

Fig 4 Half a 32 x 32 element Butler matrix

TR 79118

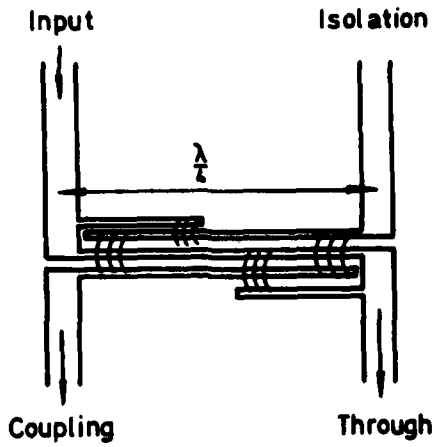

Fig 5 The 3 dB Lange coupler

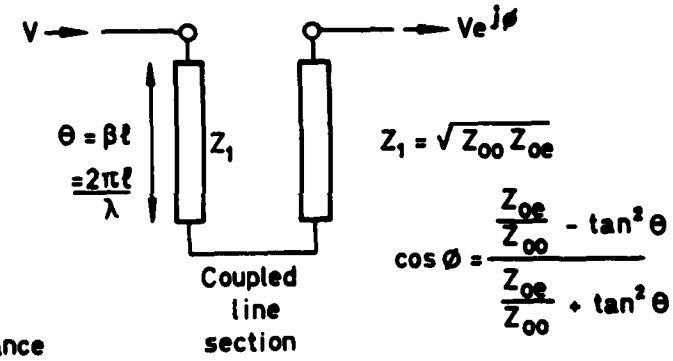

Z_1 = Image impedance
Z_{00} = Odd mode impedance
Z_{0e} = Even mode impedance

Fig 6 Schiffman coupler (simplest type)

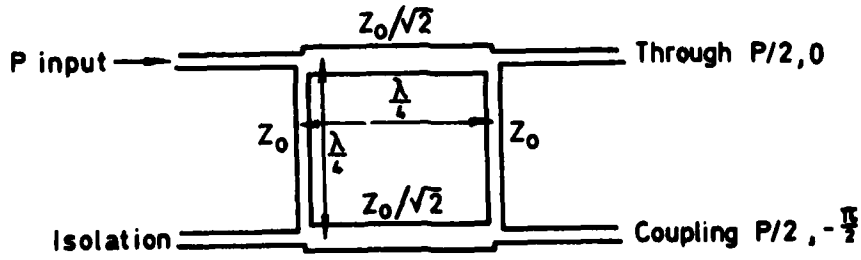

Fig 7 90° hybrid coupler

Figs 8 & 9a&b

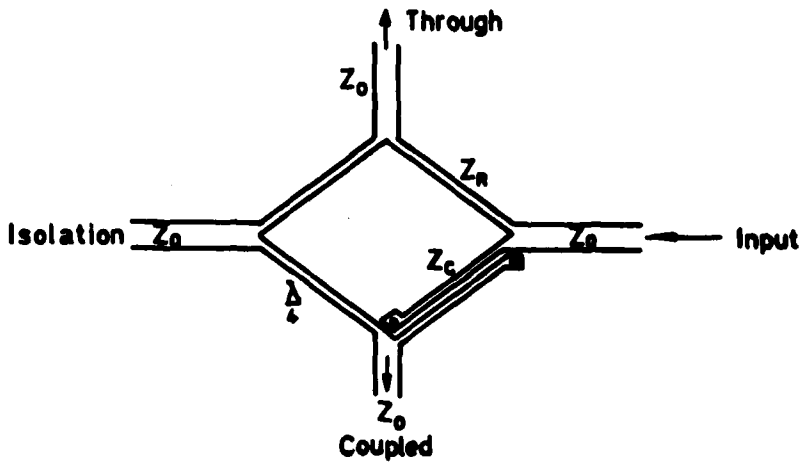

Fig 8 Wide band 180° hybrid coupler

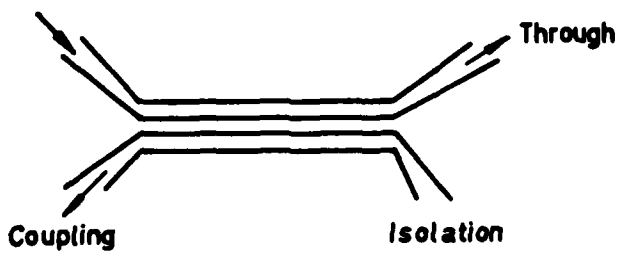

Fig 9a Broadside coupler

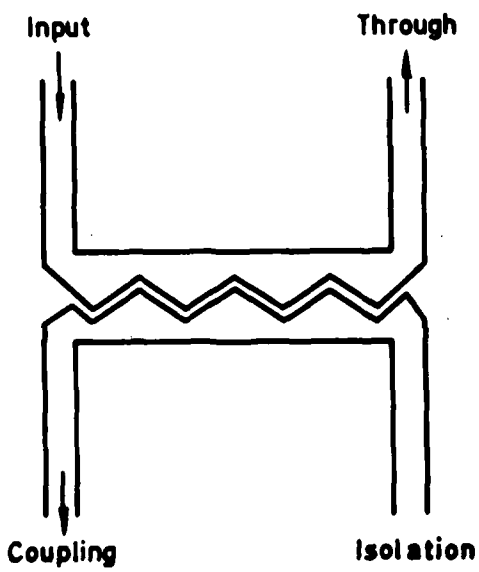

Fig 9b Podell coupler

TR 79118

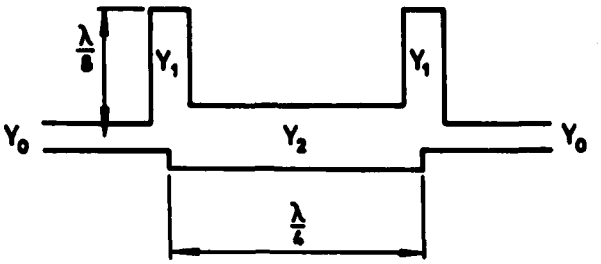

Fig 10a Loaded line section

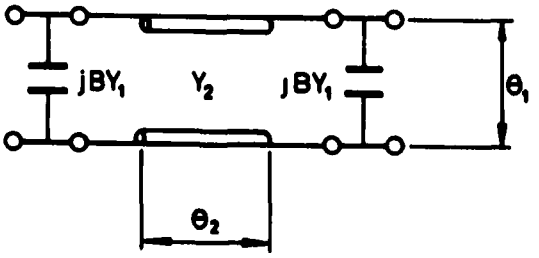

Fig 10b Loaded line equivalent circuit

Fig 11a&b

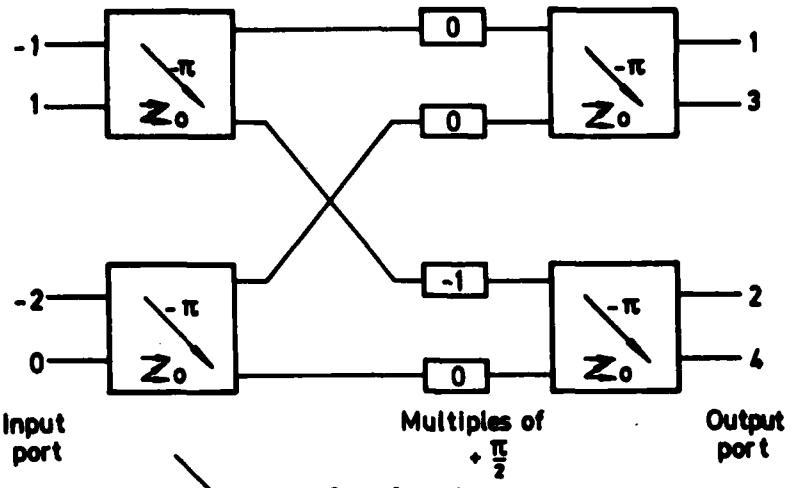

	1	2	3	4
-1	0	$\frac{-3\pi}{2}$	$-\pi$	$\frac{-5\pi}{2}$
1	0	$-\frac{\pi}{2}$	$-\pi$	$\frac{-3\pi}{2}$
-2	0	$-\pi$	0	$-\pi$
0	0	0	0	0

Fig 11a Broadside 4 x 4 Butler matrix

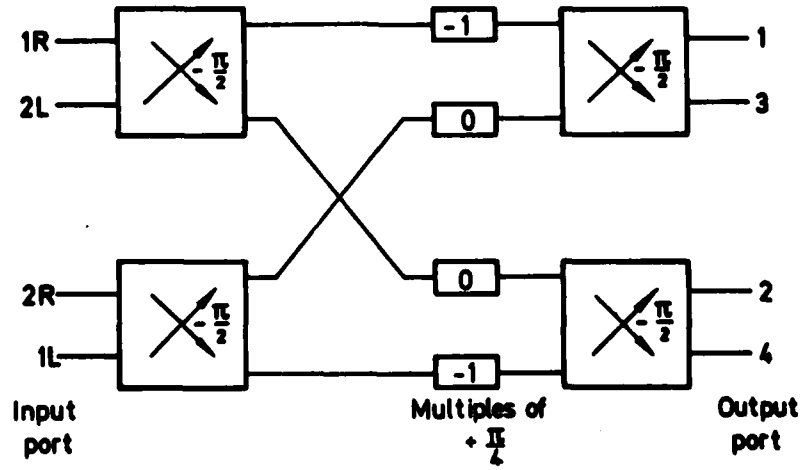

	1	2	3	4	ΔØ
1R	-1	-2	-3	-4	-1
2L	-3	-0	-5	-2	+3
2R	-2	-5	-0	-3	-3
1L	-4	-3	-2	-1	+1

Fig 11b Non-broadside 4 x 4 Butler matrix

TR 79118

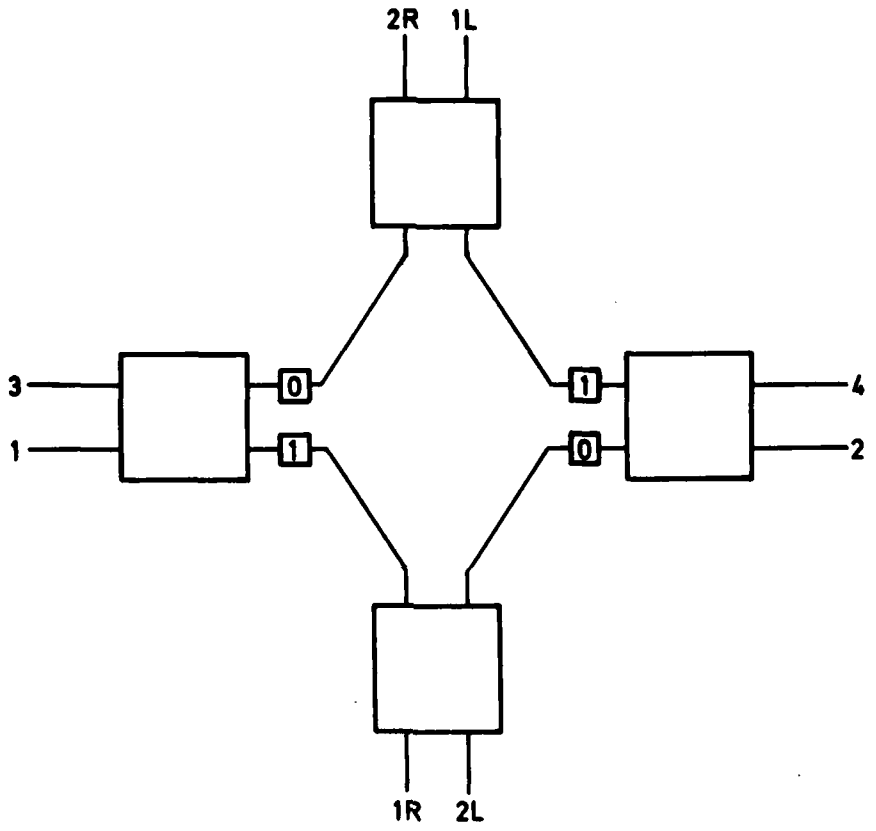

Fig 12 Alternative layout for 4 x 4 matrix avoiding crossovers

Fig 13

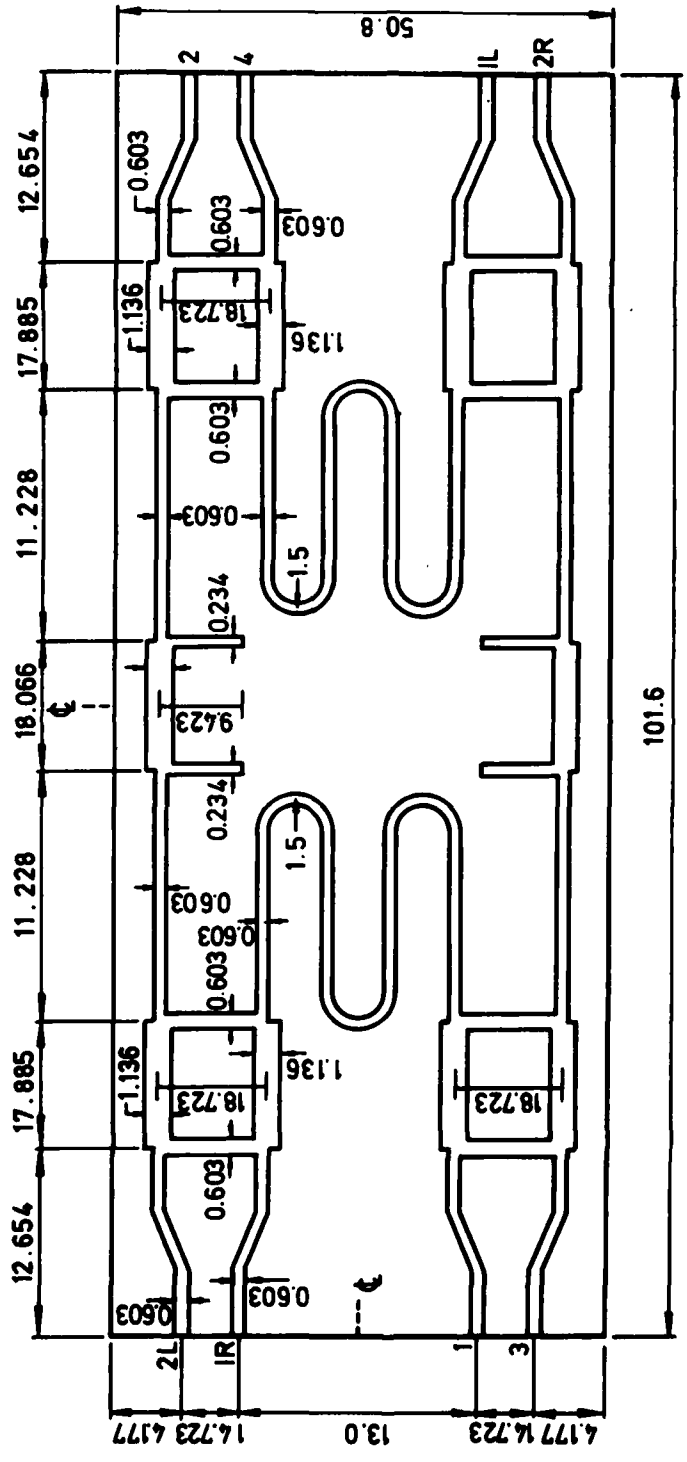

Fig 13 Design values and layout of the 4 x 4 Butler matrix

TR 79118

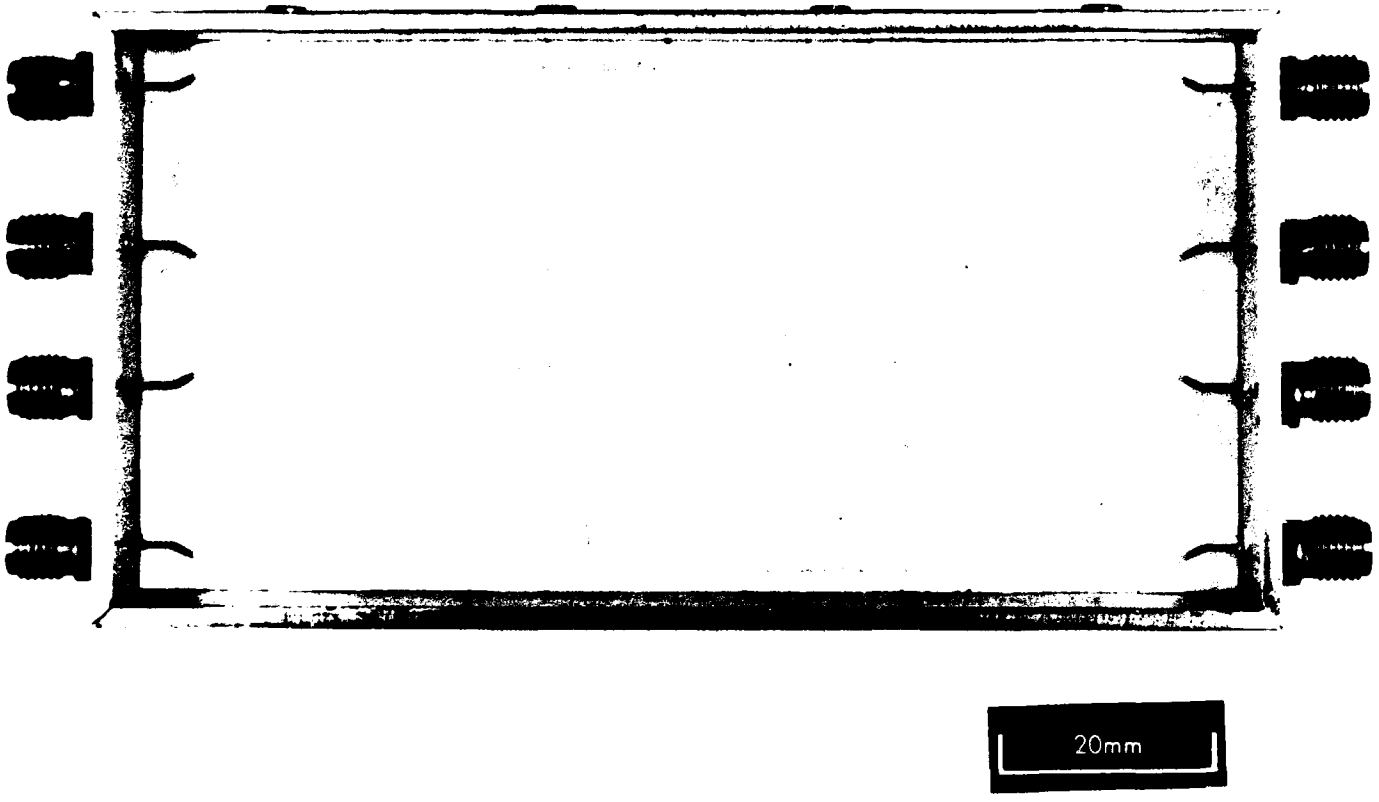

Fig 14 Breadboard model

Fig 14

Fig 15a

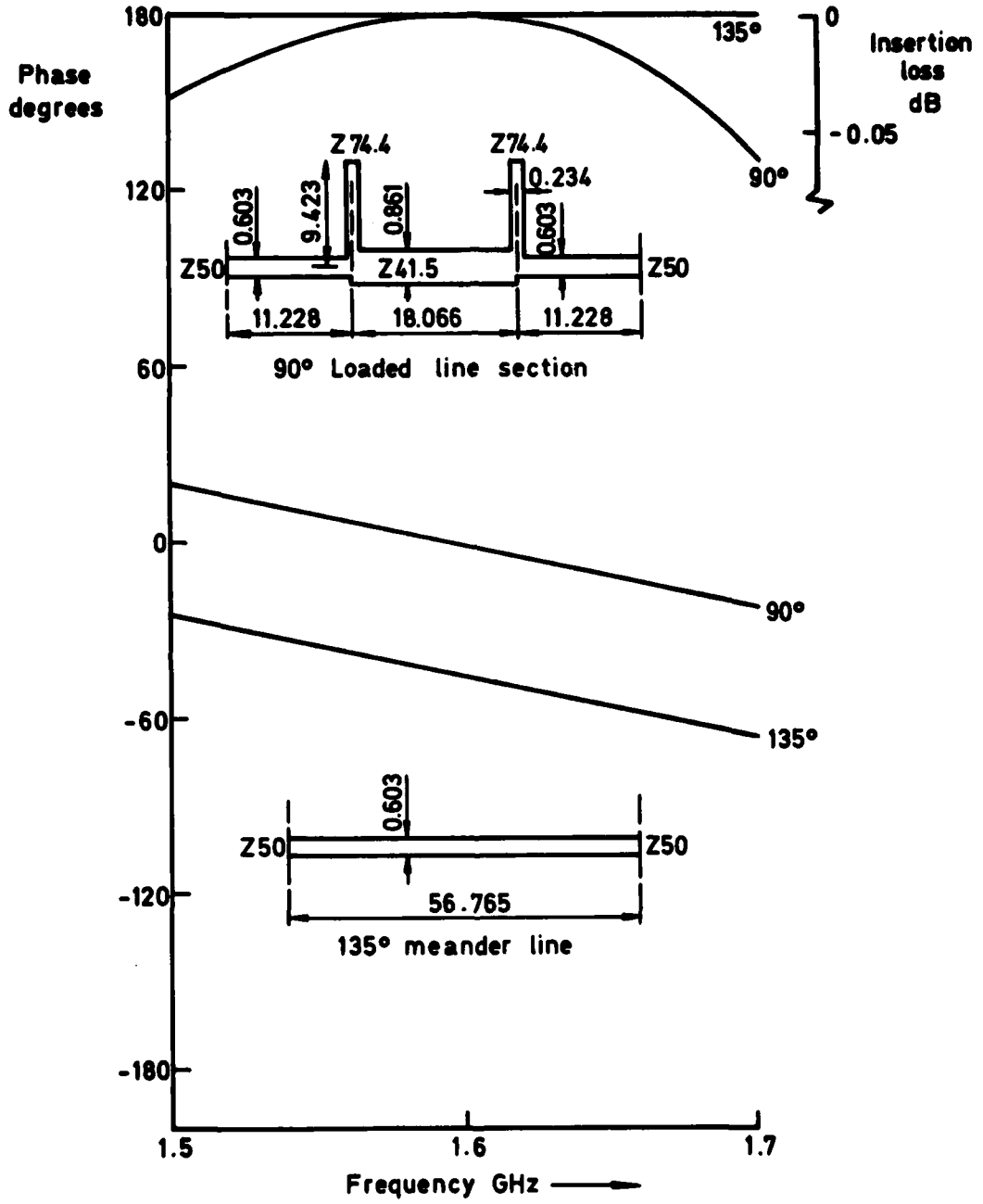

Fig 15a Computed phase shift and insertion loss for the test phase shifters (ideal lines)

TR 79118

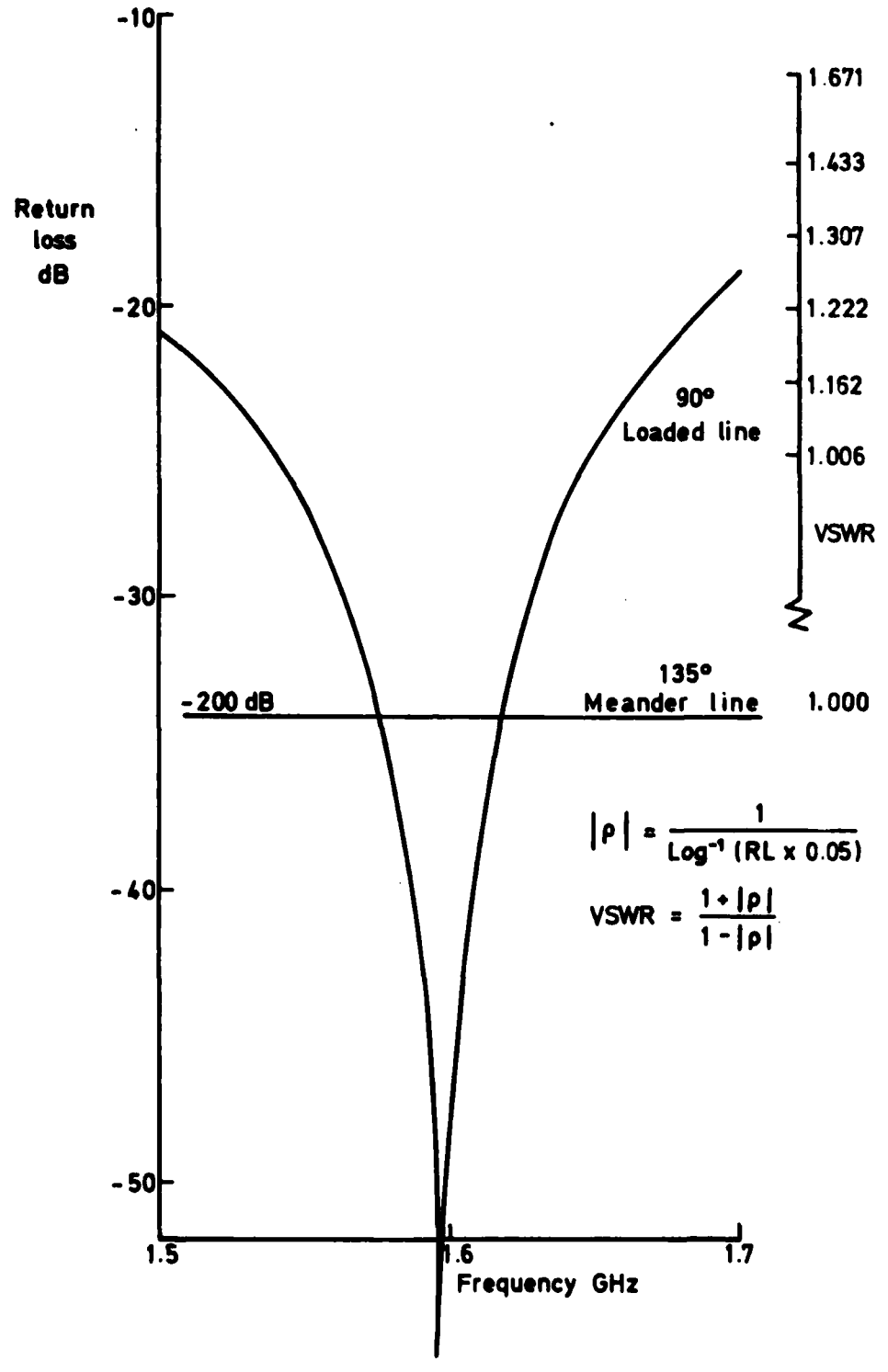

TR 79118

Fig 15b Computed return loss versus frequency for the test phase shifters

Fig 16

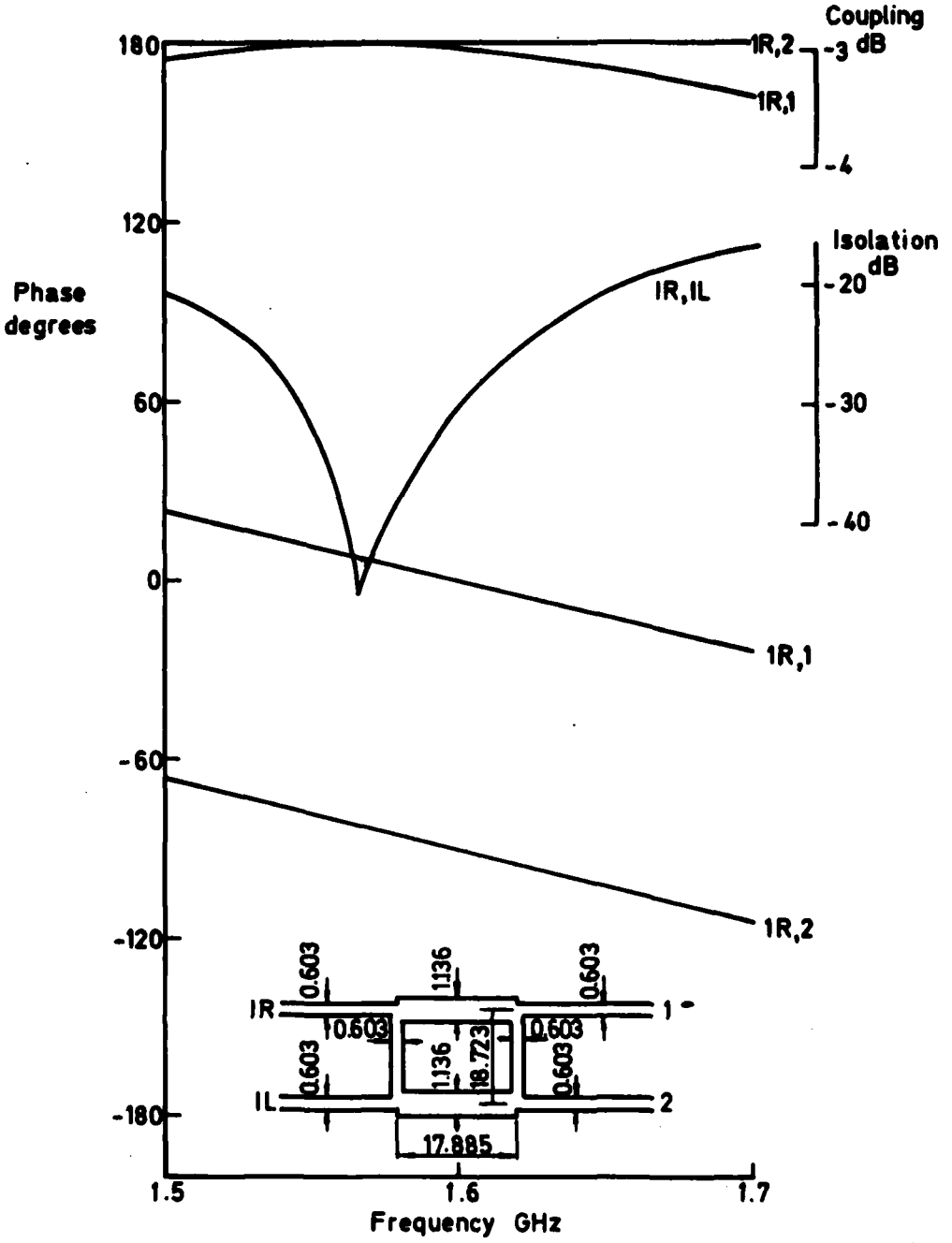

TR 79118

Fig 16 Computed phase shift, coupling and isolation versus frequency for the test 90° hybrid coupler

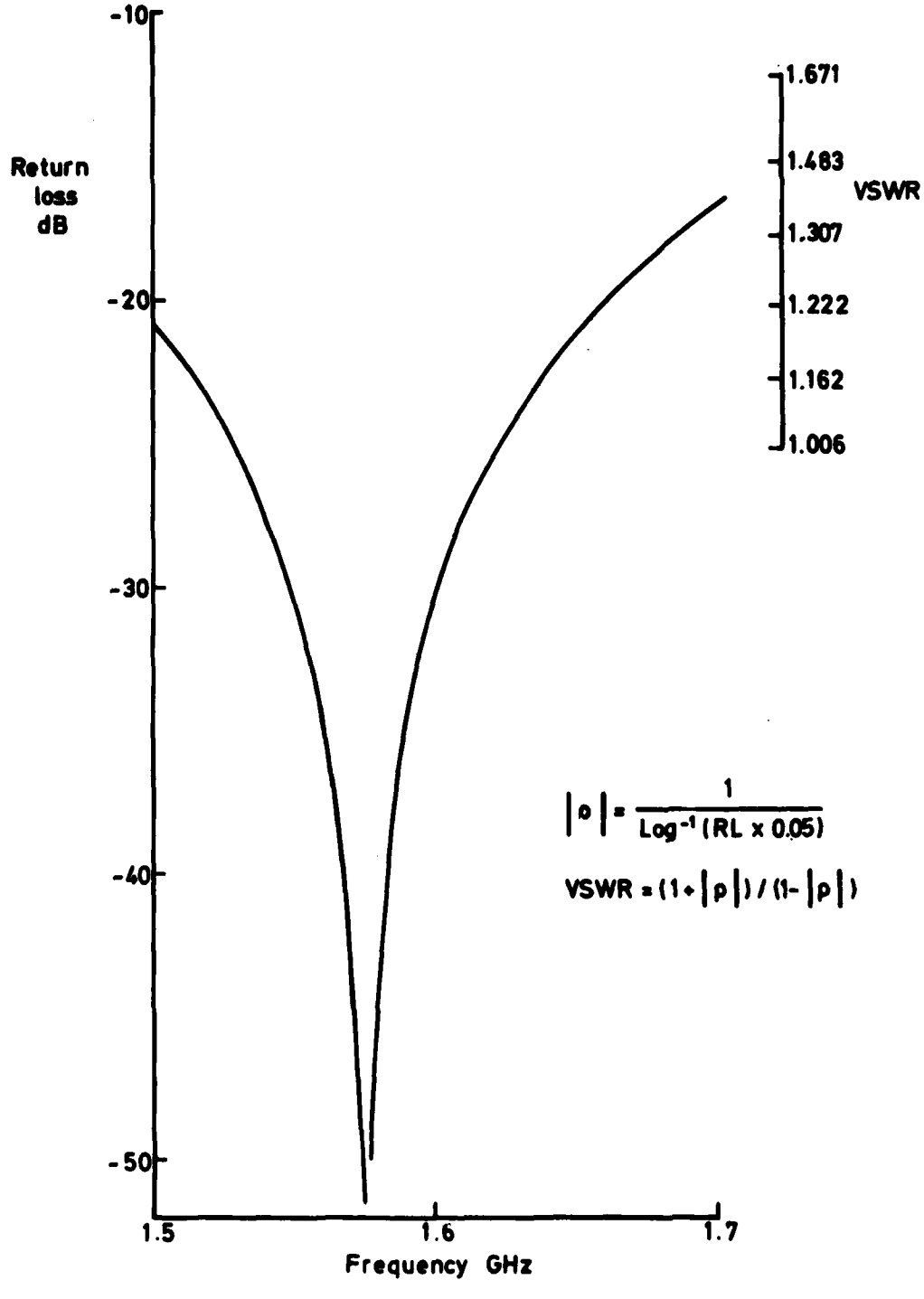

TR 79118

Fig 17 Computed return loss — all ports of coupler test circuit

Fig 18

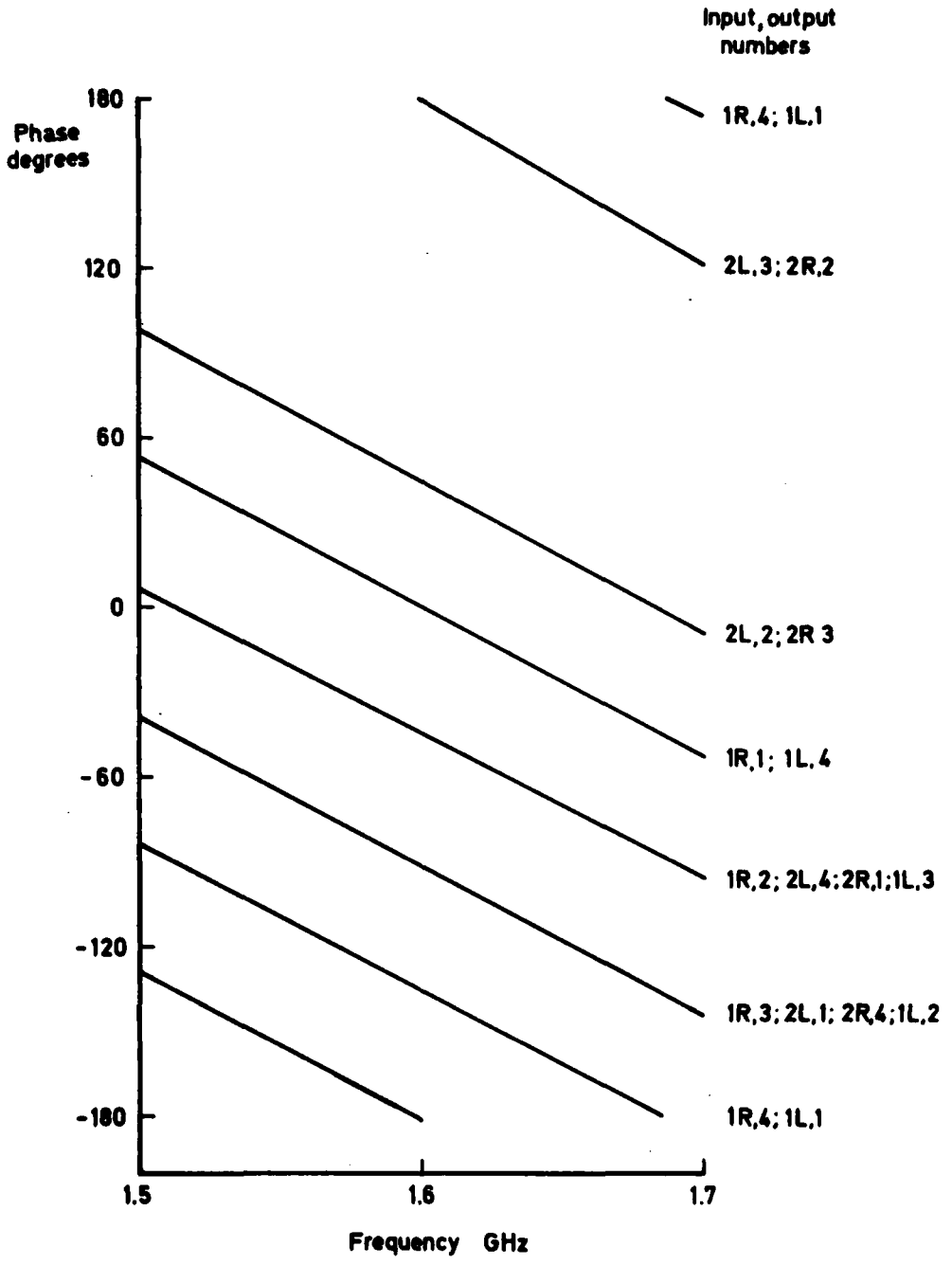

Fig 18 Computed phase response of designed Butler matrix (input to output port numbers shown)

TR 79118

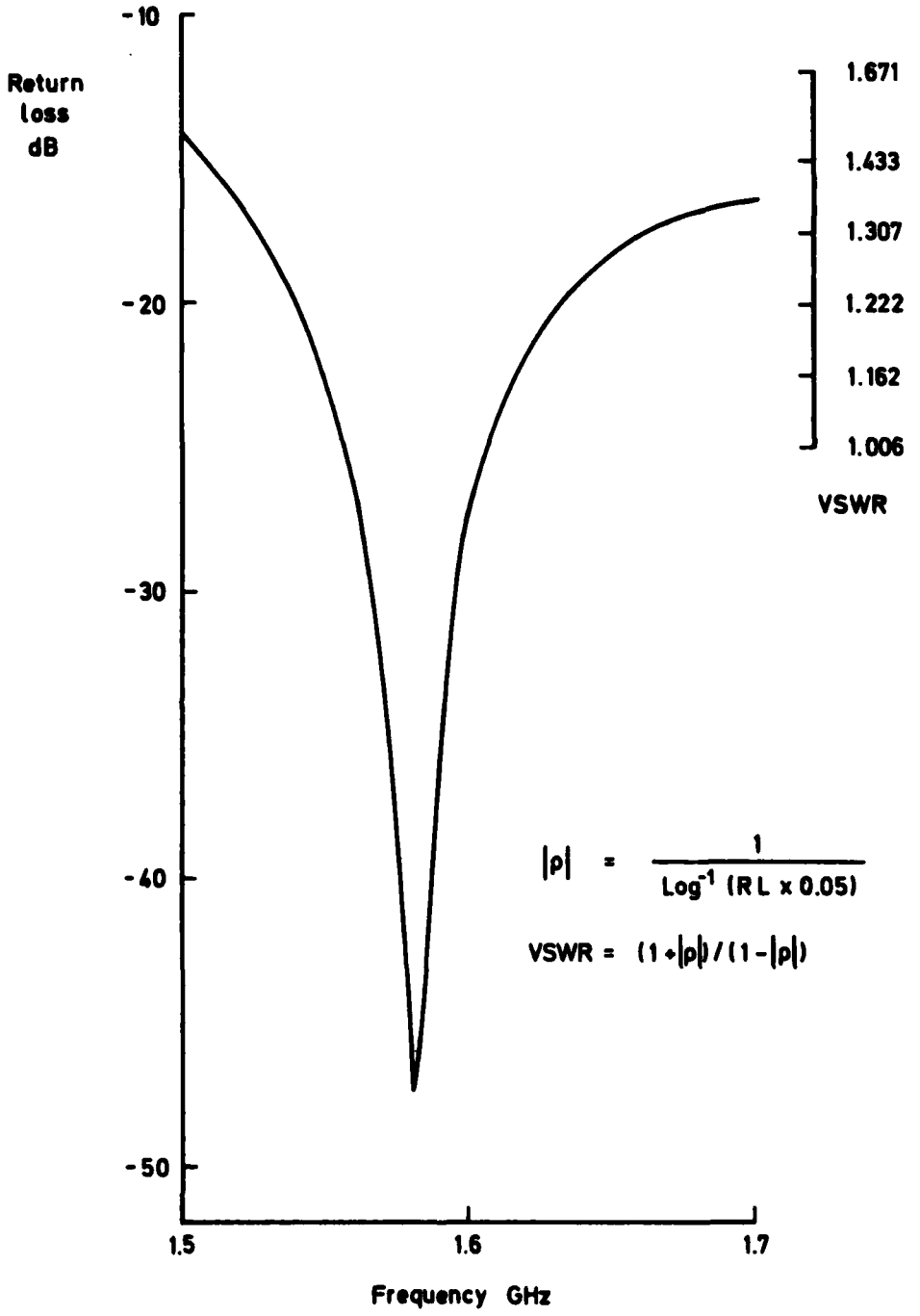

TR 79118

Fig 19 Computed return loss versus frequency for all ports of Butler matrix

Fig 20

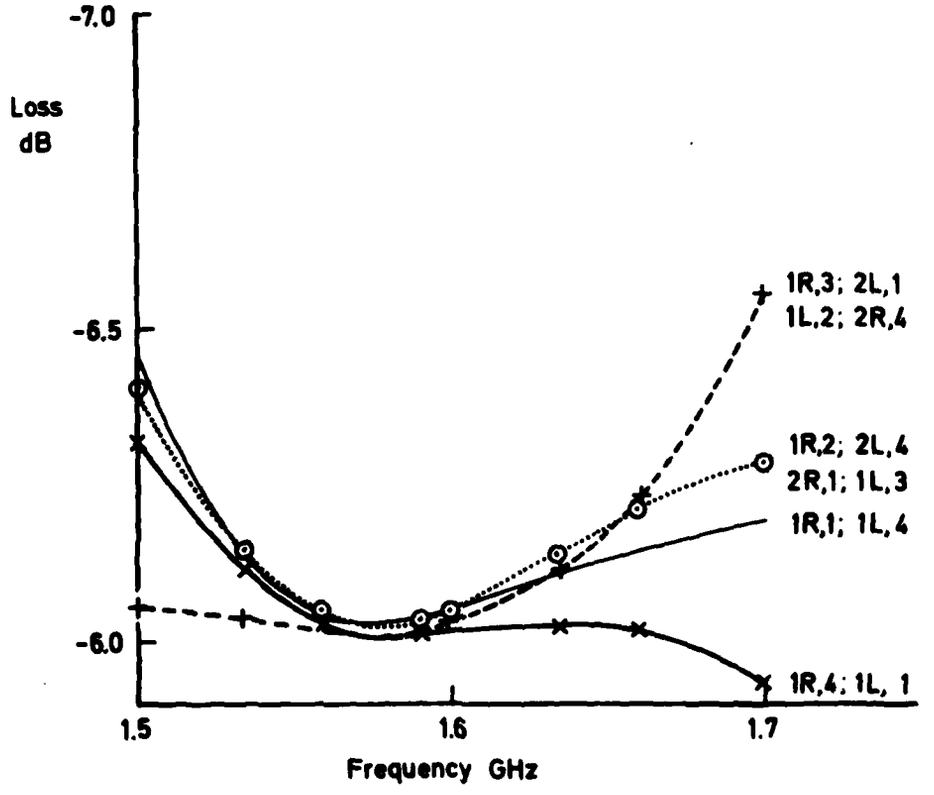

TR 79118

Fig 20 Total computed loss through the design matrix (input to output ports shown)

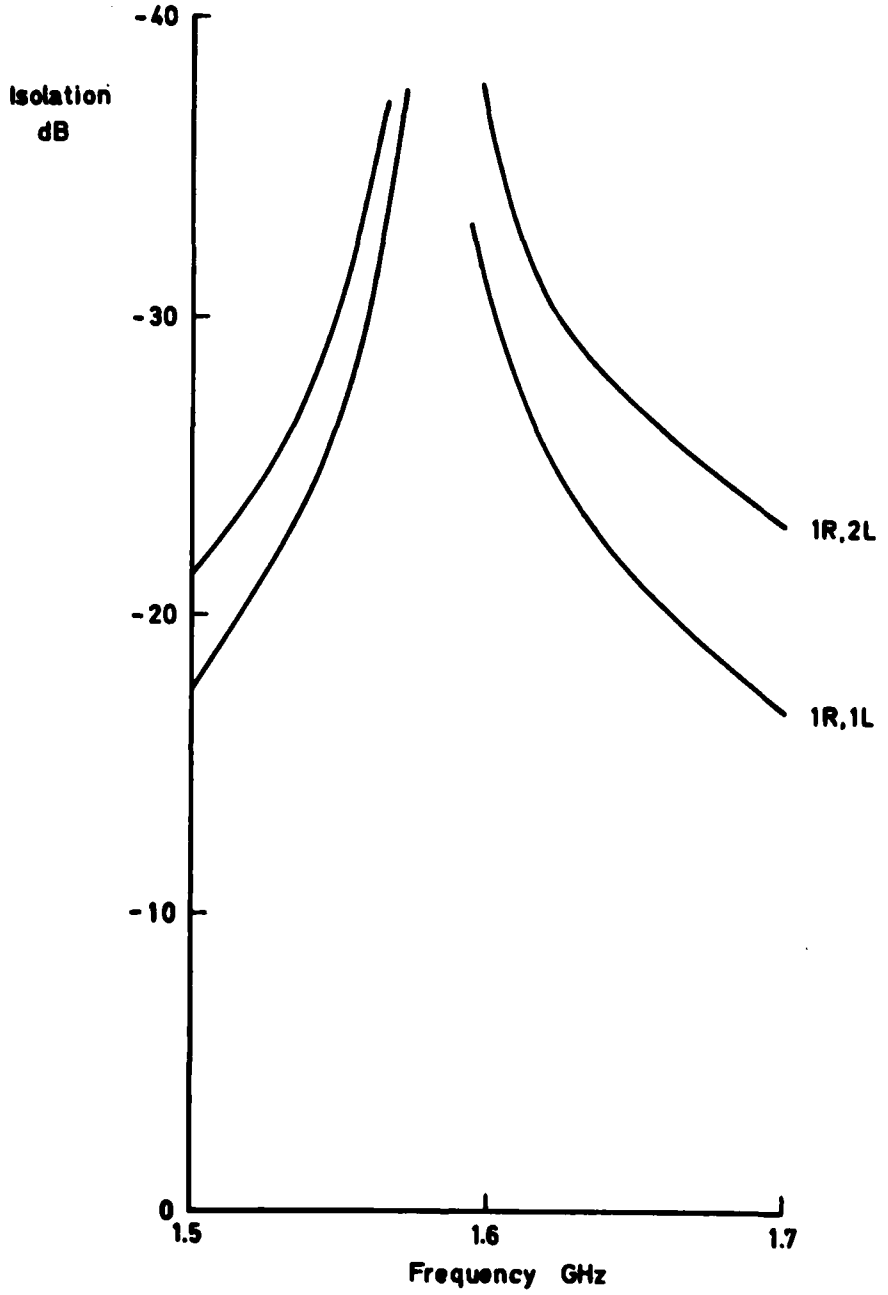

TR 79118

Fig 21 Computed isolation versus frequency input port 1R to inputs 1L and 2L

Fig 22

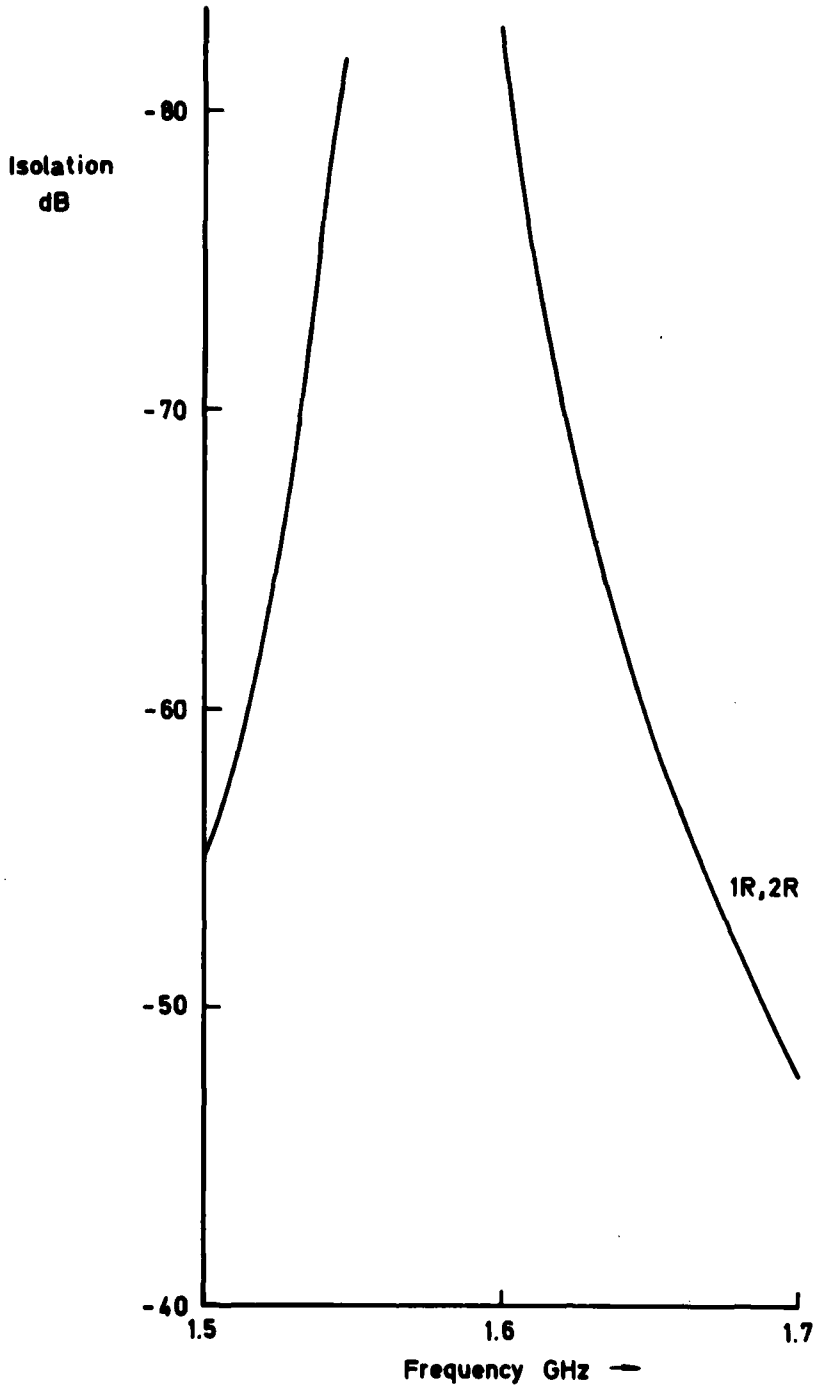

TR 79118

Fig 22 Computed isolation versus frequency input port 1R to input port 2R

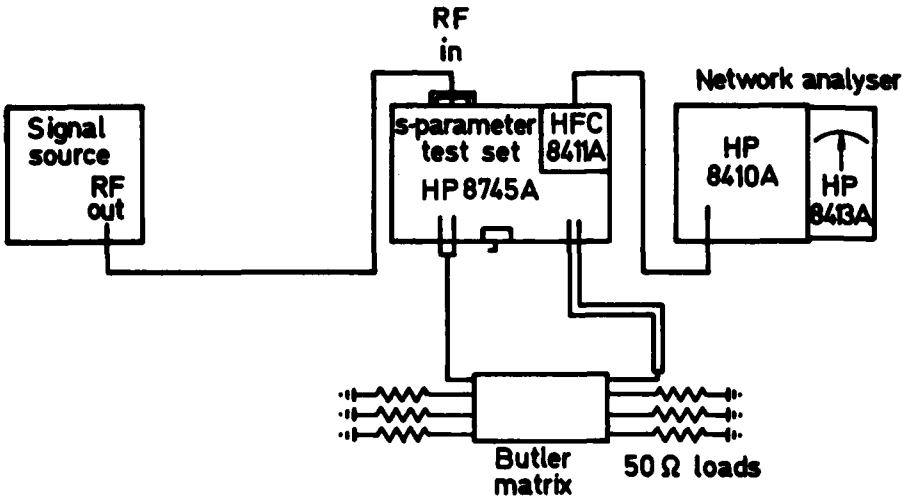

TR 79118

Fig 23 General set-up for transmission measurements

Fig 24

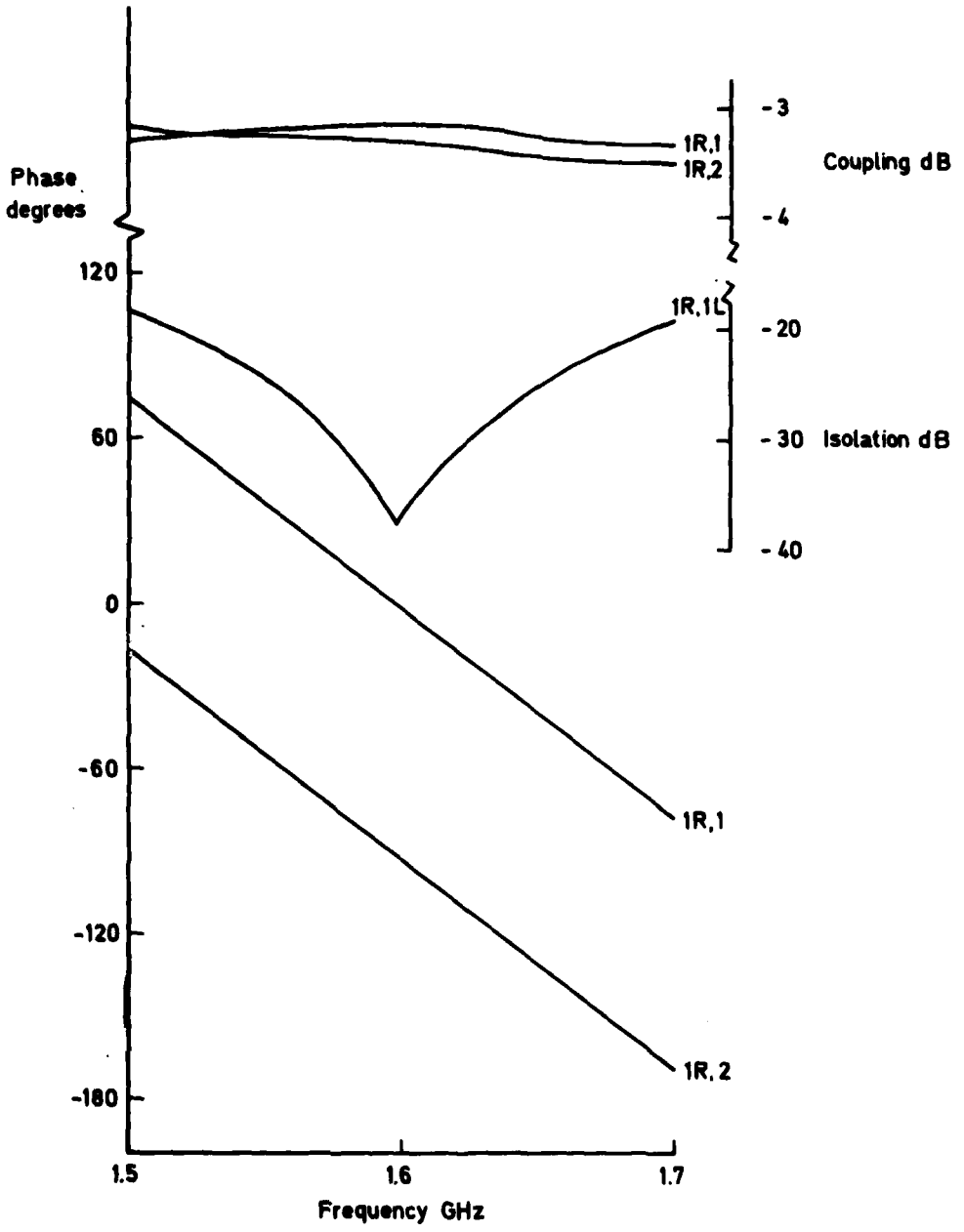

Fig 24 Measured coupling, isolation and phase shift versus frequency for the test 90° hybrid coupler

TR 79118

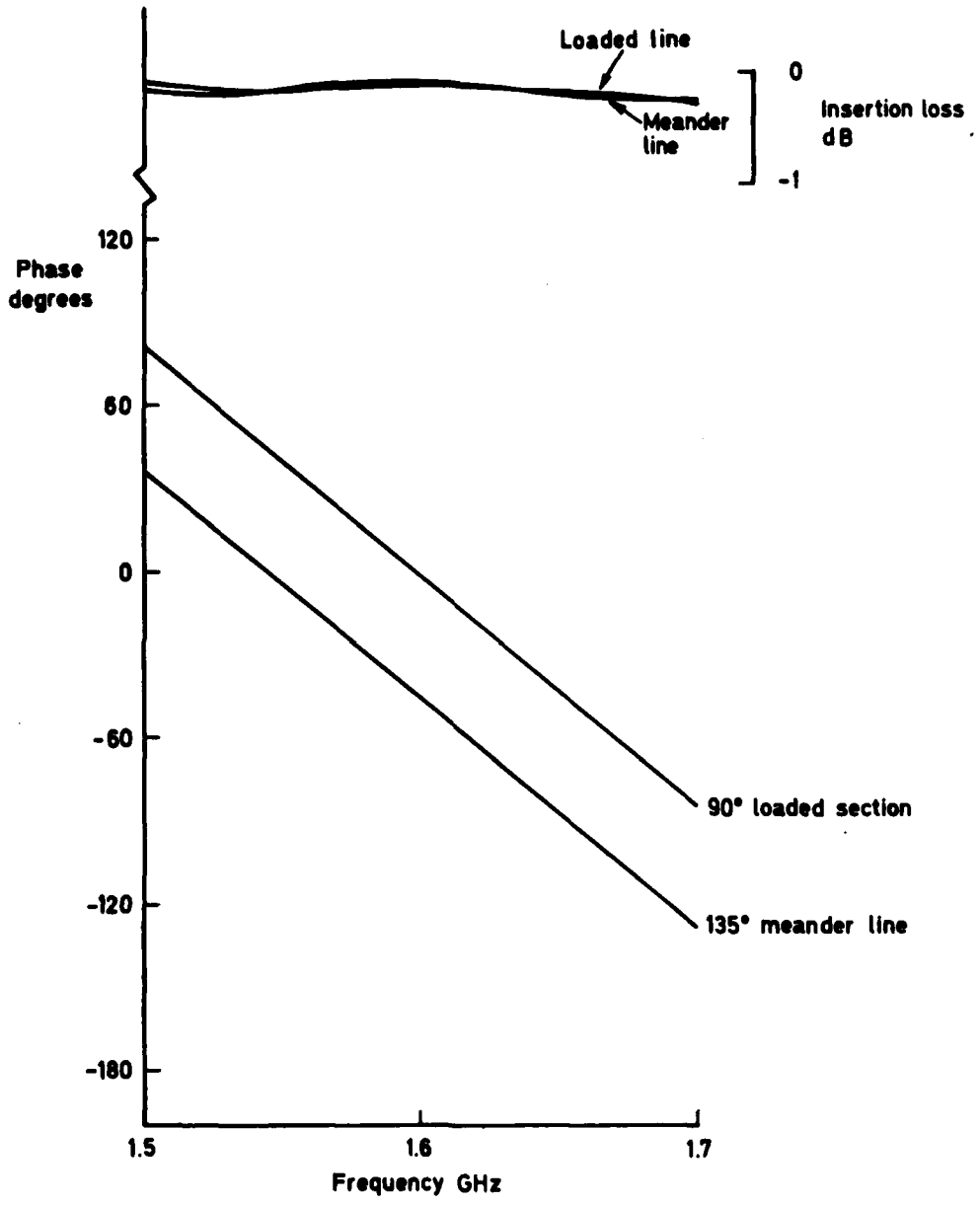

TR 79118

Fig 25 Measured insertion loss and phase shift for the test phase shifters

Fig 26

$$|\rho| = \frac{1}{\text{Log}^{-1}\ (RL \times 0.05)}$$

$$VSWR = (1+|\rho|)/(1-|\rho|)$$

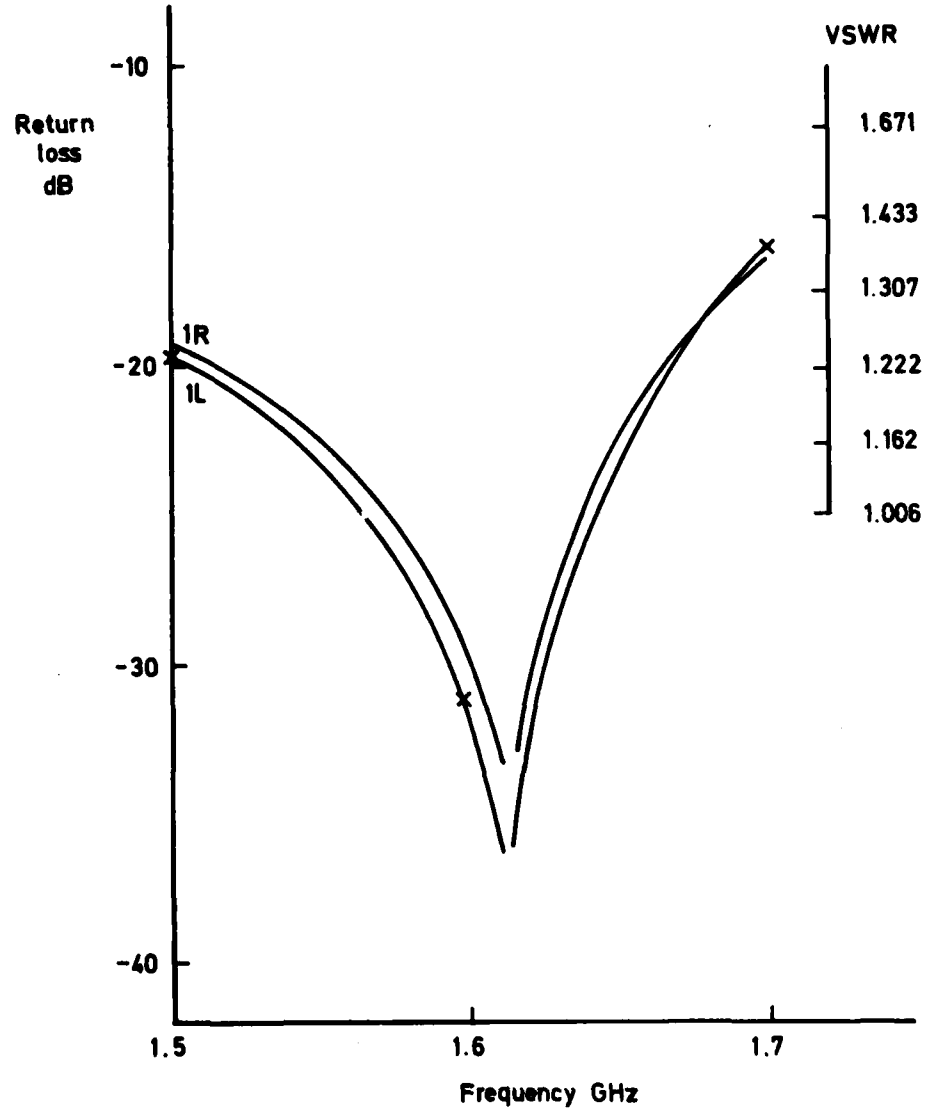

Fig 26 Measured return loss for 90° hybrid coupler. Both inputs

TR 79118

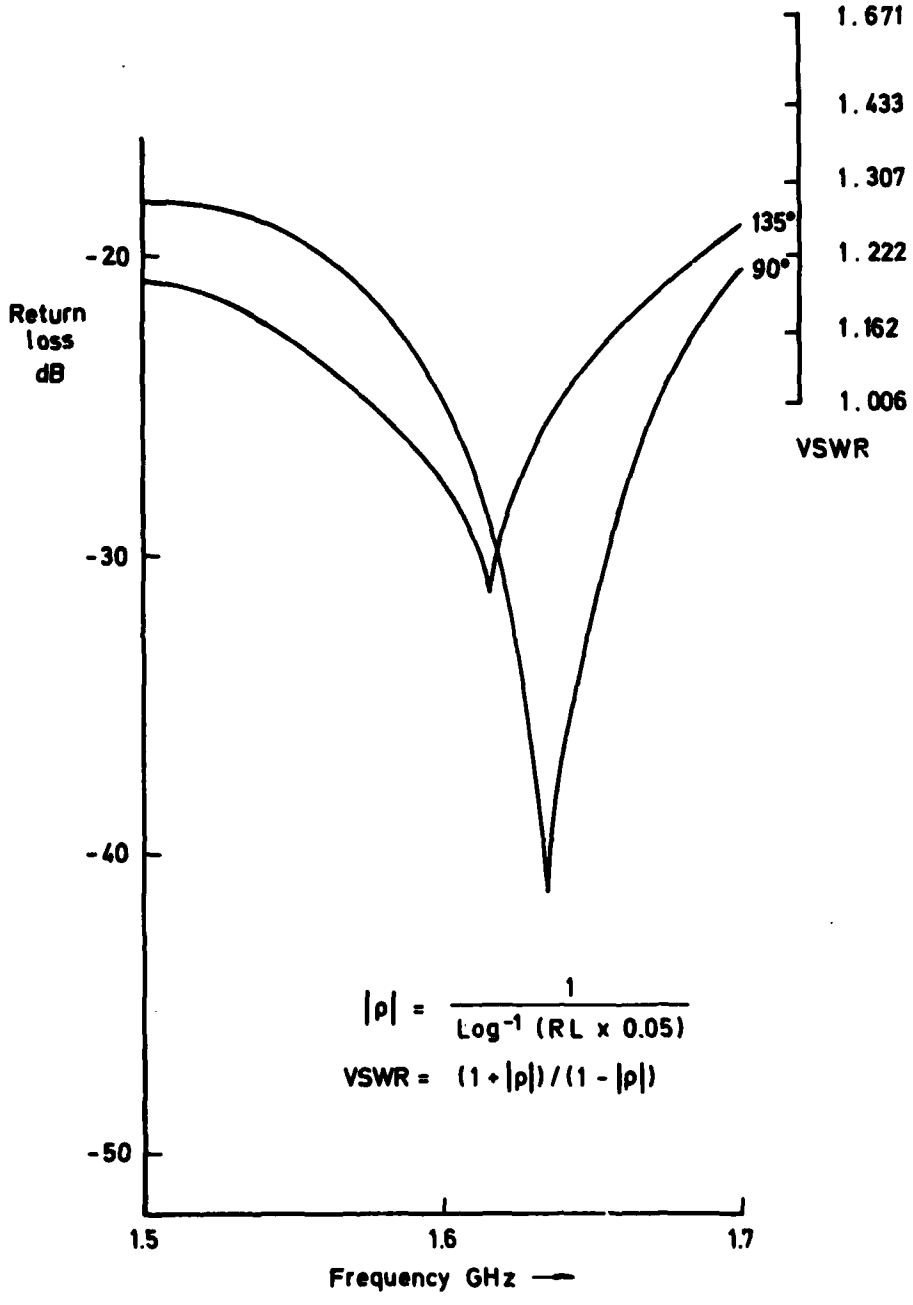

Fig 27 Measured return loss versus frequency for the test phase shifters

TR 79118

Fig 28

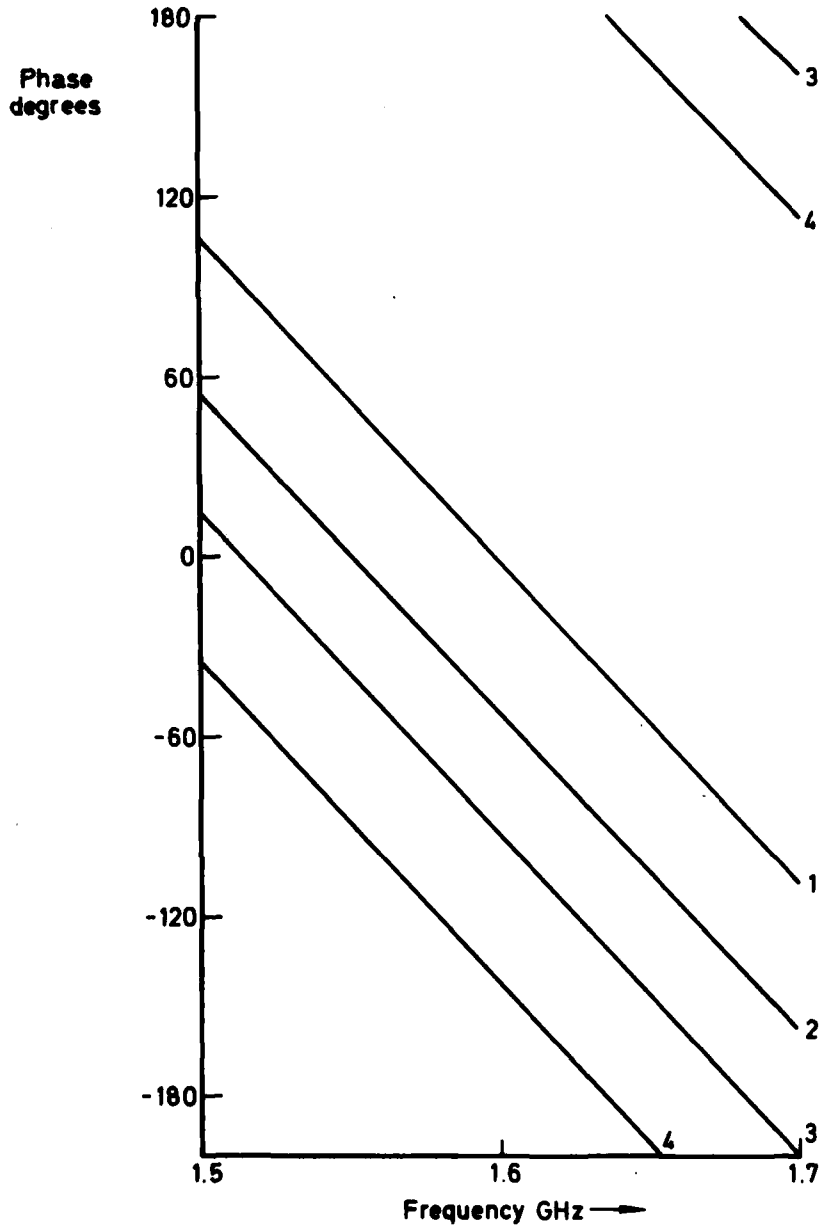

TR 79118

Fig 28 Measured phase shift versus frequency for matrix. Input port 1R to all outputs

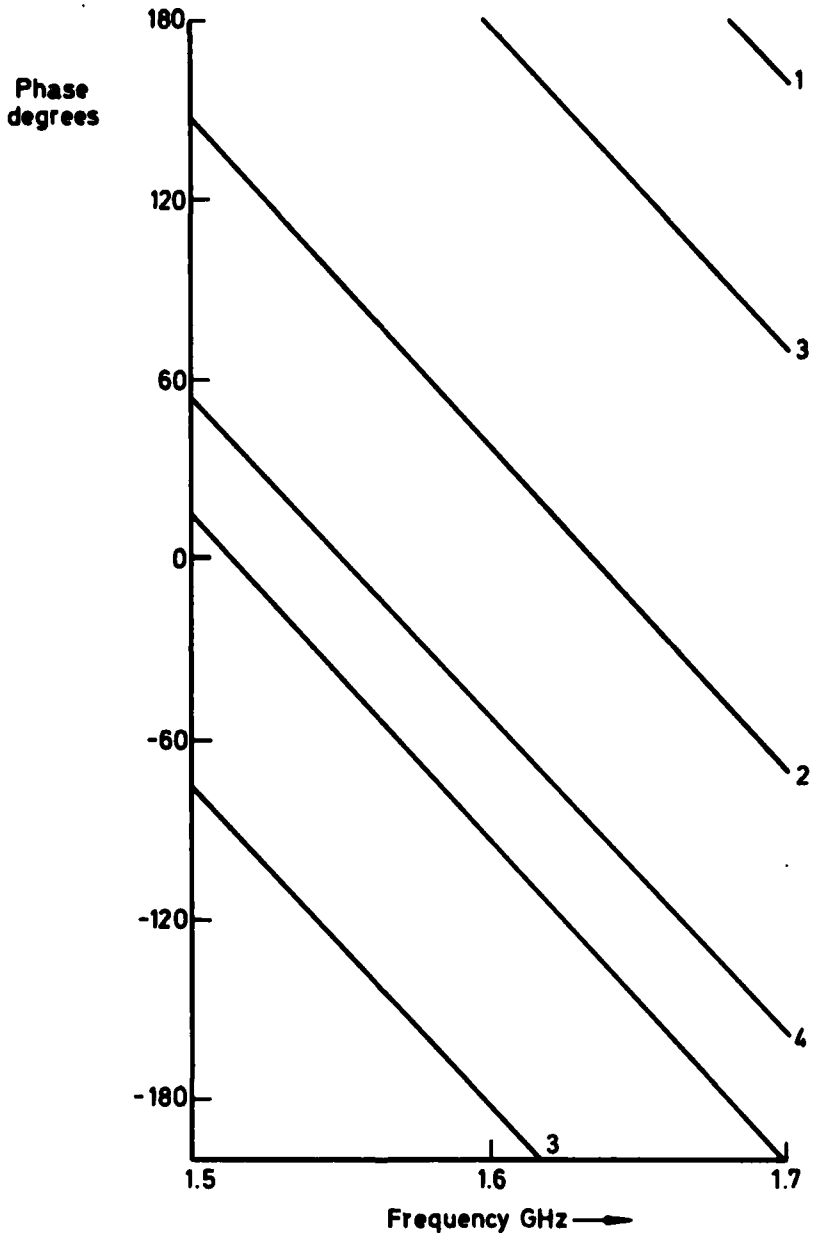

TR 79118

Fig 29 Measured phase shift versus frequency for matrix. Input 2L to all outputs

Fig 30

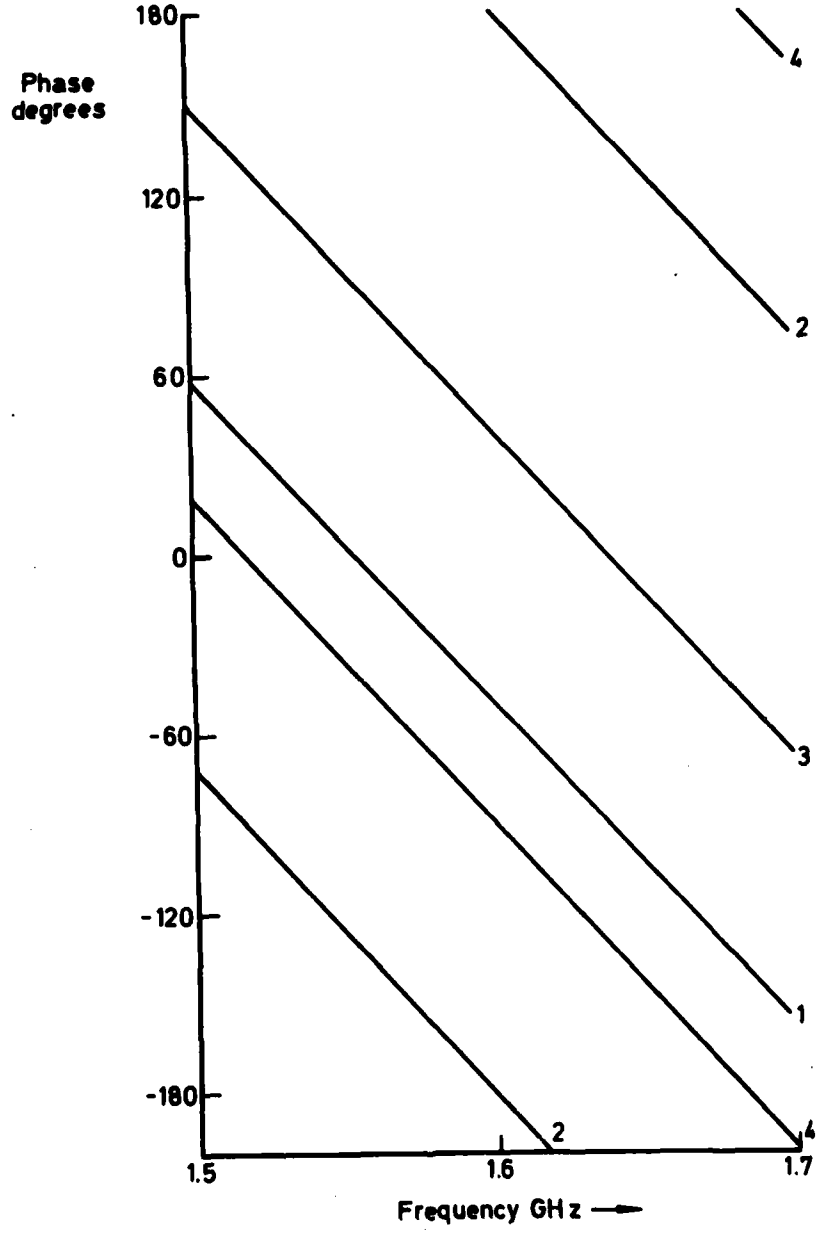

Fig 30 Measured phase shift versus frequency for matrix. Input port 2R to all outputs

TR 79118

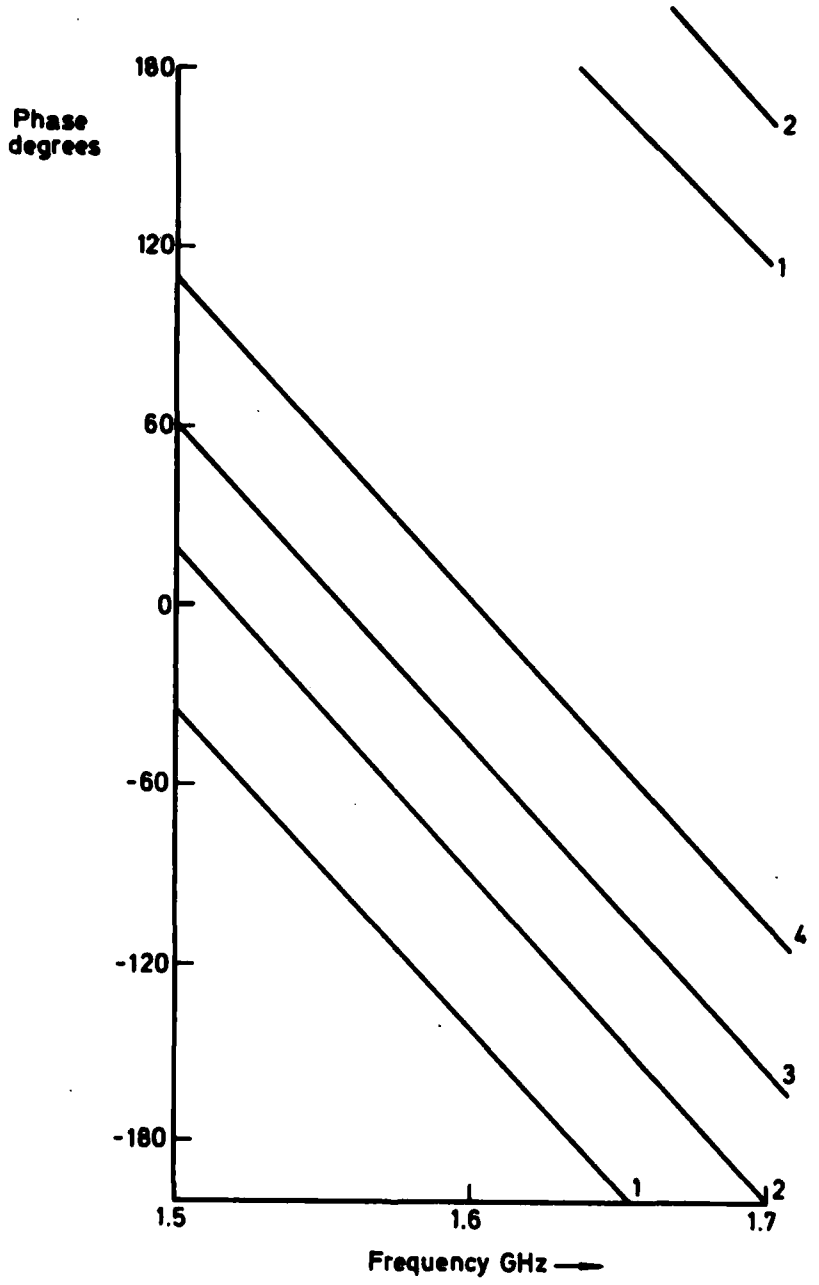

TR 79118

Fig 31 Measured phase shift versus frequency for matrix. Input port 1L to all outputs

Fig 32

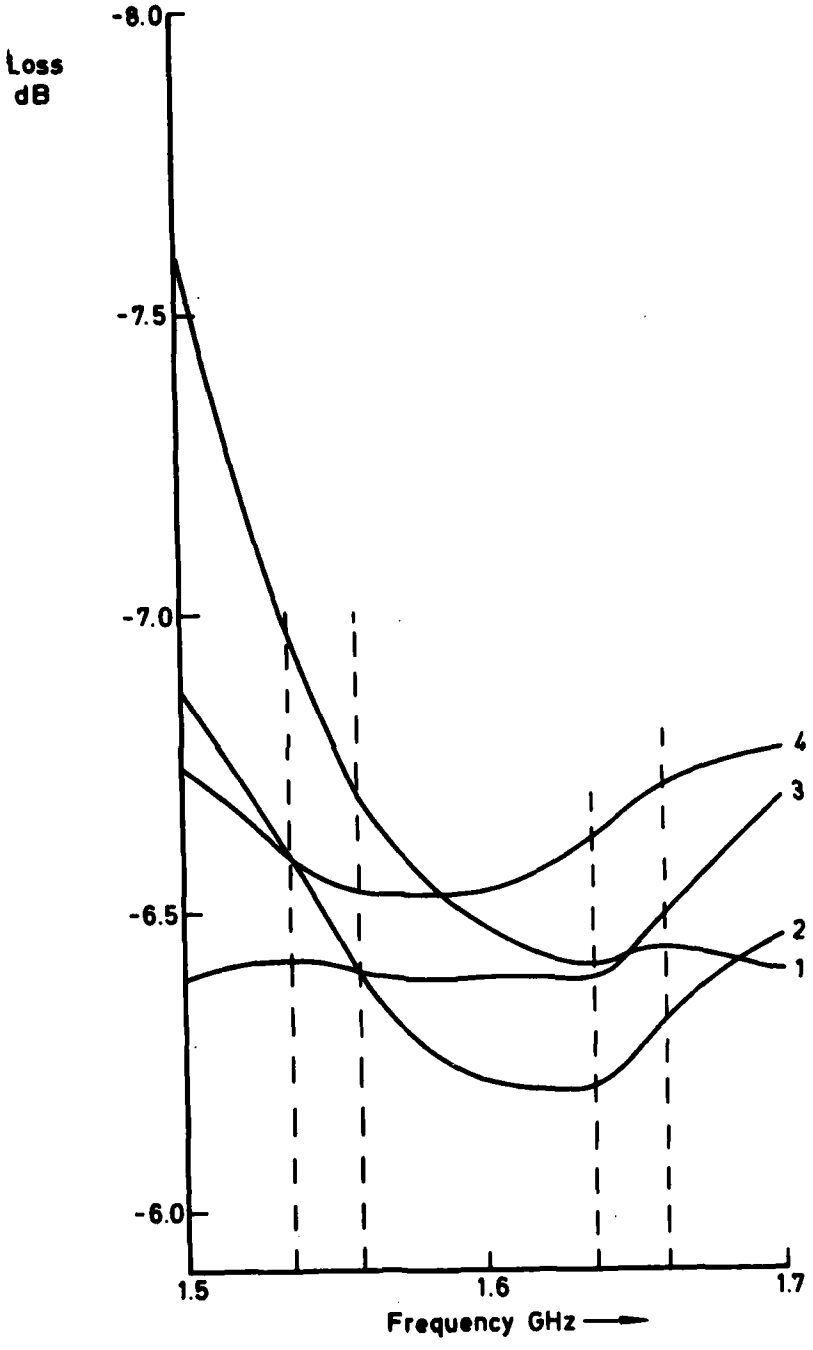

TR 79118

Fig 32 Measured loss through the matrix. Input port 1R to all outputs

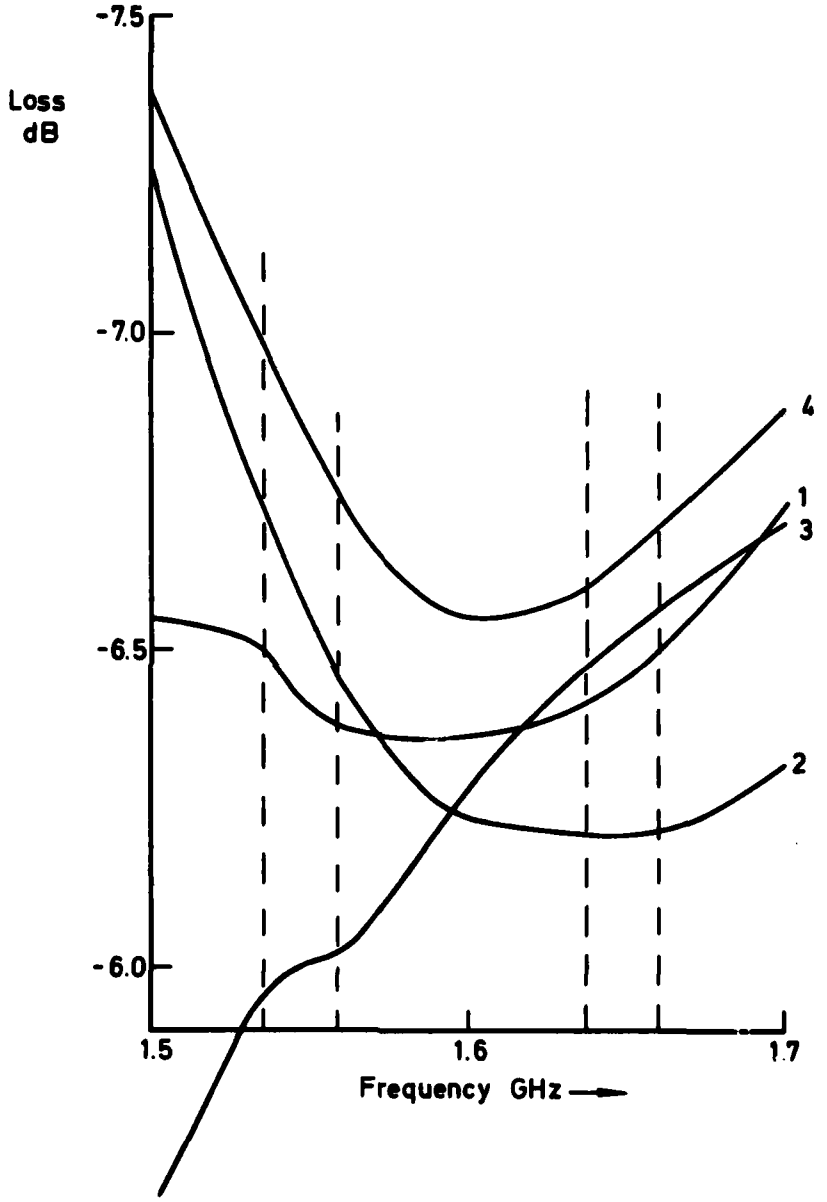

TR 79118

Fig 33 Measured loss through the matrix. Input port 2L to all outputs

Fig 34

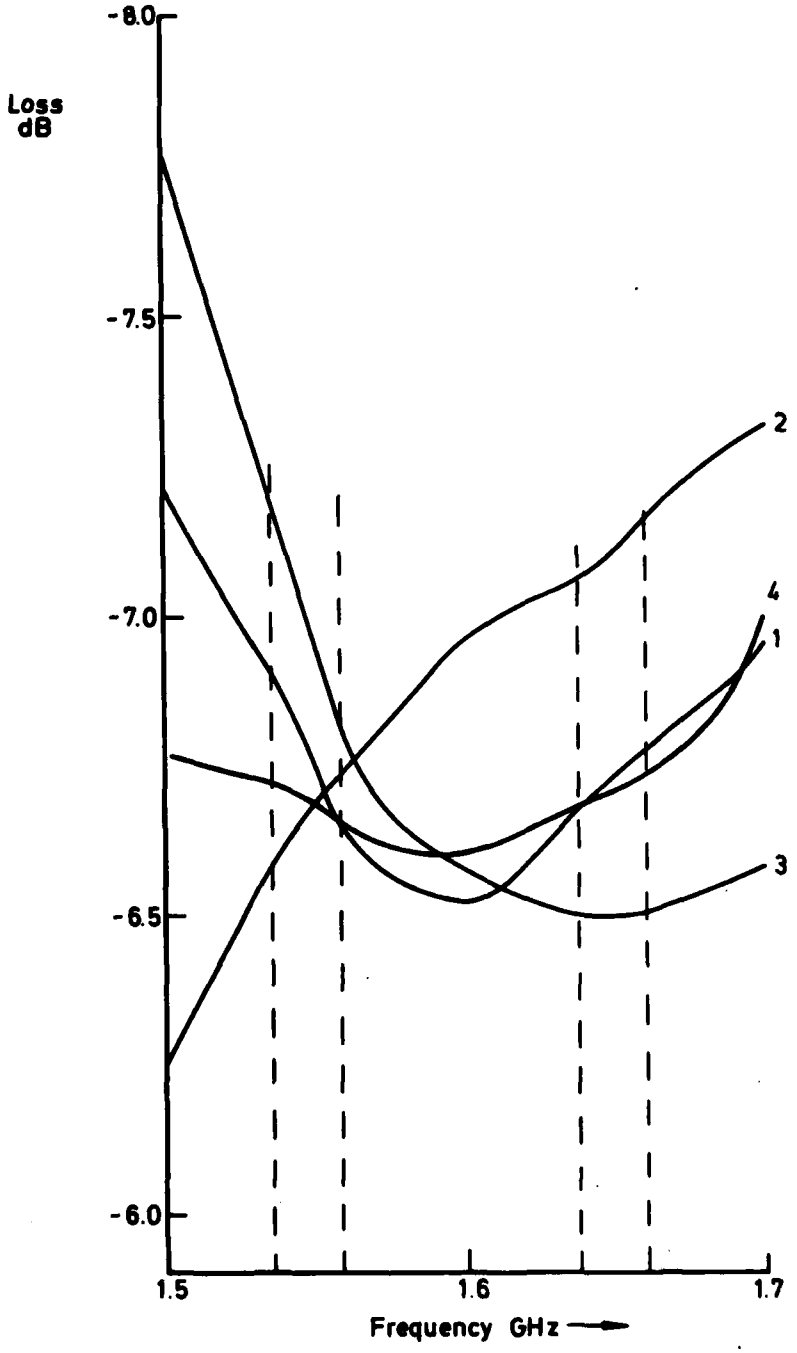

Fig 34 Measured loss through the matrix. Input port 2R to all outputs

TR 79118

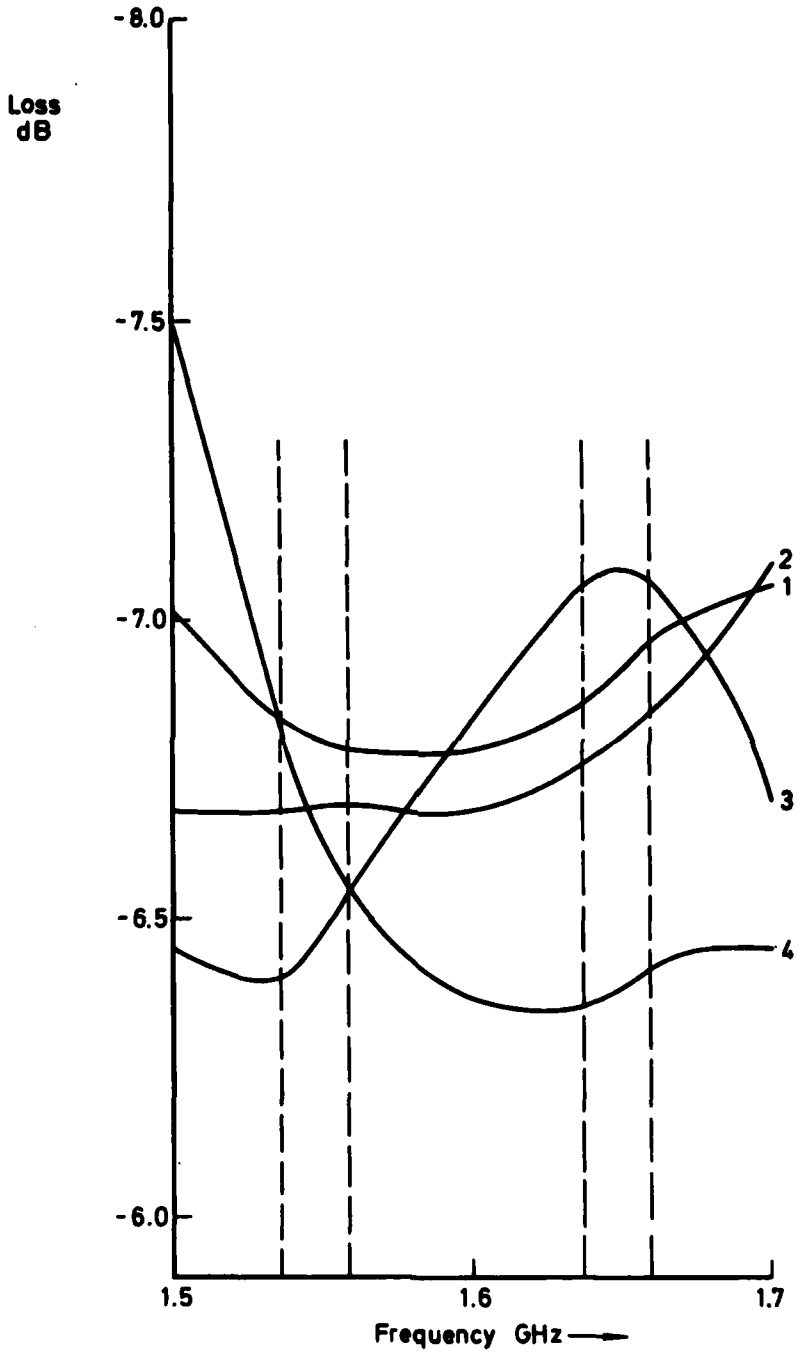

Fig 35 Measured loss through the matrix. Input port 1L to all outputs

Fig 36

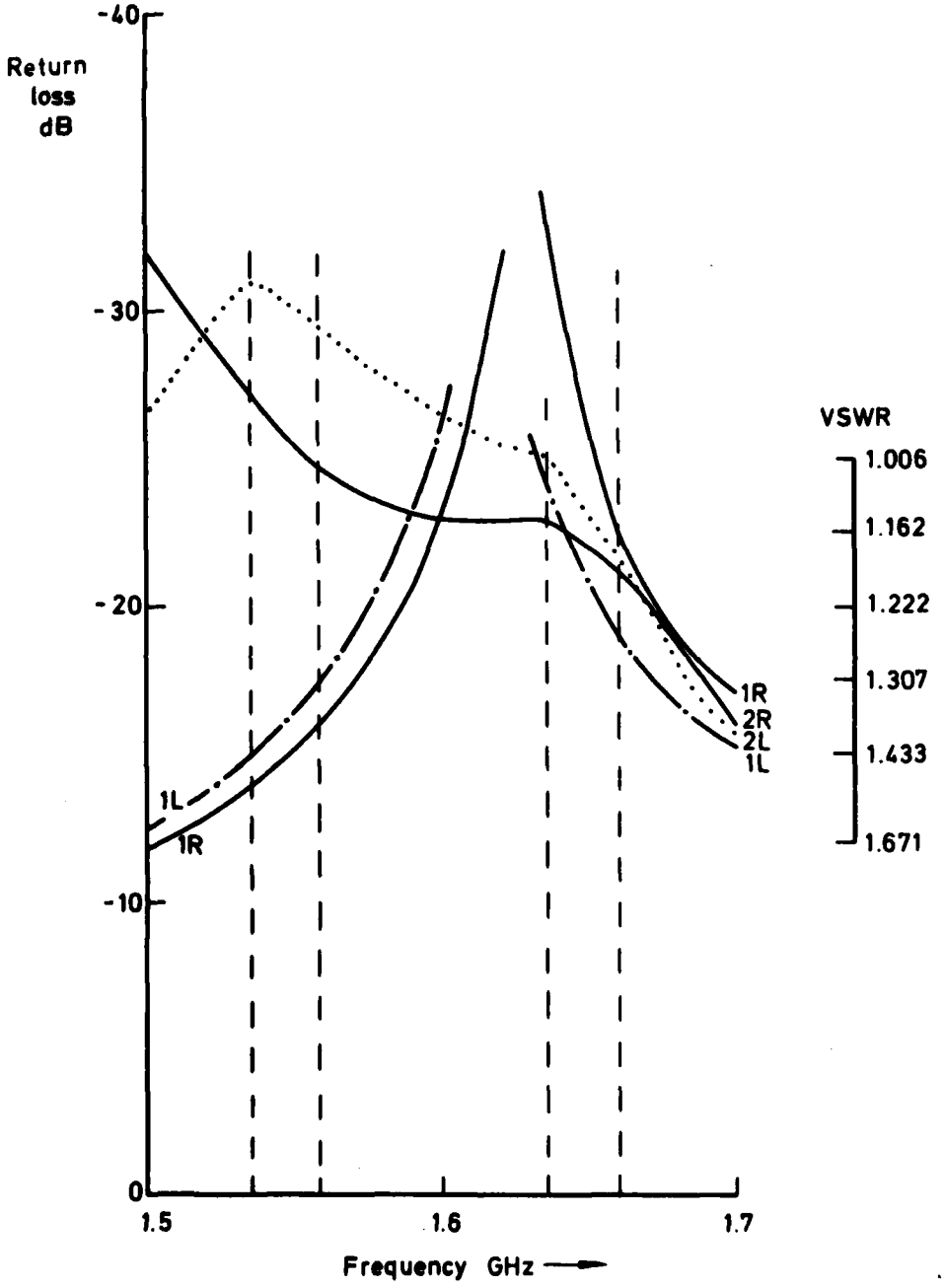

Fig 36 Measured return loss versus frequency for the matrix. All inputs

TR 79118

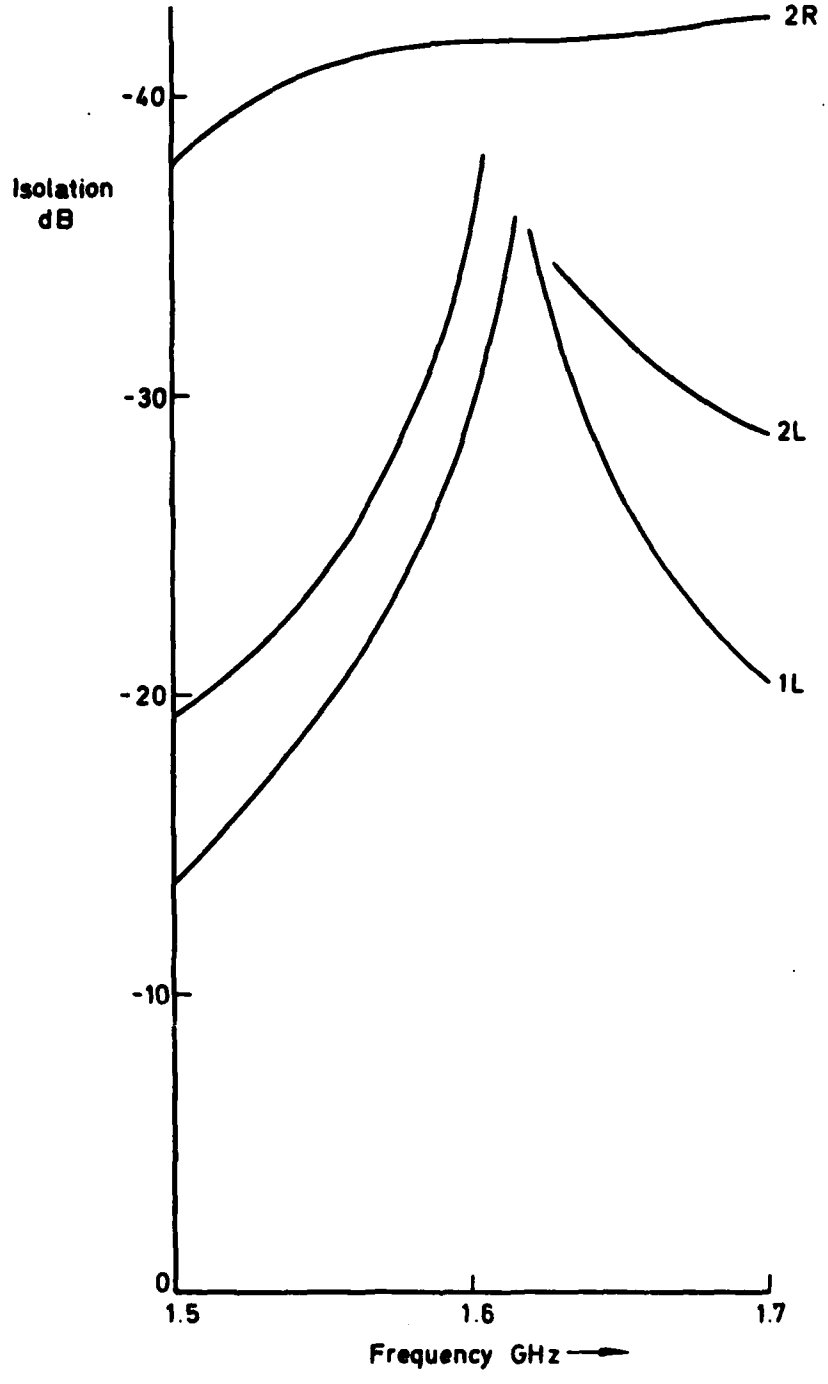

TR 79118

Fig 37 Measured isolation versus frequency for the matrix. Input port 1R to all inputs

Fig 38

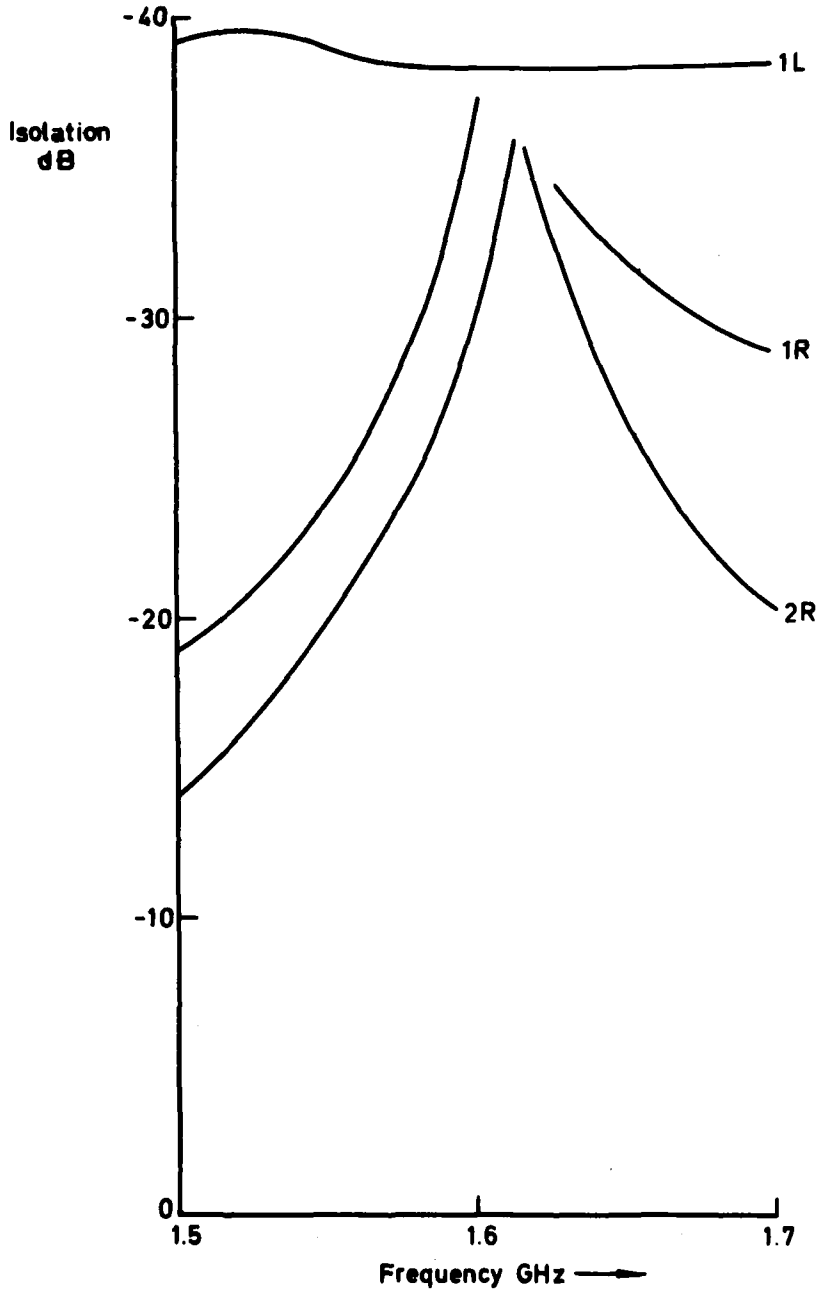

TR 79118

Fig 38 Measured isolation versus frequency for the matrix. Input port 2L to all inputs

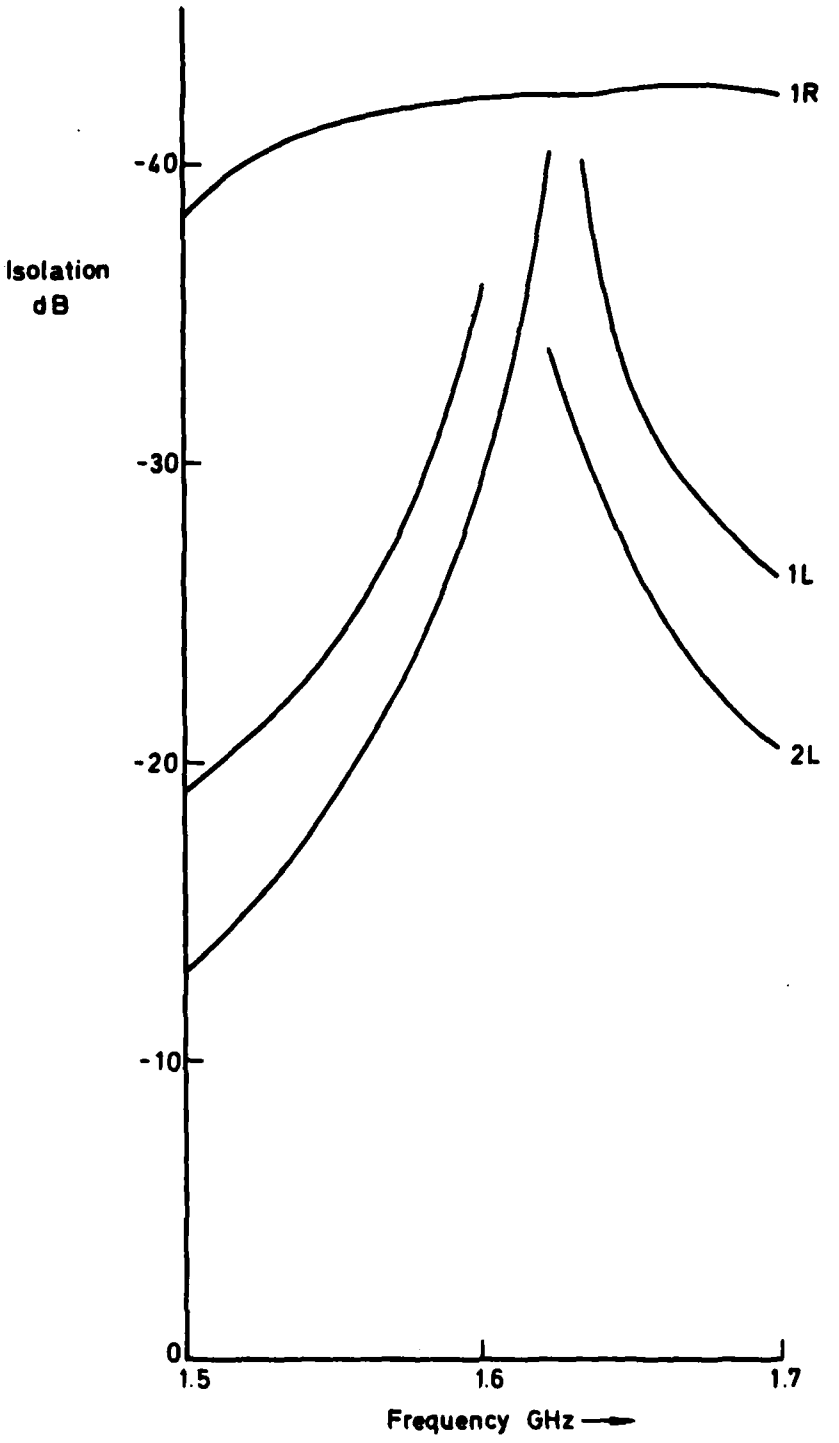

TR 79118

Fig 39 Measured isolation versus frequency for the matrix. Input port 2R to all inputs

Fig 40

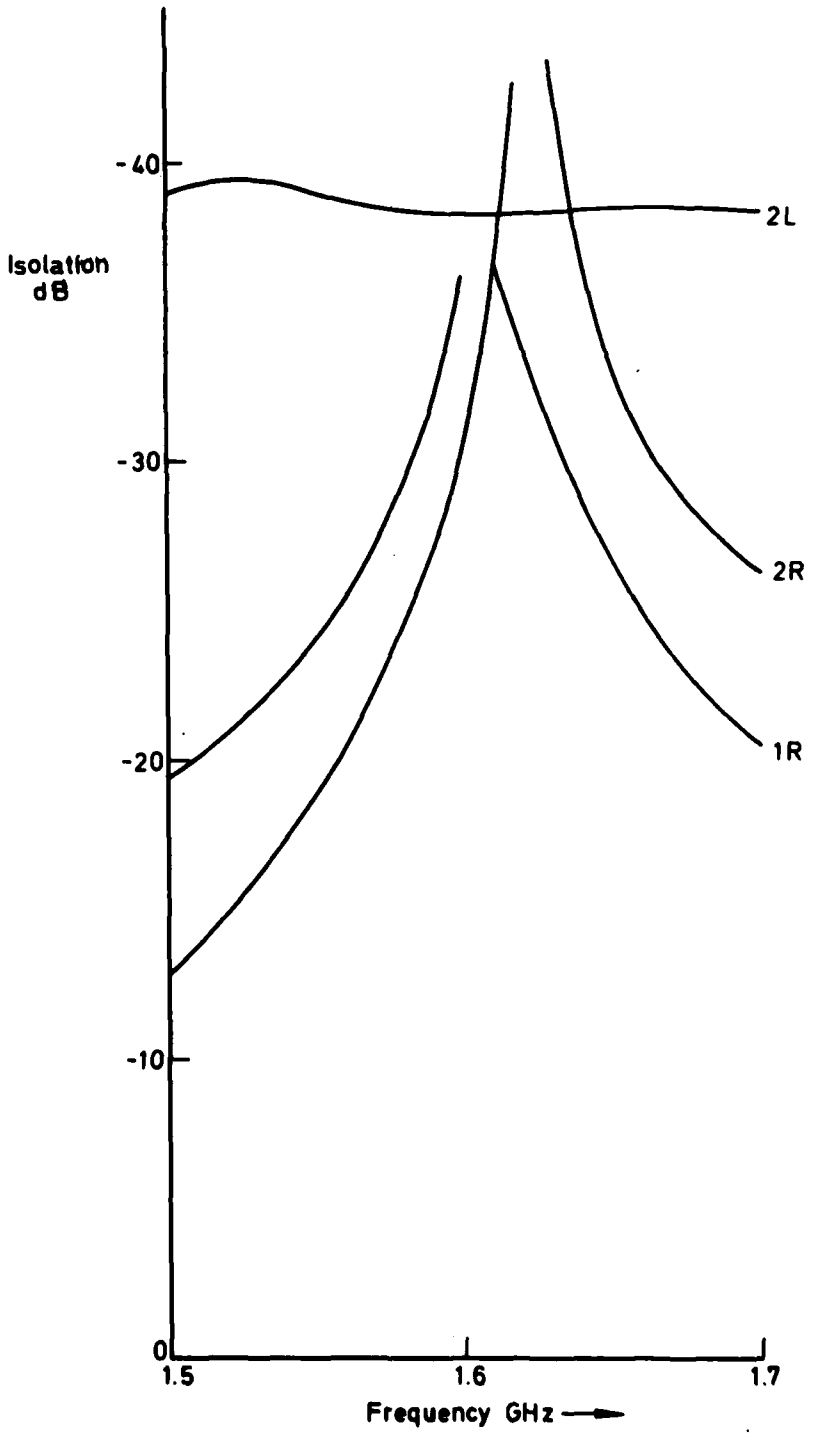

Fig 40 Measured isolation versus frequency for the matrix. Input port 1L to all inputs

TR 79118

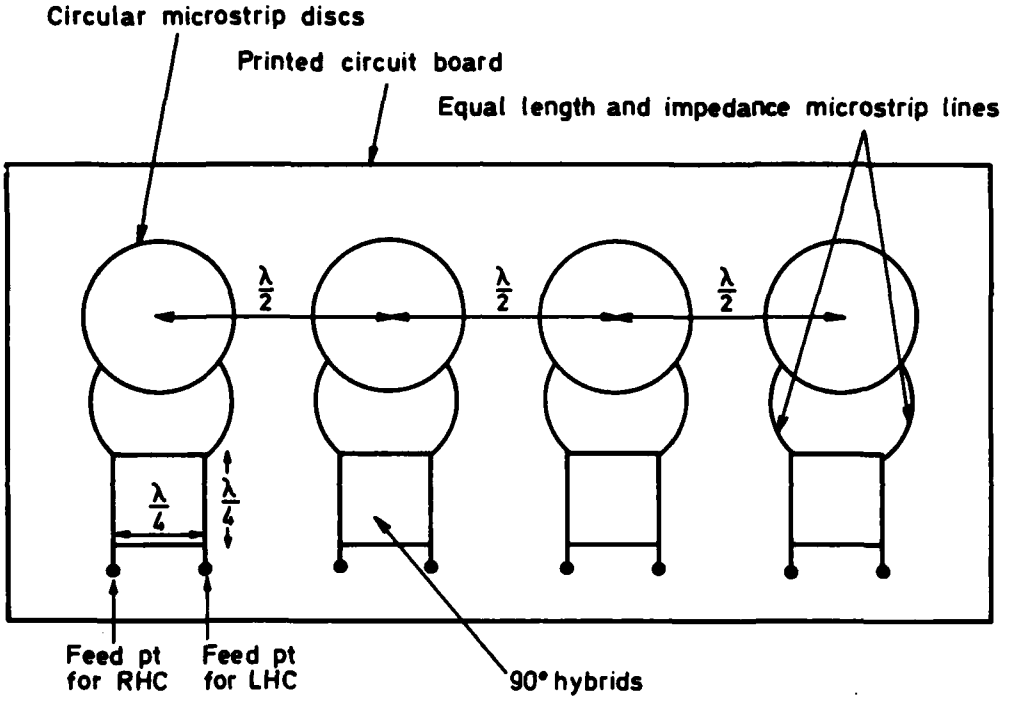

Fig 41 Block diagram of microstrip planar array (all lengths correct at 1.575 GHz)

Fig 42

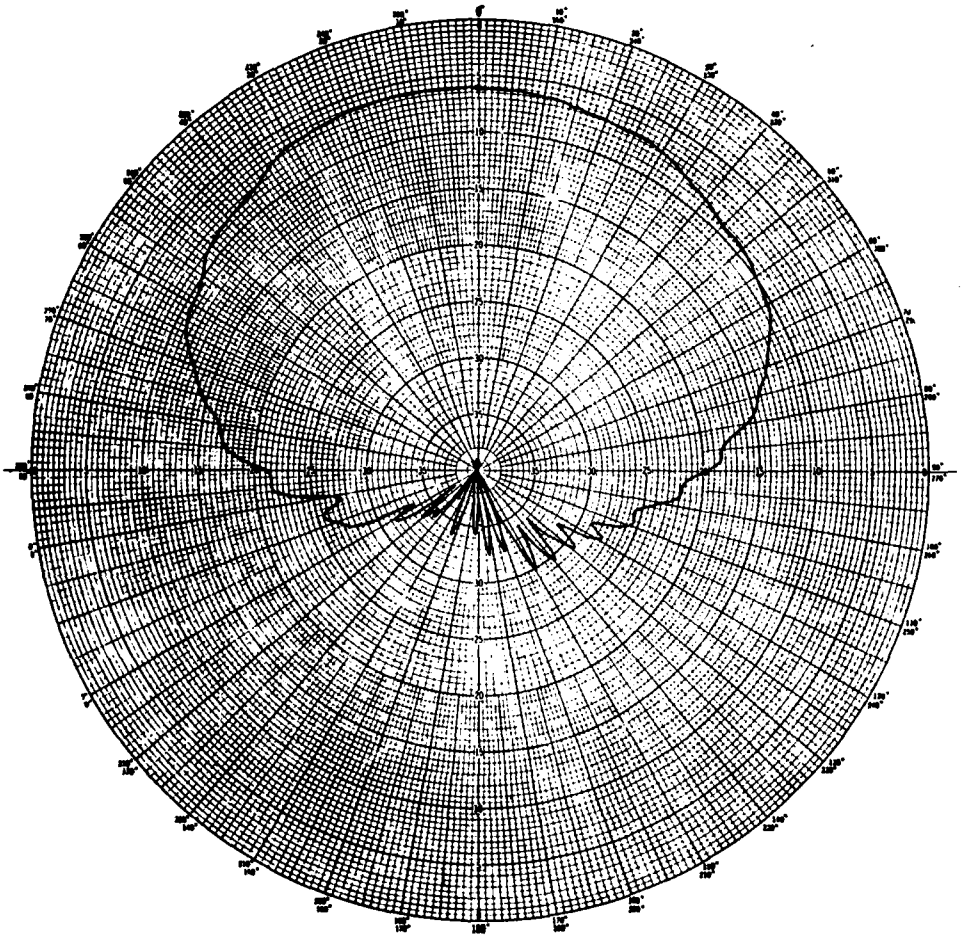

Fig 42 Radiation pattern for single element disc antenna

TR 79118

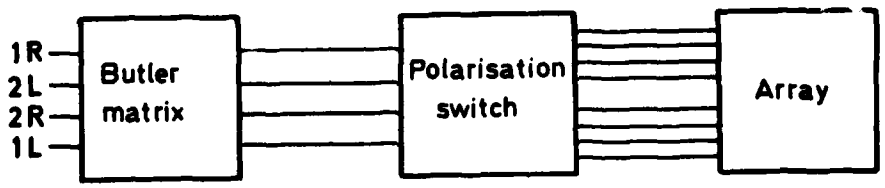

Fig 43 Basic set-up of matrix fed array

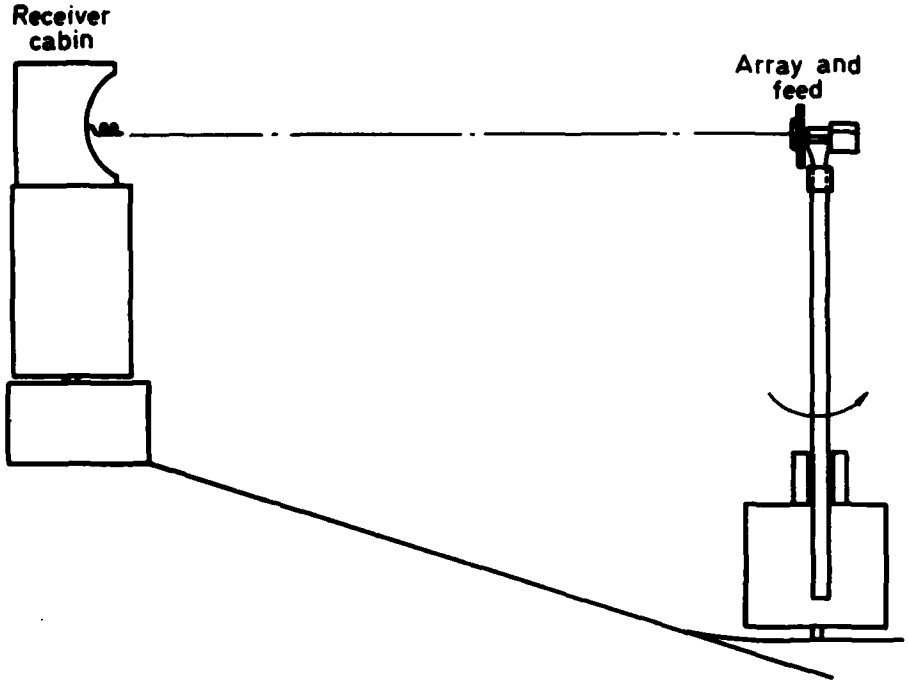

Fig 44 Range set-up for array measurement

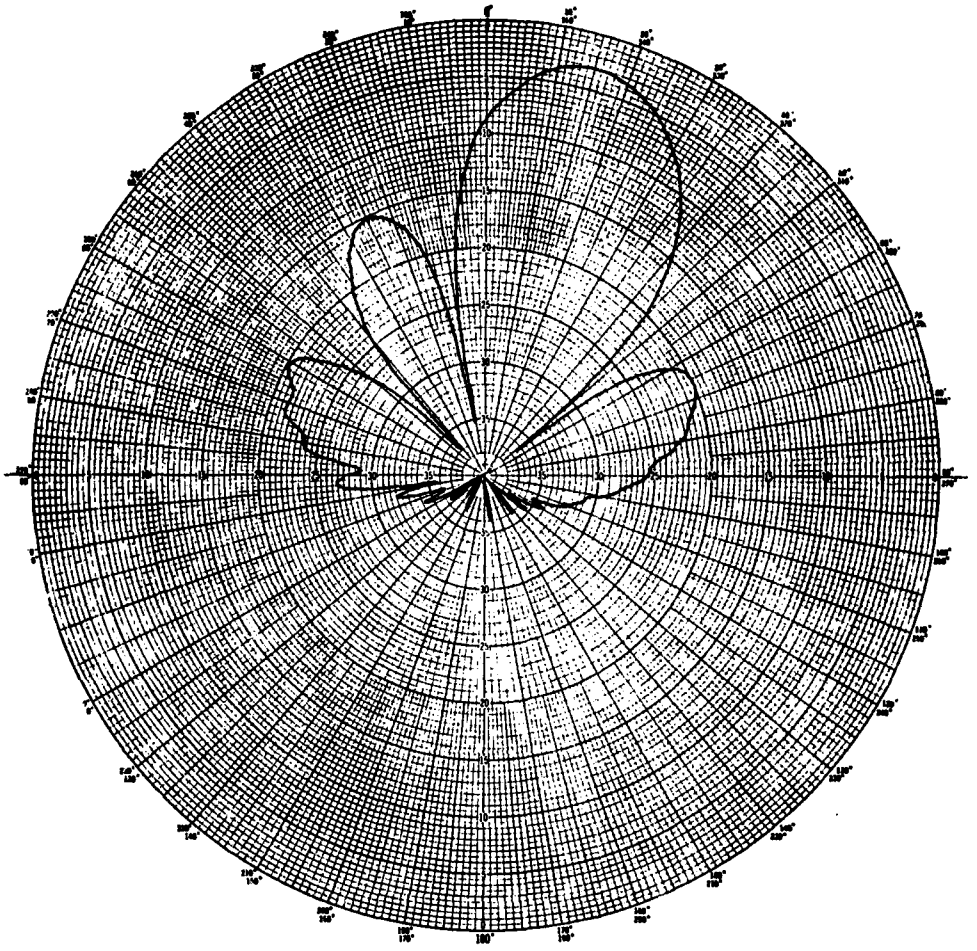

Fig 45 Polar plot. Input 1R

Fig 46

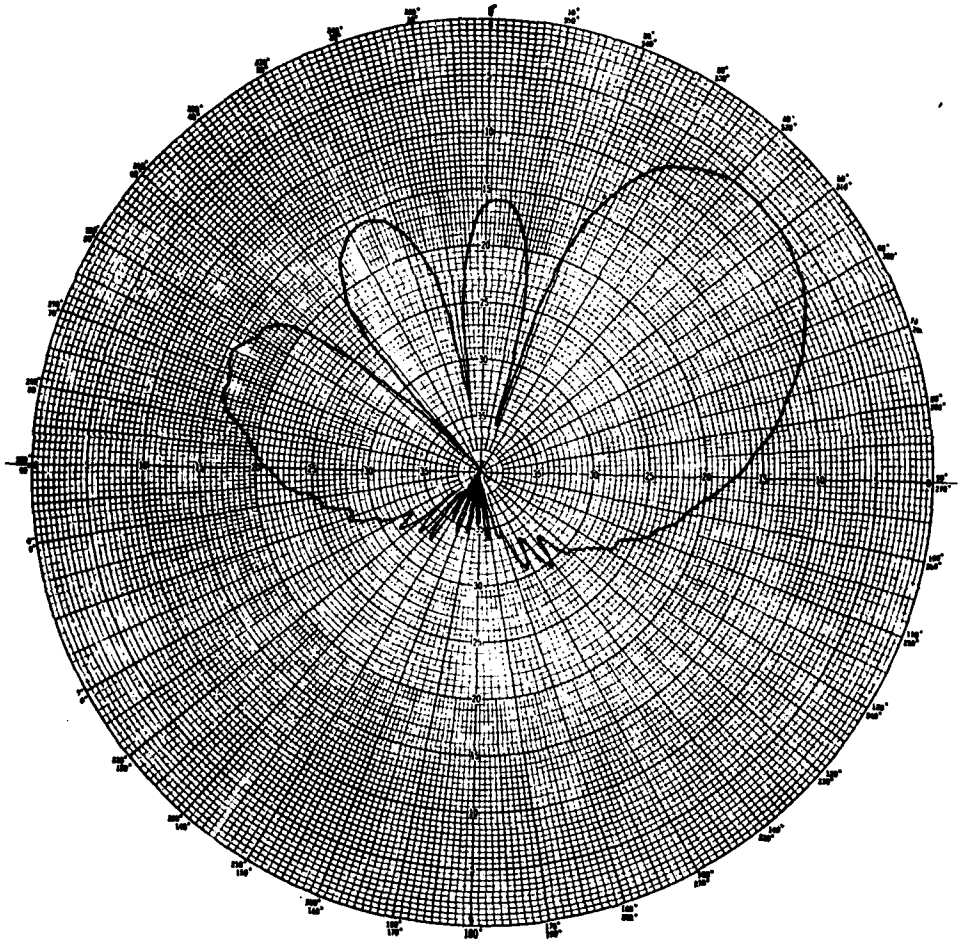

Fig 46 Polar plot. Input 2R

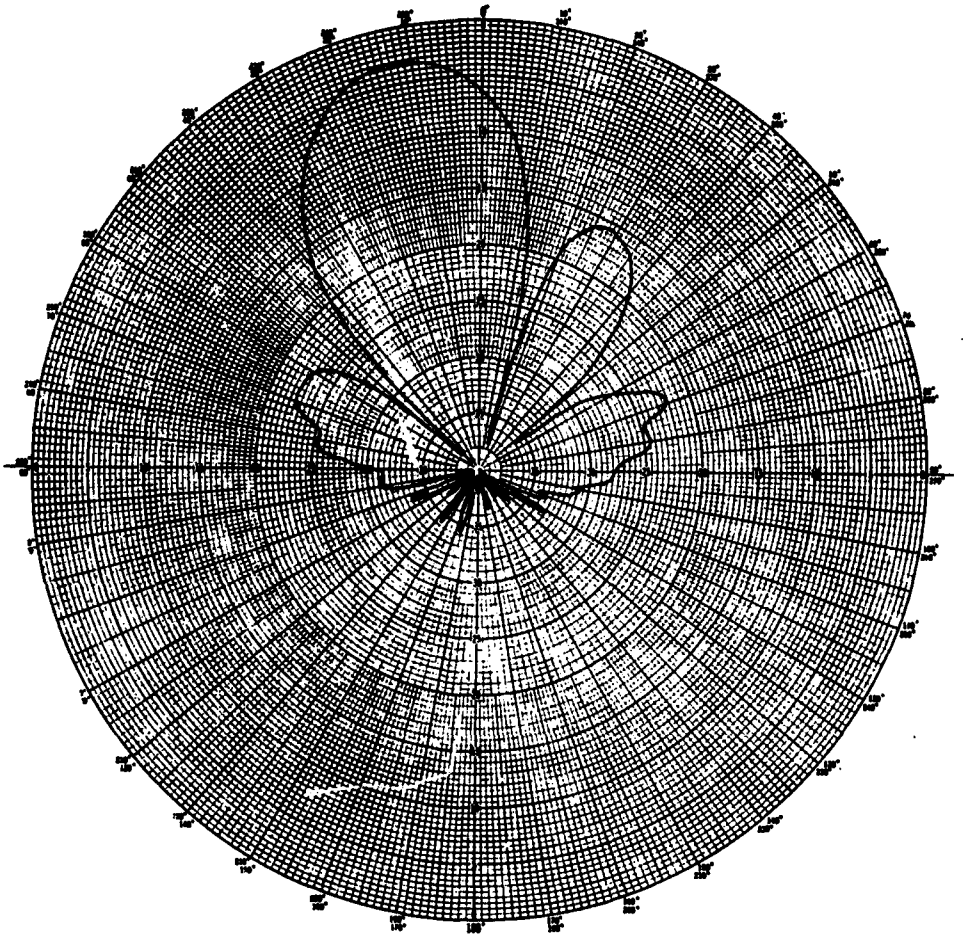

Fig 47 Polar plot. Input 1L

Fig 48

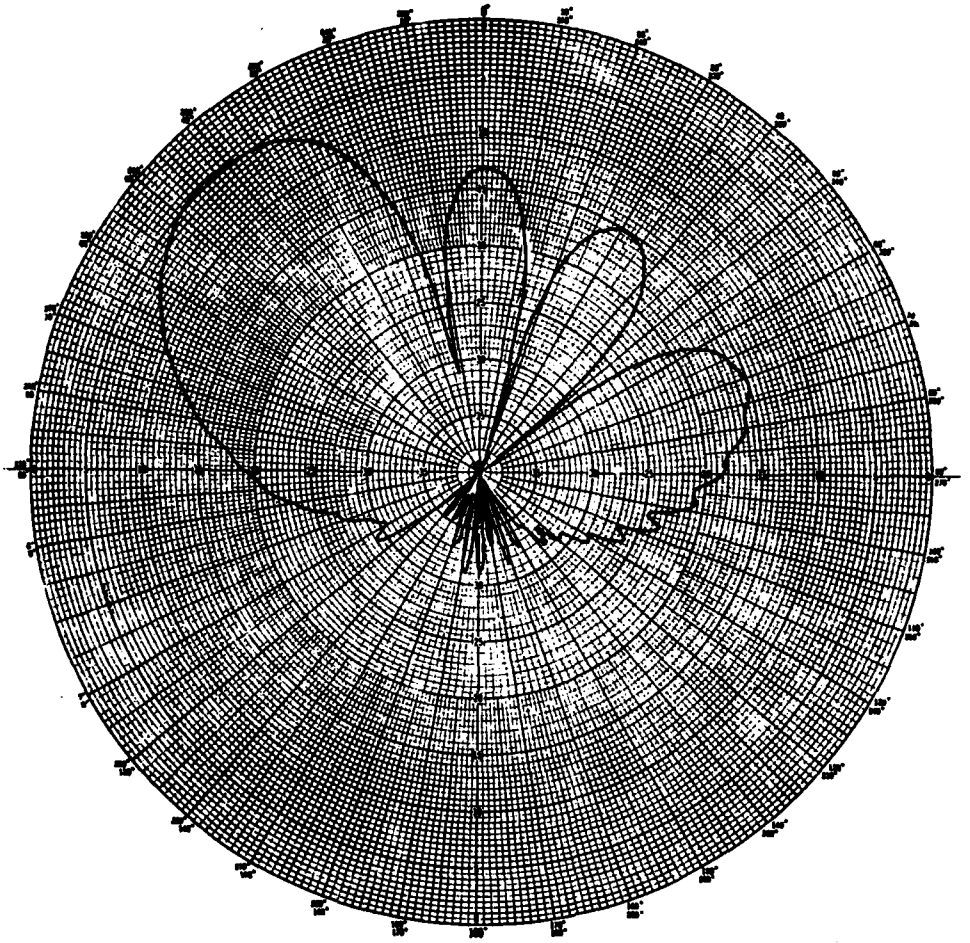

Fig 48 Polar plot. Input 2L

TR 79118

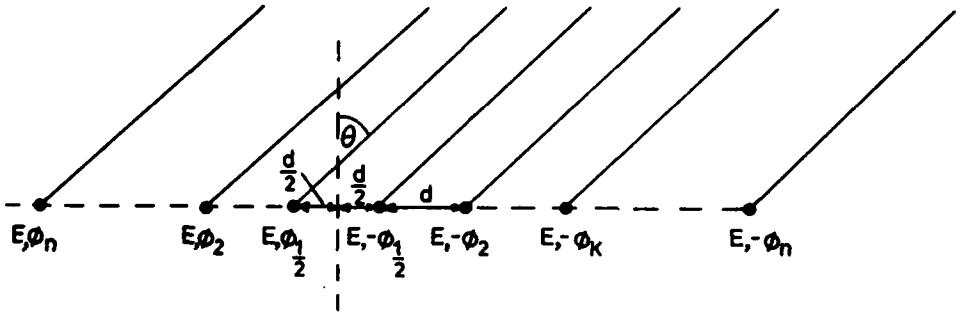

Fig 49 Array of 2n omni-radiators

Fig 50

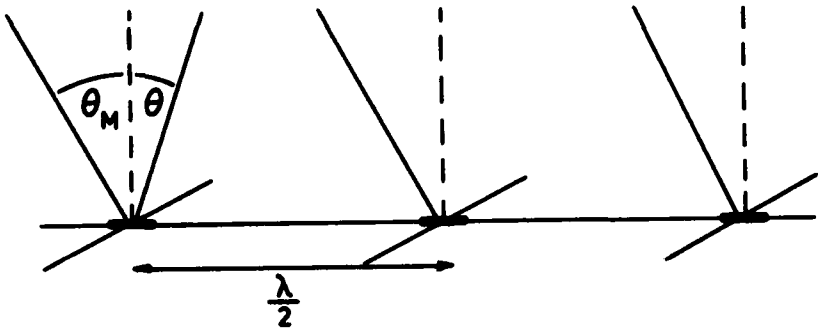

Fig 50 Dipole elements

TR 79118

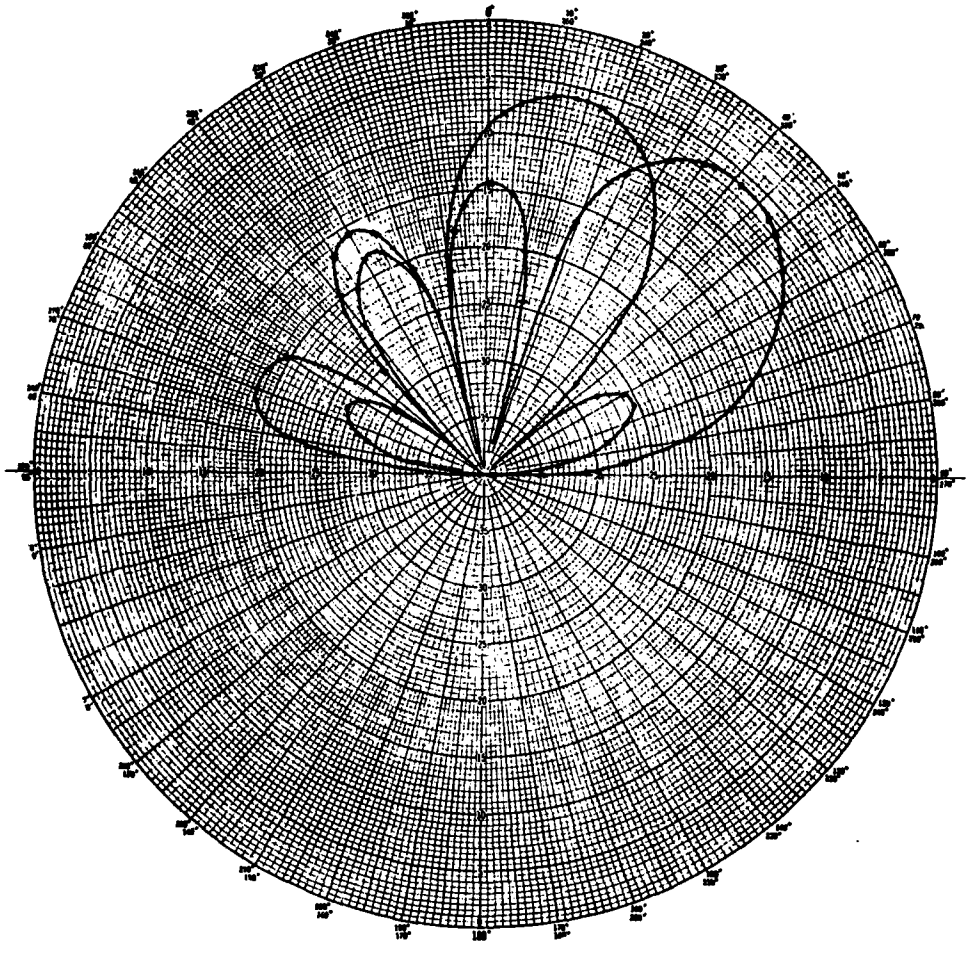

Fig 51 Array theoretical polar diagram — normalised for assumed cos θ element pattern
+++ $\theta_p = 48.6^\circ$, ... $\theta_p = 14.5^\circ$

Fig 52

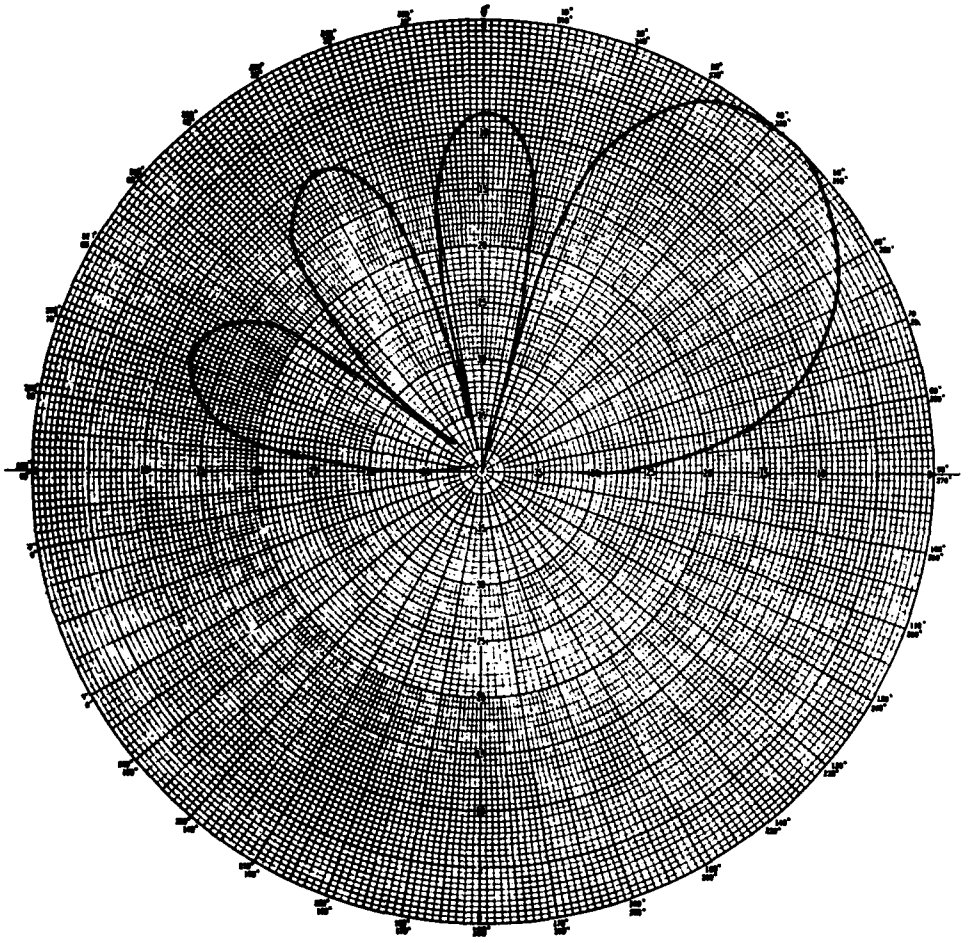

Fig 52 Expanded array. Theoretical polar diagram for $\theta_p = 48.6°$ and an element pattern of $\cos\theta$

TR 79118

REPORT DOCUMENTATION PAGE

Overall security classification of this page

UNCLASSIFIED

As far as possible this page should contain only unclassified information. If it is necessary to enter classified information, the box above must be marked to indicate the classification, e.g. Restricted, Confidential or Secret.

1. DRIC Reference (to be added by DRIC)	2. Originator's Reference	3. Agency Reference	4. Report Security Classification/Marking
	RAE TR 79118	N/A	UNCLASSIFIED

5. DRIC Code for Originator	6. Originator (Corporate Author) Name and Location
7673000W	Royal Aircraft Establishment, Farnborough, Hants, UK
5a. Sponsoring Agency's Code	**6a. Sponsoring Agency (Contract Authority) Name and Location**
N/A	N/A

7. Title
A thickfilm microstrip Butler Matrix for the frequency range 1.5-1.7 GHz

7a. (For Translations) Title in Foreign Language

7b. (For Conference Papers) Title, Place and Date of Conference

8. Author 1. Surname, Initials	9a. Author 2	9b. Authors 3, 4	10. Date	Pages	Refs.
Tabb, A.G.			September 1979	93	10

11. Contract Number	12. Period	13. Project	14. Other Reference Nos.
N/A	N/A		Space 568

15. Distribution statement
(a) Controlled by – Head of Space Department, RAE (RAL)
(b) Special limitations (if any) –

16. Descriptors (Keywords) (Descriptors marked * are selected from TEST)
Antennas*. Antenna feeds*. Beam forming network. Butler Matrix. Microstrip.

17. Abstract

This Report describes the design, construction and electrical measurement of a 4 × 4 Butler Matrix for the 1.5-1.7 GHz frequency range. The Matrix was constructed in thickfilm technology on an alumina substrate. A computer aided design package was used for the circuit synthesis.